RICE UNIVERSITY

Viscosity Evaluation of Heavy Oils from NMR Well Logging

by

Zheng Yang

A THESIS SUBMITTED
IN PARTIAL FULFILLMENT OF THE
REQUIREMENTS FOR THE DEGREE

Doctor of Philosophy

APPROVED, THESIS COMMITTEE

George J. Hirasaki, A.J. Harstook Professor, Chair
Chemical and Biomolecular Engineering

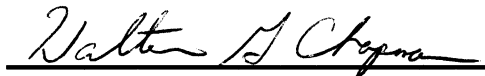

Walter G. Chapman, William W. Akers Professor
Chemical and Biomolecular Engineering

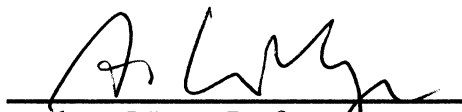

Andreas Lüttge, Professor
Earth Science and Chemistry

HOUSTON, TEXAS

APRIL, 2011

Abstract

Viscosity Evaluation of Heavy Oils from NMR Well Logging

by

Zheng Yang

Heavy oil is characterized by its high viscosity, which is a major obstacle to both logging and recovery. Due to the loss of T_2 information shorter than the echo spacing (*TE*), estimation of heavy oil properties from NMR T_2 measurements is usually problematic. In this work, a new method has been developed to overcome the echo spacing restriction of NMR spectrometer during the measurement of heavy oil. A FID measurement supplemented the CPMG in an effort to recover the lost T_2 data. Constrained by the initial magnetization (M_0) estimated from the FID and Curie's law and assuming lognormal distribution for bitumen, the corrected T_2 of bitumen can be obtained. This new method successfully overcomes the *TE* restriction of the NMR spectrometer and is nearly independent on the *TE* applied in the measurement. This method was applied in the measurement of systems at elevated temperatures (8 ~ 90 °C) and some important petrophysical properties of Athabasca bitumen, such as hydrogen index (*HI*), fluid content and viscosity were evaluated by using the corrected T_2.

Well log NMR T_2 measurements of bitumen appear to be significantly longer than the laboratory results. This is likely due to the dissolved gas in bitumen. The T_2 distribution depends on oil viscosity and dissolved gas concentration, which can vary throughout the field. In this work, the viscosity and laboratory NMR measurements were made on the recombined live bitumen sample and the synthetic Brookfield oil as a

function of dissolved gas concentrations. The effects of CH_4, CO_2, and C_2H_6 on the viscosity and T_2 response of these two heavy oils at different saturation pressures were investigated.

The investigations on live oil viscosity show that, regardless of the gas type used for saturation, the live oil T_2 correlates with viscosity/temperature ratio on a log-log scale. More importantly, the changes of T_2 and viscosity/temperature ratio caused by solution gas follows the same trend of those caused by temperature variations on the dead oil. This conclusion holds for both the bitumen and the synthetic Brookfield oil. This finding on the relationship between the oil T_2 and its corresponding viscosity/temperature ratio creates a way for in-situ viscosity evaluation of heavy oil through NMR well logging.

Acknowledgements

First of all, I wish to express my sincere gratitude to my thesis advisor Dr. George J. Hirasaki for his enlightening guidance and generous support throughout my Ph.D. thesis research. Special thanks go to Dr. Walter G. Chapman, who not only serves in my thesis committee, but also provided many helpful discussions and suggestions about my research with great patience. I also greatly appreciate Dr. Andreas Lüttge at Department of Earth Science, who serves in my thesis committee.

I am very grateful to Dr. Harold Vinegar, Dr. Matthias Appel, Dr. Daniel Reed and Dr. Sean Zou at Shell E&P Company for their invaluable guidance and ideas about my research. Thank Dr. Maura Puerto for her generous help in the design and setup of the experimental equipments. Thank Dr. M. Robert Willcott at Rice University for his interesting NMR class and insightful discussion on the NMR measurement of bitumen. Thank Dr. Gersh Zvi Taicher at Echo Medical Systems for the 20-MHz NMR measurements. Many thanks go to my colleagues in this group, especially Michael Rauschhuber, Arjun Kurup, Robert Li, Neeraj Rohilla, Jose Lopez and Tianmin Jiang, for their spiritual and academic help throughout my thesis research.

I want to acknowledge Shell E&P Company and Rice Consortium of Processes in Porous Media for the financial support.

Most of all, I wish to thank my wife Qing Zhu and my family for their constant love, support and understanding, and for all the sacrifices that they have made.

Table of Contents

List of Figures

List of Tables

Chapter 1 Introduction

Nuclear magnetic resonance (NMR) refers to the response of atomic nuclei to magnetic fields. In the presence of an external magnetic field, an atomic nucleus processes around the direction of the external field in much the same way a gyroscope processes around the earth's gravitational field. Measurable signals can be produced when these spinning magnetic nuclei interact with the external magnetic fields (Cowan 1997).

With the invention of NMR logging tools that use permanent magnets and pulsed radio frequency signals, the application of sophisticated laboratory techniques to determine formation properties *in situ* in recently drilled or while drilling well has been possible from the early 1990s (Coates, Xiao and Prammer 1999), (Dunn, Bergman and Latorraca 2002). Rather than placing the sample at the center of the instrument, the NMR logging tools turns the laboratory NMR equipment inside-out and places itself in a well bore, and is surrounded by the formation to be analyzed. A permanent magnet is placed inside the NMR logging tool to produce a magnetic field that polarizes the formation materials, and an antenna is incorporated to surround this magnet, which is used to perturb the spins and then "listen" for the decaying echo signal from those protons that are in resonance with the field from the permanent magnet.

Theoretically, NMR measurements can be made on any nucleus that has an odd number of protons or neutrons or both, such as the nucleus of hydrogen (^{1}H), carbon (^{13}C), and sodium (^{23}Na). For most of the elements found in earth formations, the nuclear magnetic signal induced by external magnetic fields is too small to be detected with a

borehole NMR logging tool. However, hydrogen, which has only one proton and no neutrons, is abundant in both water and hydrocarbons, has a relatively large gyromagnetic ratio, and produces strong signals. To date, almost all NMR logging and NMR rock studies are based on responses of the nucleus of the hydrogen atom.

Since the relationship between the proton resonance frequency and the strength of the permanent magnetic field is linear, the frequency of the transmitted and received energy can be tuned to investigate regions at different distance from an NMR logging tool. This tuning of an NMR probe to be sensitive to a specific frequency allows the magnetic resonance instruments to image narrow slices of either a hospital patient or a rock formation.

The NMR tool is characterized to be exclusively visible to fluids (Vinegar 1986). Consequently, the matrix materials do not contribute to the porosity measured by an NMR logging tool so that the calibration to formation lithology is not necessary. This response characteristic makes the NMR well logging tool fundamentally different from other conventional logging tools.

The major shortcoming for those conventional neutron, bulk-density, and acoustic-travel-time porosity-logging tools is that it can be influenced by all the components of a reservoir rock (Hearst and Nelson 1985), (Bassiouni 1994). It is well known that the reservoir rocks typically have more rock framework than fluid-filled space, therefore, these conventional tools tend to be much more sensitive to the matrix materials than to the pore fluids.

The conventional resistivity-logging tools are designed to be extremely sensitive to the fluid-filled space and traditionally are used to estimate the amount of water present

in reservoir rocks. However, they cannot be considered as the true fluid-logging devices. These tools are strongly influenced by the presence of conductive minerals and, for the proper interpretation of these tools, a detailed knowledge of the properties of both the formation and the water in the pore space is required (Coates, Xiao and Prammer 1999).

Due to the special physical principles on which NMR logging is based, the NMR logging tools are particularly powerful at providing the following information: a) quantities of the fluids in the rock; b) properties of the fluids in the rock; c) sizes of the pores that contain fluids.

Fluid quantities can be estimated by measuring the density of hydrogen nuclei in reservoir fluids with NMR logging tool. Since the density of hydrogen nuclei present in water is known and that of oils is similar, data from the NMR tool can be easily converted to an apparent water-filled porosity. Moreover, this conversion can be done without any knowledge of the minerals that make up the solid fraction of the rock.

NMR well logging technology relies on the ability to link specific rock conditions or fluid properties within a thin zone a few inches from the borehole wall in the reservoir to different NMR behavior. The NMR tools can determine the presence and quantities of different fluids (Coates, Xiao and Prammer 1999), (Dunn, Bergman and Latorraca 2002), as well as some of the specific properties of the fluids, such as viscosity (Morris et al 1994), (LaTorraca, Stonard, et al. 1999), (Lo, et al. 2002). Specific pulse-sequence settings can be run by the NMR logging tools to enhance their ability to detect particular fluid conditions.

As a result of differences in the NMR behavior between a fluid in the pore space of a reservoir rock and the fluid in bulk form (Huang 1997), enough pore-size

information can be extracted from NMR logging data to remarkably improve the estimation of some key petrophysical properties, such as permeability (Curwen and Molaro 1995) and the volume of capillary-bound water (Prammer 1994).

As mentioned in previous paragraphs, the NMR porosity is essentially matrix-independent and the NMR logging tools are only sensitive to the pore fluids. The sensitive volumes of the NMR logging tools are well defined (Coates, Xiao and Prammer 1999), and the difference in various NMR properties, such as relaxation times and diffusivity of various fluids, makes it possible to identify immobile water, movable water, gas, light oil, medium-viscosity oil, and heavy oil (Dunn, Bergman and Latorraca 2002).

The superiority of NMR logging tools at providing the above valuable petrophysical information makes these tools stand out among logging devices. In recent years, the developments of the NMR logging technology and the applications of NMR to core analysis and formation evaluation have been very rapid and widespread (Dunn, Bergman and Latorraca 2002). Currently, NMR logging tools are extensively used for determining reservoir porosity and permeability (Mirotchnik, et al. 2001), and for the real-time analysis of bottom-hole sampling of reservoir fluids (Bouton, et al. 2001), (Masak, et al. 2002).

As the conventional oil reserves in the world continue to decline and the worldwide demand for oil keeps increasing, the heavy oil and bitumen deposits attract great attention from the industry, and are considered to be a very important part for the world energy security in the future. Numerous companies have invested billions of dollars in oil sands surface mining and in situ recovery projects for heavy oil. Furthermore, as the oil price keeps going higher, the exploration of bitumen in deeper

formations is drawing more and more interest. Many *in-situ* bitumen recovery options have been designed and commercialized for recovering oil in the deeper formations (Bryan, Mai, et al. 2005). Therefore, being able to predict heavy oil properties and fluid saturation in situ and optimize the process of bitumen extraction process is of considerable value to the industry.

Heavy oil and bitumen are characterized by their high viscosities, which are the major obstacles to their recovery and properties investigations. As the most important petrophysical property, viscosity of heavy oil determines both the economics and the technical chance of success for the chosen recovery scheme and is often directly related to the recoverable reserves estimates (Miller and Erno 1995). As a result, *in-situ* oil viscosity measurement techniques would be of significant benefit to the industry.

Because of the unique operational mechanism of nuclear magnetic resonance (Coates, Xiao and Prammer 1999), the low-field NMR shows great potential as a logging tool for assessing reservoir-fluid viscosities. However, due to the loss of T_2 information shorter than echo spacing (TE), estimation of heavy oil viscosity from NMR T_2 is often problematic. In order to eventually extend the use of NMR logging tools to the competent estimation of the heavy oil viscosity in the field through logs, the development of both NMR measurement scheme and data interpretation method are required.

On the other hand, in past years, many NMR-based oil-viscosity correlations were presented in literatures to relate viscosity to different NMR parameters. Correlations were observed between oil viscosity and the mean NMR relaxation time of the oil (Kleinberg and Vinegar 1996), (Straley, et al. 1997), (Morriss, et al. 1997), (LaTorraca, Stonard, et al. 1999), and between viscosity and the apparent signal strength of the oil (Galford and

Marschall 2000), (Mirotchnik, et al. 2001). Previous work in our group focused on the development of a viscosity correlation derived from T_1 of alkanes (Lo, et al. 2002) and was tested with various crude oils in later work (Y. Zhang 2002), (Hirasaki, Lo and Zhang 2003). Unfortunately, while these correlations did a good job for predicting viscosities of conventional oils, none of them were successful when it comes to the highly viscous heavy oil and bitumen.

Another property of great importance to the recovery of heavy oil is reservoir fluid content. There are several areas in oil sands development operations where it is critical to have an estimate of the oil, water, and solids content of a given sample. During initial characterization of reservoir, determining oil and water content with depth and location in the reservoir is necessary. Fluid content determination with logging tools would be beneficial for all reservoir characterization investigations. In mining operations, obtaining enough information on the fluid and solids content of the mined oil sand ore will allow the extraction process to be better optimized and controlled.

Currently, the industry standard for accurately measuring fluid content is the Dean-Stark extraction method, which is costly and time consuming. Centrifuge technology is often used for speeding up the process, but this can cause inaccuracy because of the similar fluid densities and the presence of emulsions (Bryan and Kantzas 2005). Although, the conventional resistivity-logging tools are also traditionally used to estimate the amount of water present in reservoir rocks, they are strongly influenced by the presence of conductive minerals. Moreover, in order to properly interpreted device responses, a detailed knowledge of the properties of both the formation and the water in the pore space is also needed (Coates, Xiao and Prammer 1999).

Due to the lithology-independent and quick-response features, low-field NMR has been used as an improved method for making estimations of oil and water content in ore and froth samples. The application of this technology for heavy oil reservoirs and oil sands characterization is of particular interest.

However, NMR logging has not been very successful in characterizing heavy oil and bitumen (viscosity > 100,000 cp). The high oil viscosity still causes challenging problems for the NMR logging tools. The combination of the echo spacing (*TE*) limitation of applied NMR logging instrument and the fast relaxation of heavy oil resulting from its high viscosity inevitably result in the loss of NMR information (T_2) during measurement (Kleinberg and Vinegar 1996), (Morriss, et al. 1997), (LaTorraca, Dunn, et al. 1998), (LaTorraca, Stonard, et al. 1999), (Lo, et al. 2002), (Hirasaki, Lo and Zhang 2003), (Bryan and Kantzas 2005), (Bryan, Mai, et al. 2006) and (Bryan, Kantzas and Badry, et al. 2006). Consequently, estimation of bitumen properties, such as hydrogen index (*HI*), fluid content and viscosity, based on the captured NMR response is problematic and generally has incorrect *TE* or sample temperature dependence.

Kleinberg and Vinegar (Kleinberg and Vinegar 1996) reported an apparent hydrogen index (HI_{app}) decrease among NMR measurements on some heavy crude oil samples (API gravity < 17°) and attributed it to the oil components decaying faster than 1 msec. LaTorraca, *et al.* (LaTorraca, Stonard, et al. 1999) investigated on the effects of varying *TE* on the T_2 distributions and incorporated *TE* as a parameter into the Vinegar equation (Kleinberg and Vinegar 1996) to relate the signal loss (HI_{app} or apparent logarithmic mean T_2, $T_{2,app}$) to the viscosity for heavy oils (>1000 cp).

However, this particular method, which is based on the signal loss in NMR measurement on heavy oils, inevitably has a dependence on the value of *TE* used by the NMR logging tools and consequently needs adjustment according to various *TE* applied. Furthermore, the use of these signal-loss-based correlations rely on supplemental information from other logging tools, such as the use of resistivity and density logs for porosity and oil saturation, and estimates of the degree of invasion. The influences of high noise levels on any of these logging tools introduce error into the estimates. More importantly, the essential use of the "apparent" NMR values (HI_{app} or $T_{2,app}$) in this method makes it impossible to develop the ultimate theory-based correlations for oil properties, which undoubtedly depend on the "real" values. Therefore, the development of a new method to correct the T_2 values of the heavy oils from an incomplete T_2 distribution and overcome the echo spacing limitation of NMR spectrometer is of great necessity.

Another problem in the NMR well logging of heavy oil and bitumen is that, well log NMR T_2 measurements of the heavy oil (bitumen) appear to be significantly longer than the laboratory results. This is likely due to the dissolved gas in bitumen in the reservoir. The T_2 distribution depends on oil viscosity and dissolved gas concentration, which may vary throughout the field. Therefore, a method to determine the solution gas and the *in-situ* viscosity from NMR logs would be very useful in heavy oil and bitumen reservoir development.

The objectives of this study are to solve these two problems in the NMR well logging of heavy oils.

An improved NMR measurement scheme, combining FID and CPMG is developed in the investigation on Athabasca bitumen. A new method for the interpretation of NMR data, which uses the lognormal distribution model to fit the CPMG data supplemented with the specified initial magnetization M_0, successfully overcomes the echo spacing restriction of NMR tools in the application for viscous heavy oils. By using the corrected T_2 information, improved estimates for viscosity, fluid content and hydrogen index of bitumen were achieved.

In the second part of this study, the viscosity and laboratory NMR measurements on a recombined live bitumen sample and the Brookfield oil standard (synthetic oil, 100% PAO) as a function of dissolved gas concentrations were performed. The effects of three major reservoir gases (CH_4, CO_2, and C_2H_6) on the viscosity and T_2 response of the two different oil samples at a series of saturation pressures were investigated. The correlations between the saturation pressure, gas solubility, NMR T_2 and live oil viscosity are established to resolve the differences between the NMR log and laboratory data. The findings create a way for in-situ viscosity evaluation of heavy oil through NMR well logging.

A brief introduction of the chapters in this thesis is as follows:

Chapter 1 is for problem statement and subject introduction. The relevant literature reviews is also included in this chapter.

Chapter 2 describes the investigations performed on the Canadian Athabasca bitumen. A new NMR measurement scheme and data interpretation method were developed to successfully overcome the echo spacing restrictions during the NMR measurements on heavy oils.

Chapter 3 illustrates the work performed on the synthetic Brookfield oil. In this chapter, the facilities and procedures for the high pressure experiments are designed. The viscosity and NMR measurements were performed at various pressure levels. The dissolving behaviors of three different reservoir gases were observed and the solubility of each gas in this synthetic oil was evaluated via PVT measurements.

Chapter 4 investigates the changes of viscosity and the NMR response of the recombined live bitumen sample with three different reservoir gases. Comparisons were drawn between the results from the live bitumen and live Brookfield oil. Correlations are established to resolve the differences between the NMR log and laboratory data.

Chapter 5 is devoted to the conclusion of this study and suggestions for the future work in this research area.

Chapter 2 NMR Measurement of Bitumen at Different Temperatures

2.1 Introduction

Heavy oil and bitumen is characterized by its high viscosity and density, and represent a worldwide known oil reserve of 6 trillion barrels (Galford 2000) and (Deleersnyder 2004). As the conventional oil reserves of the world continue to decline and the exploration and production technologies keep improving, the heavy oil and bitumen deposits have attracted great attention from both the government and the industry, and will be the future of the world oil industry for years to come.

Low field NMR has displayed great potential in many heavy oil well logging cases (California, Venezuela, China) (Deleersnyder 2004). However, the echo spacing (*TE*) limitation of applied NMR logging tools and the fast relaxation of heavy oil resulting from its high viscosity have combined to make the NMR information (T_2) inevitably lost during measurements. Consequently, estimation of heavy oil properties, such as hydrogen index (*HI*), fluid content and viscosity, based on the captured NMR response is problematic and generally has incorrect *TE* or sample temperature dependence.

In this chapter, new methods for both NMR measurement and subsequent raw data interpretation are developed to correct the T_2 relaxation times of heavy oil (bitumen). The new methods can overcome the echo spacing limitation of NMR spectrometer and have only minor *TE* dependence. Further improvement was also made to eliminate the

incorrect temperature dependence during the application of the new methods at different sample temperatures (8 ~ 90 °C). The petrophysical properties, such as hydrogen index, fluid saturation and viscosity can be directly estimated from the corrected relaxation times.

2.2 Equipment and Experimental Procedures

The major nuclear magnetic resonance (NMR) spectrometer used in this work is a low field Maran-II spectrometer (Maran-SS), which is operating at a proton resonance frequency of 2.0 MHz. The effective vertical height of the magnetic field is around 5 cm. The temperature of magnetic field system is controlled at 30 °C with an error of ± 0.1 °C.

The heavy oil sample used in this work is froth separated Athabasca bitumen from Alberta, Canada. It consists of bitumen, water and a small amount of clay. The bitumen sample used for the measurements with Maran-II is contained in a glass tube (I.D. 4.66 cm) with a sample height of 3.60 cm. The sample tube was carefully sealed and stored at room temperature.

The NMR measurements were performed at different sample temperatures from 8 to 90 °C. The temperature of magnet was kept at 30 °C for all measurements. Before each measurement, the bitumen sample was placed in a thermal water bath at the desired temperature for over 4 hours to reach the sample temperature equilibrium. The sample tube was wrapped with four-layer paper insulation during the measurement. A single measurement took less than 1 min. The measurement at each temperature was repeated at least three times to ensure the data reliability.

The 90 °C case was employed to demonstrate the temperature change during heating process and NMR measurement. The temperature at the center was used to represent the bitumen sample temperature. As shown in Fig. 2.2.1, it only took about 90 min. to heat the bitumen sample from room temperature to 90 °C. The sample was equilibrated for over 4 hours. During the subsequent NMR measurement, the sample temperature was 90±1.5 °C within 1 min. 90 °C is the highest temperature used in this work and has the largest temperature difference from the magnet temperature (30 °C). According to the results displayed in Fig. 2.2.1, it is reasonable to assume that 4-hour thermal water bath was enough to reach equilibrium at any interested temperature in this work. And the temperature deviation during the measurement was acceptable.

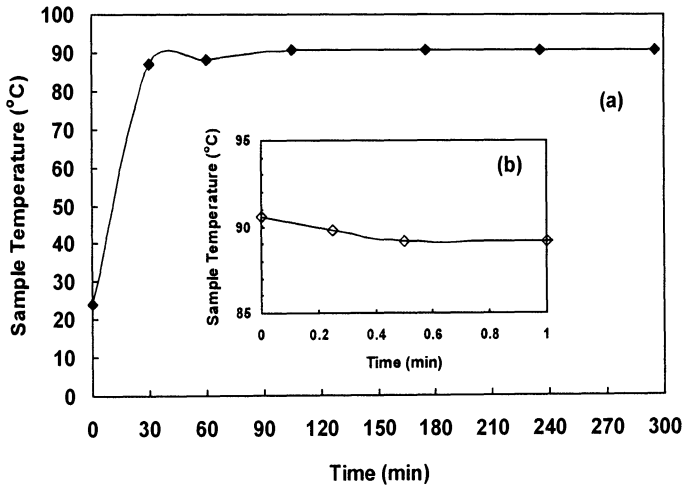

Figure 2.2.1 Temperature change of Athabasca bitumen sample: (a) during heating process, (b) during NMR measurement

2.3 Results

2.3.1 Regular CPMG Measurement on Bitumen Sample

Regular CPMG measurements were performed on the Athabasca bitumen sample of 30 °C with the Maran-II spectrometer. For the bitumen sample, the applied width of $\pi/2$ pulse was 9.45 μsec and that of π pulse was 16.60 μsec. Three different echo spacings (*TE*) 0.4 msec, 0.8 msec and 1.2 msec were applied respectively. The CPMG raw data were fitted to the standard multi-exponential decay model as follows (Dunn, LaTorraca, et al. 1994):

$$M(t) = \sum_i f_i \cdot e^{-\frac{t}{T_{2,i}}} \tag{2.1}$$

The interpreted T_2 relaxation time distributions of this bitumen sample are shown in Fig. 2.3.1. It is clear that, the T_2 distribution of bitumen sample has a strong dependence on the applied echo spacing. When the echo spacing increases, the bitumen peak shifts to the larger relaxation time, while the area of the bitumen peak significantly decreases. It implies that, due to the short T_2 relaxation time (less than 1 msec) of bitumen resulting from its high viscosity (on the order of 10^6 cp), the T_2 of some components of bitumen is even shorter than the echo spacing of the NMR spectrometer. Therefore, as larger echo spacing was applied, more T_2 distribution information of bitumen was lost.

Another observation that can be made from Fig. 2.3.1 is that the bitumen signal and water signal are separated clearly in the T_2 relaxation time distribution at 30 °C. The entire signal from the bitumen is found in the first peak from the left of the sample

spectra (Bryan, Mai, et al. 2006). Thus, in this case, the local minimum after the bitumen peak was employed as the cut-off between oil and water peaks.

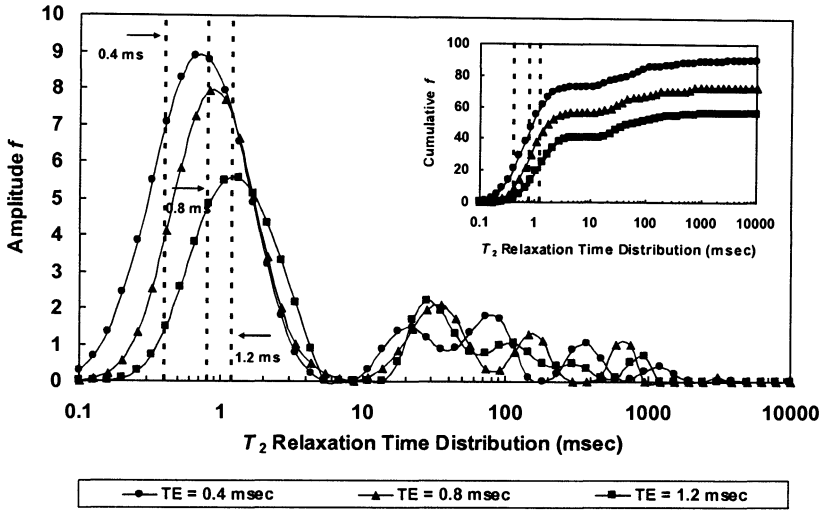

Figure 2.3.1 T_2 distribution of bitumen has strong dependence on echo spacing

The NMR responses (amplitude *f*) from water and bitumen in the sample are calculated respectively and shown in Table 2.3.1. We can easily find that, due to the loss of T_2 information shorter than the applied echo spacing, the summation of amplitude from bitumen keeps deceasing when the applied echo spacing increases. On the other hand, the summation of amplitudes from the water response, which can be taken as the indication of area covered by water peaks, only has very slight changes. This implies insensitive response of water to the applied echo spacing, which results from its significantly lower viscosity and larger T_2 relaxation time. Here, the water relaxation time is less than the value of bulk water because of surface relaxation due to interaction with bitumen and clay solids.

Table 2.3.1 NMR response of bitumen sample in regular CPMG

Echo spacing (TE) (msec)	Σf of bitumen in sample	Σf of water in sample	Σf of total bitumen sample
0.4	69.0	17.1	86.1
0.8	57.1	16.8	73.9
1.2	37.9	16.9	54.8

2.3.2 Improved Experimental Scheme for Correcting T_2 of Bitumen

In order to overcome the inevitable echo spacing restriction of the Maran-II, a modified scheme for CPMG measurement was developed to correct the T_2 relaxation time of bitumen. In this new scheme, a regular FID was imposed at the start of each CPMG measurement. Then the initial magnetization of the bitumen sample M_0, can be obtained from the extrapolation of FID as shown in Fig. 2.3.2.

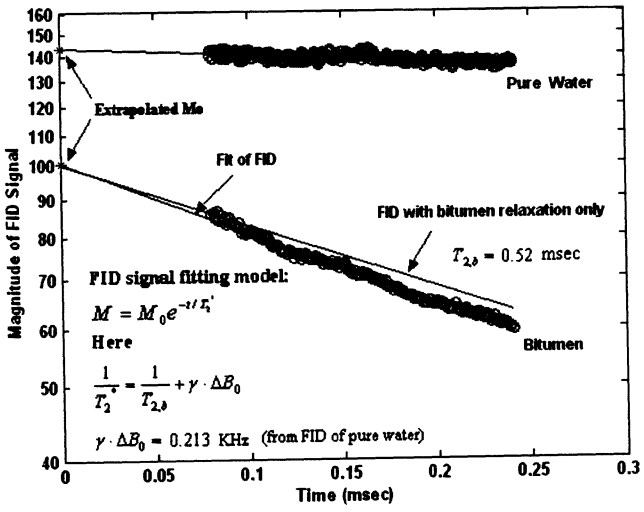

Figure 2.3.2 Estimations of M_0 and T_2 from the extrapolation of FID

The transverse relaxation of the measured FID signal follows a first order rate process with a characteristic time constant T_2^* (Coates, Xiao and Prammer 1999):

$$M(t) = M_0 \cdot e^{-\frac{t}{T_2^*}}. \tag{2.2}$$

Here, M_0 is the initial magnetization of the sample. The constant T_2^* is called transverse relaxation time and is affected by the inhomogeneity of the static magnetic field. The time constant describing the decay of the transverse magnetization due to both the spin-spin relaxation of bulk sample (T_2) and the inhomogeneity of the static field is given as:

$$\frac{1}{T_2^*} = \frac{1}{T_{2,b}} + \gamma \cdot \Delta B_0 . \tag{2.3}$$

where $T_{2,b}$ is the intrinsic transverse relaxation time of bitumen, $\gamma \cdot \Delta B_0$ is the inhomogeneity of the static field in unit, KHz.

From the Eq. [2.2] and Eq. [2.3], we can see that in order to determine the inhomogeneity of magnetic field, a sample with the property that $T_2^* \ll T_{2,b}$ must be used. The pure water (deionized), which has a $T_{2,b}$ relaxation time of around 2.9 sec, serves this purpose well. Then, the inhomogeneity $\gamma \cdot \Delta B_0$ of the applied magnetic field in this work can be estimated, which is 0.213 KHz as shown in Fig. 2.3.2.

Due to the high viscosity of bitumen, the $T_{2,b}$ of bitumen is small and comparable to the inhomogeneity of magnetic field. Therefore, both terms on the right side of Eq. [2.3] count for the single exponential fitting. Given the inhomogeneity obtained from the FID of pure water (Fig. 2.3.2), the estimated T_2 of bitumen is 0.52 msec.

2.3.3 Improved Interpretation Method for Correcting T_2 of Bitumen

After incorporating the improved experimental scheme described in section 2.3.2, a new interpretation method was also developed for interpreting the CPMG raw data of bitumen sample. In this new method, the initial magnetization of bitumen sample, which was obtained from FID measurement, was supplemented to the regular CPMG raw data.

First, the standard multi-exponential model Eq. [2.1] was still used to interpret the supplemented CPMG data. The case of TE = 0.4 msec was employed as an example and the result of interpretation by using the standard multi-exponential model is shown in Fig. 2.3.3. It is clear that, simply using the supplemented CPMG data for interpretation hardly changed the position of bitumen peak. Instead, a long tail showed up at the left side of the bitumen peak as the compensation of the supplemented M_0. In this manner, the estimate of the bitumen T_2 distribution was not improved. A new model which is able to better collaborate with the supplementation of CPMG data was necessary.

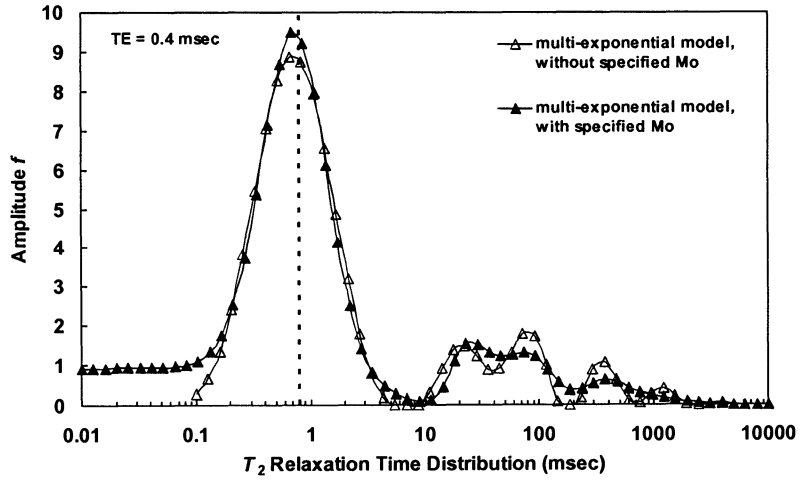

Figure 2.3.3 T_2 distribution of bitumen sample with supplemented M_0. Here, the standard multi-exponential model was used.

The bitumen peaks shown in Fig. 2.3.1 are quite symmetric on the semi-logarithmic scale. Furthermore, the logarithmic mean of T_2 is more commonly used in different property correlations. Based on these two points, instead of the standard multi-exponential model, a lognormal distribution model was assumed to represent the T_2 distribution of bitumen. The derivation of this lognormal distribution based model is shown as below:

The multi-exponential model is expressed by Eq. [2.1]. Since it consists of two parts, bitumen and water, it can also be expressed as Eq. [2.4]:

$$M(t) = M_b(t) + M_w(t) = \sum_j f_{b,j} \cdot e^{-\frac{t}{T_{2,j}}} + \sum_k f_{w,k} \cdot e^{-\frac{t}{T_{2,k}}} \tag{2.4}$$

On the right side of Eq. [2.4], the first term is for bitumen and the second term is for water part in the bitumen sample. Here, we assume the interpretation for water part is correct from standard multi-exponential model and replace the bitumen part in Eq. [2.4] with a lognormal distribution model. Then, the $M_b(t)$ in Eq. [2.4] becomes:

$$M_b(t) = f_{b,0} \sum_j g_{b,j} \cdot e^{-\frac{t}{T_{2,j}}} \tag{2.5}$$

In Eq. [2.5], g_j follows lognormal distribution, as shown in Eq. [2.6]:

$$g_{b,j} = \frac{1}{\sigma\sqrt{2\pi}} \cdot e^{-\frac{[\ln(T_{2,j})-\mu]^2}{2\sigma^2}} \cdot \Delta \ln(T_{2,j}) \tag{2.6}$$

$$\text{Where } \sum_{j=1}^{\infty} g_{b,j} \to 1 \tag{2.7}$$

It's clear that, in this lognormal distribution model, there are two unknowns, the log mean T_2 of bitumen, μ, and the standard deviation, σ. In order to optimize the

fitting computation, the $\ln(T_{2,j})$ was chosen at μ, $\mu \pm \sigma/2$, $\mu \pm \sigma$, $\mu \pm 3\sigma/2$, $\mu \pm 2\sigma$, $\mu \pm 5\sigma/2$. Then, the T_2 distribution of bitumen could be represented by using eleven points with a lognormal distribution. Thus, in Eq. [2.6]:

$$\Delta \ln(T_{2,j}) = \frac{\sigma}{2} \tag{2.8}$$

Here, we assume that only bitumen and water in the bitumen sample give NMR response. Therefore, the total response of bitumen $f_{b,0}$ is equal to the difference between the initial magnetization M_0 of bitumen sample and the total NMR response of water part. Then, the $f_{b,0}$ in Eq. [2.5] can be expressed as:

$$f_{b,0} = M_0 - \sum_k f_{w,k} \tag{2.9}$$

Finally, the new model, which combines the original multi-exponential model for water part and a lognormal distribution model for bitumen part, can be expressed as below:

$$M(t) = f_{b,0} \sum_j g_{b,j} \cdot e^{-\frac{t}{T_{2,j}}} + \sum_k f_{w,k} \cdot e^{-\frac{t}{T_{2,k}}} \tag{2.10}$$

2.3.4 Interpretation of CPMG Raw Data at 30 °C with New Model

The M_0 obtained from the FID supplemented the CPMG data. The newly developed model as shown by Eq. [2.10] was employed to fit the augmented CPMG data at 30 °C. The Matlab code used for the lognormal distribution fitting is displayed in Appendix A. The supplemented CPMG data is input by a file named "t_and_g.dat" and the data of fitted result is saved in a file named "t_and_h_fitting_result.dat".

The fitting results for the CPMG signal obtained with three different echo spacing are shown in Fig. 2.3.4(a). The zoom-in for the first 10 msec in Fig. 2.3.4(a), which is mainly from the decay of bitumen part, is shown in Fig. 2.3.4(b). From Fig. 2.3.4, we can find that the new model fit the CPMG raw data of bitumen very well.

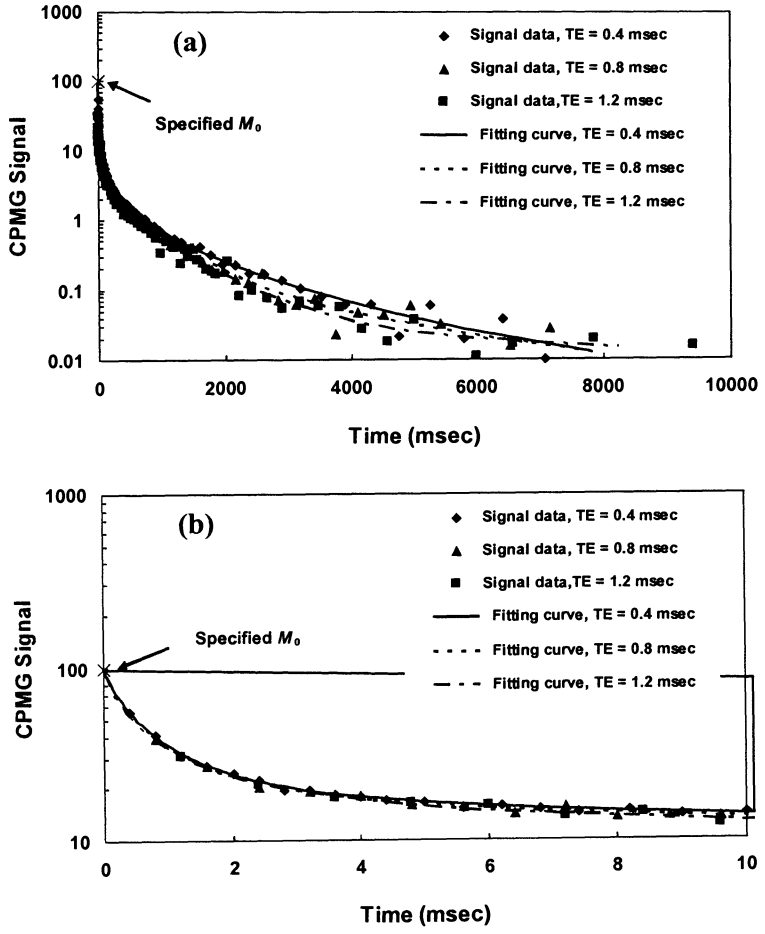

Figure 2.3.4 Fit CPMG data supplemented with M_0 from FID and assume lognormal distribution for bitumen. Here, Fig. 2.3.4(b) is Zoom-in for the CPMG fitting of first 10 msec in Fig. 2.3.4(a).

The interpretations of CPMG data are shown in Fig. 2.3.5. The T_2 distributions of bitumen sample obtained from the standard multi-exponential model without specified M_0 are compared with the results from the new model. As displayed in Fig. 2.3.5, the T_2 of bitumen estimated by specifying M_0 in CPMG data and assuming lognormal distribution for bitumen are 0.58, 0.56 and 0.54 msec for $TE = 0.4$, 0.8 and 1.2 msec, respectively. However, the corresponding T_2 obtained from the regular CPMG interpretation are 0.74, 0.83, 1.33 msec, respectively. Apparently, the T_2 of bitumen obtained by using the new model are remarkably shorter. More importantly, the corrected T_2 of bitumen has little dependence on echo spacing and is close to the T_2 estimated from FID (0.52 msec).

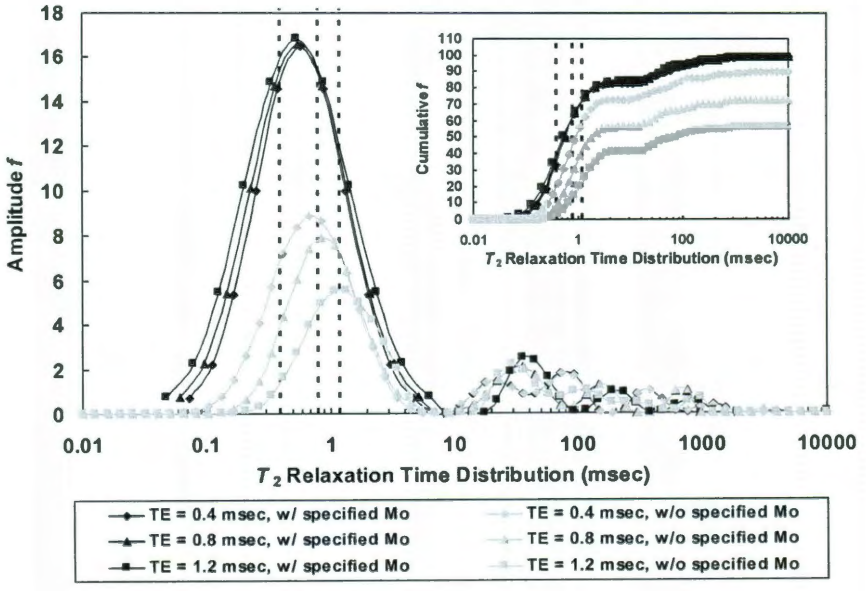

Figure 2.3.5 T_2 distribution of bitumen sample with supplemented M_0 and assuming lognormal distribution for bitumen.

As shown in the cumulative T_2 distribution in Fig. 2.3.5, the area of the bitumen peak is significantly increased by using the new interpretation method. This is due to the compensation for the loss of T_2 information shorter than echo spacing in regular CPMG measurements.

2.3.5 Application at Different Sample Temperature

It is well known that the temperature of the environment for well logging varies with each application. Therefore, after the successful application in 30 °C case, this new method was also applied for the measurements at different sample temperatures. The temperature range in this work is from 8 °C to 90 °C, which is adequate for the Canadian bitumen logging. Some important properties of bitumen at different temperatures were evaluated by using its T_2 obtained from the new method.

2.3.5.1 Calculation Method of *HI* and Saturation at Different Temperatures

The hydrogen index (*HI*) of a fluid is defined as the proton density of the fluid at any given temperature and pressure divided by the proton density of pure water in standard conditions. It can be expressed as below (Dunn, Bergman and Latorraca 2002):

$$HI = \frac{\text{Amount of Hydrogen in Sample}}{\text{Amount of Hydrogen in an equal volume of Pure Water}} \tag{2.11}$$

The hydrogen index should be a quantity independent of measurement methods. In this work, the hydrogen index of bitumen can be expressed as Eq. [2.12].

$$HI_b = \frac{\left(\sum f_{b/b+w}/V_{b/b+w}\right)_{\text{at conditions of interest}}}{\left(T_{\text{standard}}/T_{\text{interest}}\right)\cdot\left(M_{0,w}/V_t\right)_{\text{at standard condition}}} \tag{2.12}$$

Here,

$\sum f_{b/b+w}$, sum of f of bitumen part in the bitumen sample;

$\sum f_{w/b+w}$, sum of f of water part in the bitumen sample;

$M_{0,w}$, initial magnetization of pure water;

$V_{b/b+w}$, volume of bitumen part in the bitumen sample;

$V_{w/b+w}$, volume of water part in the bitumen sample;

V_t, total volume of bitumen sample and volume of pure water standard;

T_{standard}, standard temperature of pure water sample;

T_{interest}, interested temperature of pure water sample;

In this work, the total volume of bitumen sample is equal to the volume of pure water as standard, thus the volumes of water and bitumen in the mixture sample can be estimated by Eq. [2.13] and Eq. [2.14] respectively:

$$V_{w/b+w} = V_t \cdot \frac{\left(\sum f_{w/b+w}\right)_{\text{at conditions of interest}}}{\left(T_{\text{standard}} / T_{\text{interest}}\right) \cdot \left(M_{0,w}\right)_{\text{at standard condition}}} \tag{2.13}$$

$$V_{b/b+w} = V_t - V_{w/b+w} \tag{2.14}$$

Another assumption, which was necessary for the investigation on bitumen sample at different temperature, is that the difference of sample volume within our interested temperature range is negligible. Consequently, Eq. [2.12] becomes,

$$HI_b = \frac{\sum f_{b/b+w}}{1 - \frac{\left(\sum f_{w/b+w} / M_{0,w}\right)_{\text{at conditions of interest}}}{\left(T_{\text{standard}} / T_{\text{interest}}\right) \cdot \left(M_{0,w} / V_t\right)_{\text{at standard condition}}}} \tag{2.15}$$

The equation for calculating water saturation S_w can be derived from Eq. [2.13] and expressed as:

$$S_w = \frac{V_{w/b+w}}{V_t} = \frac{\left(\sum f_{w/b+w}\right)_{\text{at conditions of interest}}}{\left(T_{\text{standard}} / T_{\text{interest}}\right) \cdot \left(M_{0,w}\right)_{\text{at standard condition}}} \tag{2.16}$$

2.3.5.2 Investigation on Bitumen Sample at Different Temperatures

Besides 30 °C, the bitumen sample was also measured at 8, 20, 40, 50, 60, 70, 80, 90 °C, respectively. The same interpretation method as used in 30 °C case was employed. The *HI* and viscosity of bitumen as well as the water saturation in the sample were estimated by using the T_2 of bitumen obtained from the new method.

2.3.5.2.1 M_0 from FID at Different Temperatures

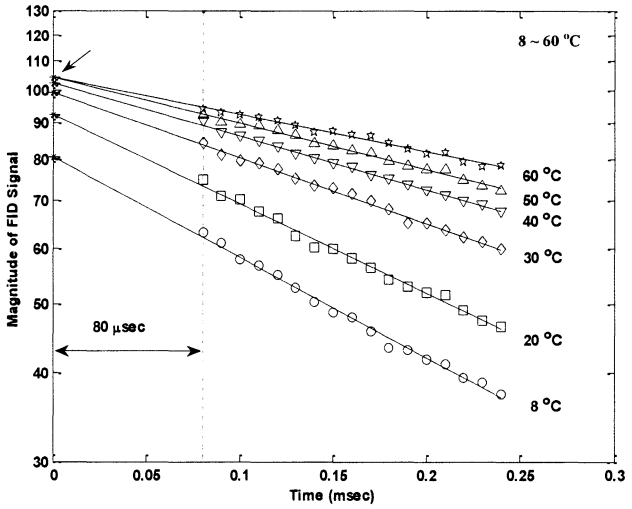

Figure 2.3.6 Extrapolate M_0 of bitumen sample from FID at temperatures: 8 ~ 60 °C

Fig. 2.3.6 displays the initial magnetization of bitumen sample at 8, 20, 30, 40, 50, 60 °C, which were estimated from extrapolation of FID. According to the Curie's Law (Cowan 1997), when temperature increases, the M_0 of sample should decreases correspondingly. However, within the range from 8 to 60 °C, the extrapolated M_0 of bitumen increases as temperature rises, which is opposite to the Curie's Law's prediction. Moreover, when the temperature is over 40 °C, the extrapolated M_0 becomes very close to each other (indicated by the arrow). The flatter attenuation trend of FID signal at higher temperature is indicative of the significant decrease in sample viscosity when the temperature increases.

Fig. 2.3.7 displays the initial magnetization of bitumen sample extrapolated from FID at 60, 70, 80, 90 °C. It's clearly shown that, when temperature is increased over 60 °C, the bitumen M_0 starts decreasing as sample temperature increases. This follows the trend of Curie's Law.

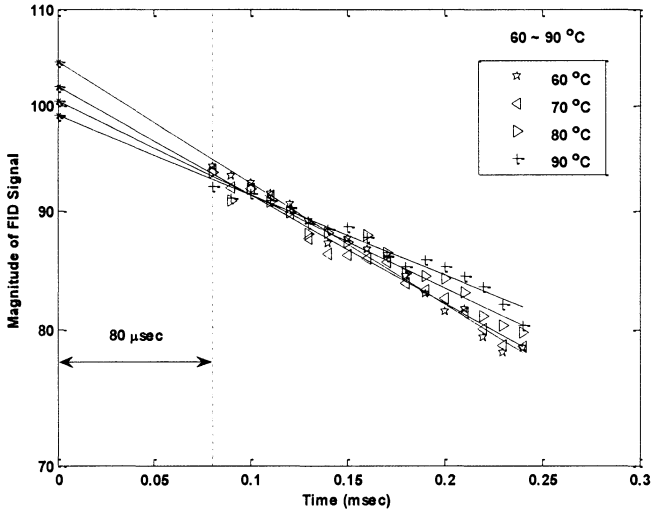

Figure 2.3.7 Extrapolate M_0 of bitumen sample from FID at temperatures: 60 ~ 90 °C

The extrapolated M_0 of bitumen sample at different temperatures shown in Fig. 2.3.6 and Fig. 2.3.7 are also summarized in Fig. 2.3.8. The following is the explanation to the unexpected results of extrapolated M_0 at temperature < 60 °C shown in Fig. 2.3.6 and Fig. 2.3.7.

The NMR spectrometer, MARAN 2 used in this work has a 80 μsec dead time before the first FID signal can be collected (as shown in Fig. 2.3.6 and Fig. 2.3.7). Due to the high viscosity of bitumen, the lost FID signal within the first 80 μsec may attenuate much faster than that within the following part. When the temperature decreases, the viscosity of bitumen increases, resulting in an even faster attenuation of FID signal (indicated by the steeper FID at lower temperature). Then, more FID information of bitumen will be lost within the dead time and possible departure from a straight line has a greater effect upon the extrapolation. Thus, M_0 directly extrapolated from the collected FID data was not accurate for those temperatures < 60 °C.

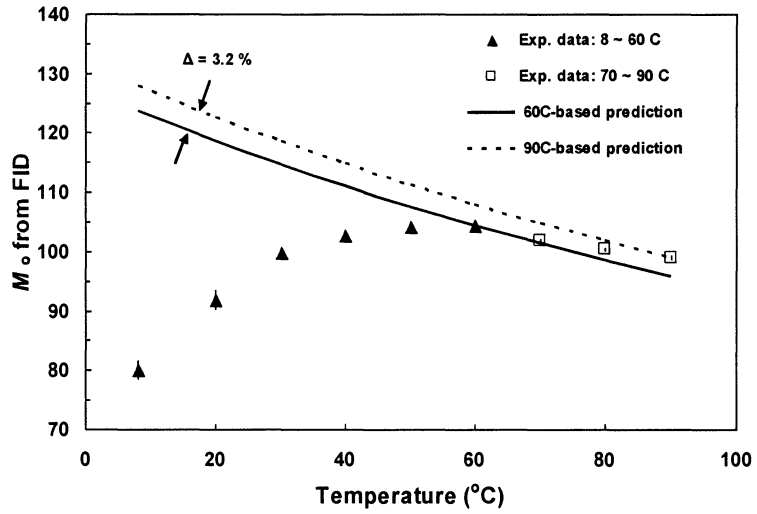

Figure 2.3.8 M_0 of bitumen sample at different temperatures

This proposed explanation was supported by the results from the measurement with 20 MHz Bruker minispec spectrometer, which had a dead time of 50 μsec rather than the 80 μsec of the 2 MHz Maran-II. Fig. 2.3.9 displays the Bruker FID signal measured on the same Athabasca bitumen but smaller sample size at 8 °C and 20 °C. As we expected that, the faster attenuations of bitumen FID signal are observed before 80 μsec especially at the lower temperature (8 °C).

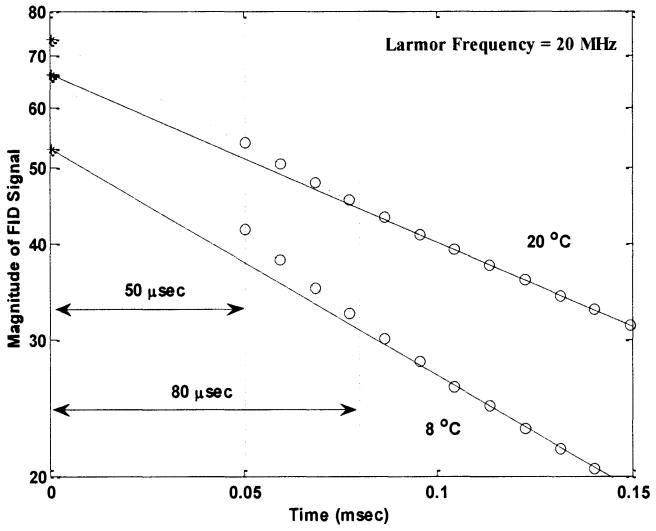

Figure 2.3.9 FID of bitumen sample at 8 °C and 20 °C with the 20 MHz Bruker minispec NMR spectrometer. Here, the 20 MHz Bruker minispec has a dead time of 50 μsec. Dashed lines are extrapolation from data 50 ~ 80 μsec. Solid lines are extrapolation from data ≥ 80 μsec.

The underestimation of the extrapolated M_0 at low temperatures (< 60 °C) can be corrected by the Curie's Law. Given a real M_0 value at certain temperature, the M_0 of the same sample at any other temperatures can be predicted by using Curie's Law. When the temperature of bitumen is over 60 °C, the sample viscosity is low enough that complete

FID information is assumed to be collected and the extrapolated M_0 decreases with increasing temperature as expected. Therefore, the extrapolated M_0 value at temperature $\geq$ 60 °C can be assumed to be the real values and used as the basis for the Curie's Law correction. As shown in Fig. 2.3.8, the difference between the 60 °C-based prediction (solid line) and the 90 °C-based prediction (dashed line) is 3.2 %. In this work, the 60 °C-based prediction of M_0 were employed for all the following calculations.

2.3.5.2.2 Interpretation of CPMG at Different Temperatures

Supplementing the Curie's Law corrected M_0 into the regular CPMG raw data, the experimental data with specified M_0 at each temperature were fitted to the lognormal distribution based model and the fitting results are shown in Fig. 2.3.10. The correspondingly interpreted T_2 distribution of bitumen is shown in Fig. 2.3.11 (a).

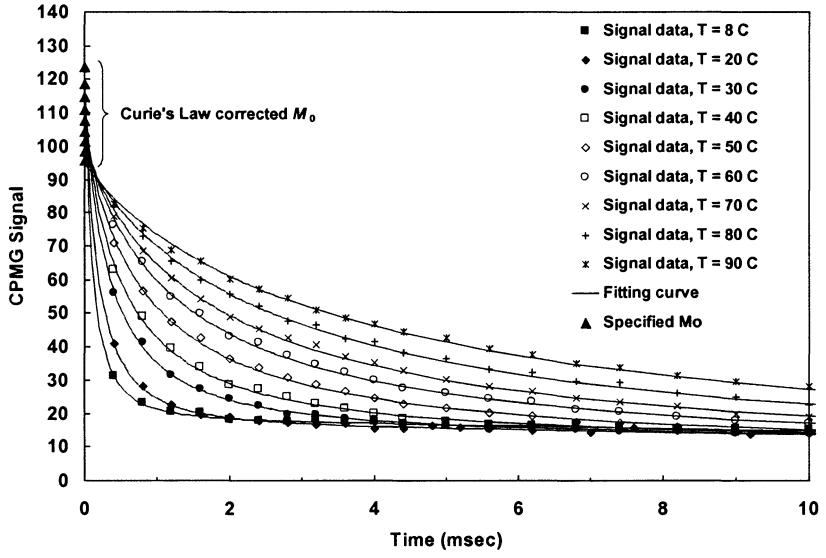

Figure 2.3.10 Fitting supplemented CPMG data by assuming lognormal distribution for bitumen. Here, the specified M_0 is corrected by Curie's Law

Fig. 2.3.11 (b) demonstrates the T_2 distribution of bitumen interpreted by using the apparent M_0. Comparing Fig. 2.3.11 (a) and Fig. 2.3.11 (b), we can find that the T_2 distributions of bitumen obtained by simply using the apparent M_0, which directly extrapolated from FID, have remarkable difference from those obtained by using Curie's Law corrected M_0. Both peak area and peak position vary when different M_0 is employed during the interpretation. Moreover, the lower the temperature, the larger the difference.

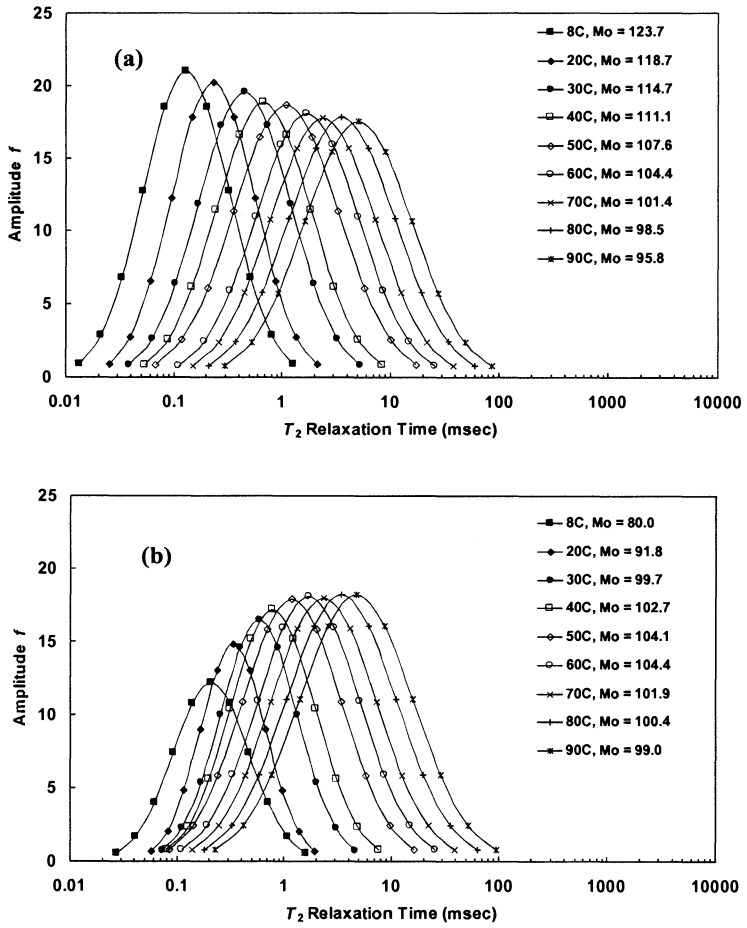

Figure 2.3.11 T_2 distribution of bitumen part obtained by assuming lognormal distribution for bitumen part and specifying M_0. Here, (a) is using Curie's Law corrected M_0; (b) is using apparent M_0 without Curie's Law correction.

As shown in Fig. 2.3.11 that, at sample temperature < 60 °C, the estimated T_2 of bitumen by using the Currie's Law corrected M_0 are uniformly shorter than those estimated with the extrapolated apparent M_0 at each temperature. When the temperature rises over 60 °C, the difference between the two T_2 of bitumen becomes very small.

Furthermore, after using the Curie's Law corrected M_0, the area of bitumen peak at temperature < 60 °C is significantly increased. Also, the NMR responses from bitumen, which is indicated by the bitumen peak area, start following the Curie's Law and decreases with increasing temperature.

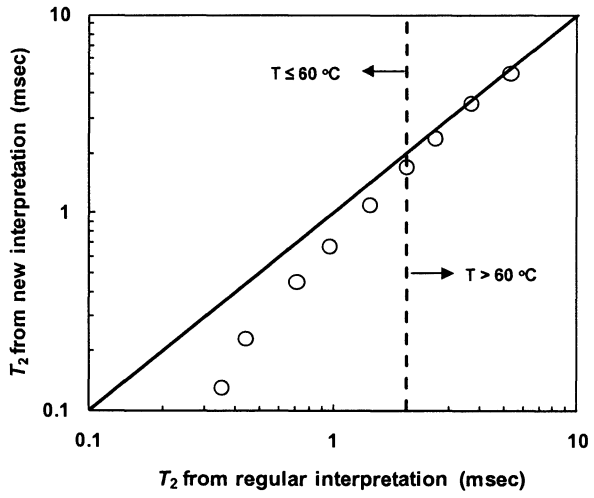

Figure 2.3.12 Comparison of T_2 values obtained from two different methods.

The comparison between the T_2 values obtained from two different methods is displayed in Fig. 2.3.12. It is clearly shown that, the higher the sample temperature, the smaller the difference between the T_2 obtained from the two different methods. When

sample temperature was raised to be above 60 °C, almost no difference was observed for the Athabasca bitumen T_2 values from different methods.

2.3.5.2.3 Estimated Water Saturation in Sample at Different Temperatures

The T_2 distribution of water part in bitumen sample, which was interpreted from the standard multi-exponential model, is assumed to be correct. The local minimum after oil peak is employed as the cut-off between oil peak and water response of bitumen sample. In this manner, the water saturation of bitumen sample at each temperature was estimated by using Eq. [2.16].

As shown by the inset of Fig. 2.3.13, the estimated S_w suddenly decreases when the temperature $\geq$ 60 °C. The solid horizontal line is the average value of S_w at 8 ~ 50 °C and the corresponding percentage standard deviation is 2.5 %.

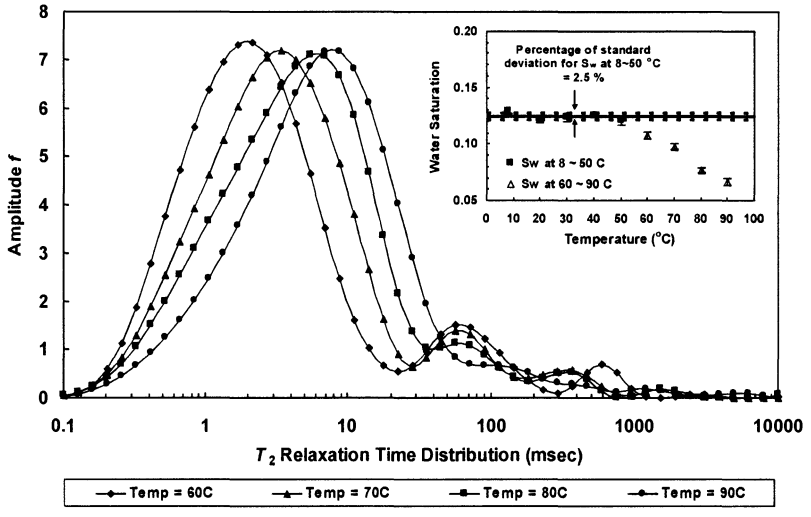

Figure 2.3.13 T_2 distribution of bitumen at temperatures 60, 70, 80, 90 °C, respectively. Here, the CPMG data were interpreted by using the multi-exponential model.

A proposed explanation to the sudden decrease of S_w at temperature $\geq$ 60 °C is that the cut-off we used in this work to distinguish oil peak and water peaks is not proper in those high temperature cases. When the sample temperature is lower than 60 °C, the bitumen peak is clearly separated from the water peaks. We can simply use the local minimum after the bitumen peak as the cut-off. However, when the sample temperature is raised over 60 °C, due to the comparable T_2 of emulsified water and bitumen, the water peaks run into the bitumen peak, as shown in Fig. 2.3.13. Using the local minimum as the cut-off may not be proper under these conditions.

A more sophisticated oil-water cut-off is necessary in the research on bitumen at high temperatures. In this work, the sample tube was well-sealed. We purposely shuffled the experiment sequence to avoid any unexpected temperature-sequence-dependent results. For example, the 20 °C measurement was performed after the 90 °C one. Based on the experimental data of water saturation shown in Fig. 2.3.13, it's reasonable to assume that the real water saturation of bitumen sample does not change within the temperature range of this work.

Therefore, we may be able to use the water saturation data at low temperatures (8 ~ 50 °C) to calibrate the cut-off at high temperatures (60 ~ 90 °C) in the following research. On the other hand, due to the significant difference between the diffusivities of bitumen and water, we may also use Diffusion Editing measurement (Hürlimann, Venkataramanan and Flaum 2002) to evaluate the NMR response of emulsified water in bitumen samples.

2.3.5.2.4 Estimated *HI* of Bitumen at Different Temperatures

The hydrogen index (*HI*) of bitumen at different temperature can be calculated by using Eq. [2.15] and the results are shown in Fig. 2.3.14. It is clear that, when the extrapolated M_0 from FID is not corrected by Curie's Law, the apparent *HI* of bitumen has a temperature-dependence. This is due to the underestimation of apparent M_0 (as shown in Fig. 2.3.6 and Fig. 2.3.8) when sample temperature < 60 °C, and the inaccurate cut-off for calculating the water saturation (as shown in Fig. 2.3.13) at temperature ≥ 60 °C.

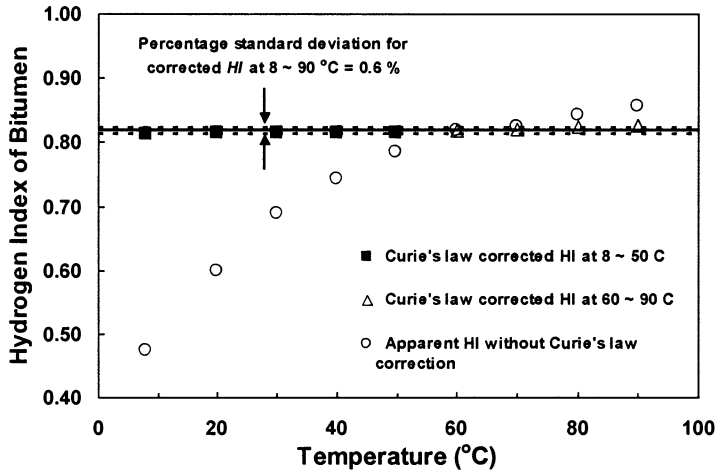

Figure 2.3.14 Hydrogen Index of bitumen at different temperatures

However, after the correction for M_0, the incorrect temperature dependence is eliminated and the bitumen *HI* stays constant at different temperature. The average value is 0.82 and the percentage standard deviation is only 0.6 %.

2.3.5.2.5 Estimated Viscosity of Bitumen at Different Temperatures

A correlation of log-mean T_2 with the ratio of viscosity and temperature, which was derived from alkanes T_1, was developed in previous work of our group (Lo, et al. 2002) and (Hirasaki, Lo and Zhang 2003). As displayed in Fig. 2.3.15, given the corrected T_2, the viscosities of bitumen at different temperatures were estimated by using the alkane correlation.

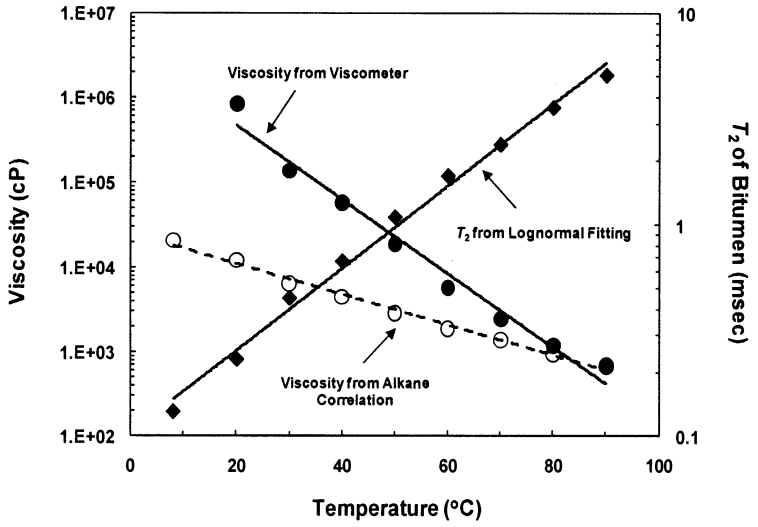

Figure 2.3.15 Comparison of bitumen viscosity from two different methods

It is clearly shown in Fig. 2.3.15 that the viscosity of bitumen estimated from the alkane correlation has significant discrepancy from the experimental value measured by viscometer at low temperatures. As the sample temperature increases, the viscosity of bitumen decreases and the difference between the two viscosity values keeps decreasing. When it reaches 90 °C, the calculated value becomes equal to the experimental value. This means that the alkane correlation, as many other NMR Relaxation Time vs.

Viscosity correlations (Kleinberg and Vinegar 1996), (Morriss, et al. 1997), (Straley, et al. 1997) and (LaTorraca, Stonard, et al. 1999), is only good for the oil with relatively low viscosity, but not suitable for those with extremely high viscosity like bitumen. In order to find out the reason responsible for the discrepancy, we need to start from the theoretical basis on highly viscous oil relaxation.

Dead crude oils relax mainly by intramolecular dipole-dipole interactions (Zhang, PhD Thesis 2002). By normalizing the relaxation time, viscosity and viscosity/temperature ratio with respect to 2 MHz as shown in Eq. [2.17] and Eq. [2.18]:

$$T_{1,2N} = \frac{2}{\omega_0} T_{1,2} \tag{2.17}$$

$$\eta_N = \frac{\omega_0}{2} \eta \tag{2.18}$$

The intramolecular dipole-dipole interaction model for a rigid spherical molecule can be expressed as follows (Hirasaki, Lo and Zhang 2003) and (Zhang, PhD Thesis 2002):

$$\frac{1}{T_{1N}} = \frac{W_2 S}{2} \left(\frac{\eta}{T}\right)_N \left\{ \frac{2/3}{1+\left[S\left(\frac{\eta}{T}\right)_N\right]^2} + \frac{8/3}{1+\left[2S\left(\frac{\eta}{T}\right)_N\right]^2} \right\} \tag{2.19}$$

$$\frac{1}{T_{2N}} = \frac{W_2 S}{2} \left(\frac{\eta}{T}\right)_N \left\{ 1 + \frac{5/3}{1+\left[S\left(\frac{\eta}{T}\right)_N\right]^2} + \frac{2/3}{1+\left[2S\left(\frac{\eta}{T}\right)_N\right]^2} \right\} \tag{2.20}$$

$$S = \frac{8\pi a^3}{3k}. \tag{2.21}$$

The experimental results between normalized T_1 or T_2 relaxation times and normalized viscosity/temperature ratio are shown in Fig. 2.3.16. Also, some literature

data are included on the plot (Vinegar, et al. 1991), (LaTorraca, Dunn, et al. 1998), (MaCann, Vinegar and Hirasaki 1999), and (Zhang, PhD Thesis 2002). The 20 MHz data of bitumen in Fig. 2.3.16 were obtained from the measurements by using a 20 MHz Bruker minispec NMR spectrometer (Acknowledgement to Dr. Gersh Zvi Taicher at Echo Medical Systems for the use of the 20-MHz Bruker minispec NMR spectrometer). The magnet was operating at 40 °C for all experiments and a shorter *TE* (0.184 msec) was employed for the CPMG. The experimental procedure was the same as that used for 2 MHz Maran-II.

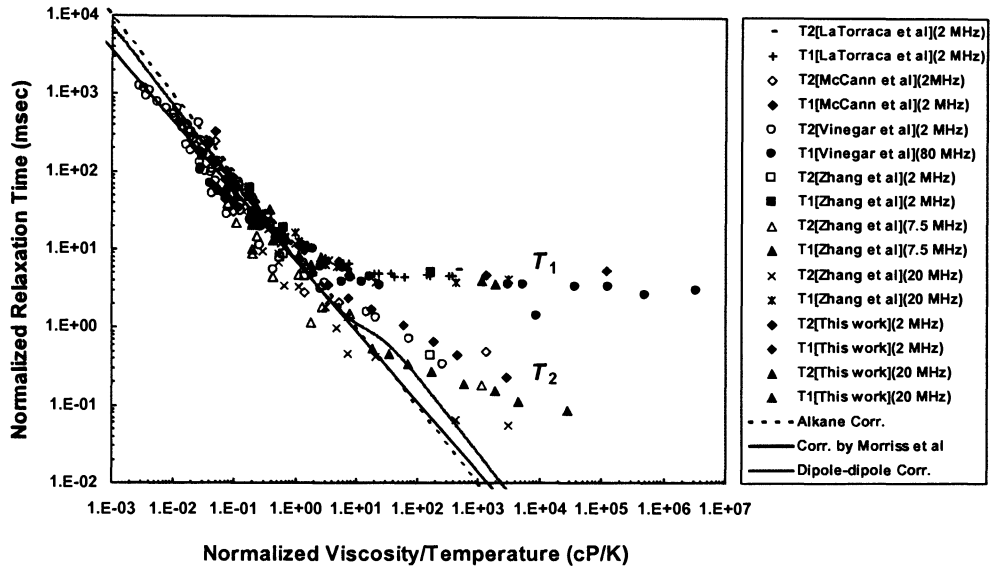

Figure 2.3.16 Relationship between normalized relaxation times and normalized viscosity/temperature ratio for Athabasca bitumen.

As shown in Fig. 2.3.16, the frequency-normalized T_1 data of bitumen from this work fall on the same plateau for different Larmor frequencies and follow the curve shown by other literature data. Zhang (Zhang, PhD Thesis 2002) and Hirasaki et al.

(Hirasaki, Lo and Zhang 2003) reported in their work that, the measured T_1 for viscous samples do not follow the theoretical trend, which predicted by the intramolecular dipole-dipole interaction model. The experimental T_1 levels off at high viscosity and reaches a plateau for normalized viscosity/temperature greater than 1 cP/K.

The experimental T_2 continues to shorten with increasing viscosity. Moreover, T_2 is considerably less than T_1 in all cases for heavy oils. As shown in Fig. 2.3.16, the measured bitumen normalized T_2 at either Larmor frequency in this work follows the trend of previous literature data. The black solid line in Fig. 2.3.16 is from the T_2 correlation by Morriss et al. (Morriss, et al. 1997) and the dashed line is from the Alkane correlation (Hirasaki, Lo and Zhang 2003). Although the viscosity predictions from the two correlations have difference for light oils, they are quite similar at high viscosities. Viscosity prediction is adaptable for relatively low viscosity crude oils. However, highly viscous samples significantly depart from both of two correlations.

The correlation derived from the intramolecular dipole-dipole interactions model (expressed by Eq. [2.20]) was also employed to fit the experimental data. The only variable in Eq. [2.20] is S and its estimated value in this case is 0.082. The fitted results are plotted as the green solid line in Fig. 2.3.16. It is clear that the experimental data of heavy oils also have great departure from the dipole-dipole correlation.

In this manner, further work is undergoing and a new correlation will be developed to better correlate T_2 relaxation time and heavy oil viscosity.

2.4 Conclusions

The echo spacing restriction of regular CPMG measurement on highly viscous bitumen can be overcome by specifying the M_0 in CPMG raw data and assuming lognormal distribution for bitumen during the interpretation.

Apparent M_0 of bitumen from FID at low temperatures (< 60 °C) has incorrect dependence on temperature due to the loss of FID signal within the initial decay period. This incorrect temperature dependence can be corrected by the Curie's Law. Given a correct M_0 value at certain temperature, the M_0 of the same sample at any other temperatures can be predicted by using the equation of Curie's Law.

Given Curie's Law corrected M_0 and proper cut-off between oil and water, the hydrogen index (HI) and water saturation (S_w) of bitumen sample can be evaluated by using the method in this work. The estimated HI of Athabasca bitumen is 0.82.

The T_1 and T_2 of Athabasca bitumen follow the trend of previous literature data. The existing T_2 vs. viscosity correlations, which are good for the oil with relatively low viscosity, are not suitable for the samples with extremely high viscosity like Canadian bitumen.

Chapter 3 NMR Measurement and Viscosity Evaluation of Live Brookfield Oil

3.1 Introduction

The laboratory NMR measurements have shown that the laboratory results of the Canadian bitumen sample appear to be remarkably shorter than the corresponding well log NMR T_2. This is likely due to the dissolved gas in the bitumen. The T_2 distribution depends on oil viscosity and dissolved gas concentration, which may vary throughout the heavy oil field. Thus, a method to determine the gas solubility and the in-situ viscosity from NMR logs would be very useful in heavy oil and bitumen reservoir development.

In this chapter, the viscosity and laboratory NMR measurements on the recombined live Brookfield oil sample as a function of dissolved gas concentrations were performed. The effects of three different gases (CH_4, CO_2, and C_2H_6) on the viscosity of Brookfield oil at a series of saturation pressures were investigated. The correlations among the saturation pressure, gas solubility, NMR T_2 and live oil viscosity are established to resolve the differences between the NMR log and laboratory data. The findings create a way for in-situ viscosity evaluation of heavy oil through NMR well logging.

3.2 Equipment and Experimental Procedures

The 2-MHz nuclear magnetic resonance (NMR) spectrometer used in this part of work was the Maran-M. A 40-mm NMR probe, which has the minimum echo spacing of 0.2 msec was used for the most NMR measurements in this work. The typical applied width of $\pi/2$ pulse was ~8.3 μs and that of π pulse was ~15.5 μs. Another 50-mm NMR probe with a minimum echo spacing of 0.4 msec was used for static gradient measurements. The temperature of magnetic field system is controlled at 30 °C with an error of ± 0.1 °C.

The sweet spot of the 40 mm probe was evaluated by using 5 mL 0.5% CuSO4 solution, resulting in a single height of 0.5 cm. FID measurements were performed when the sample tube was placed at different height and M_0 was estimated correspondingly. The measurement results are shown in Fig. 3.2.1. Setting 5% deviation from the maximum amplitude value as the threshold, the sweet spot of the probe was found to be between 2.8 cm and 6.8 cm away from the bottom of probe, resulting in a length of 4 cm.

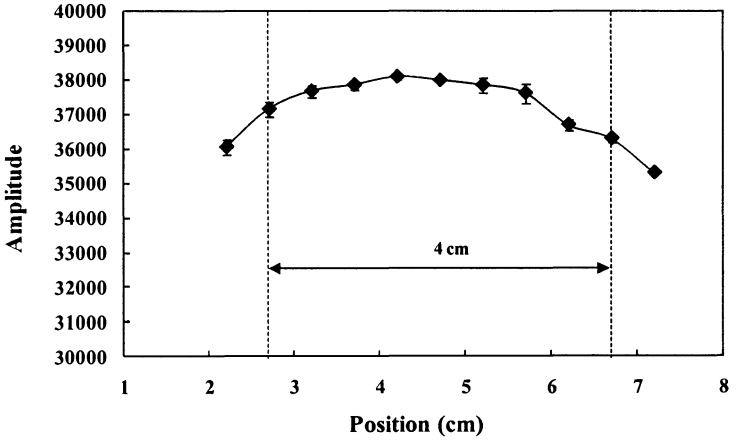

Figure 3.2.1 Evaluating sweet spot of 40 mm probe on Maran-II spectrometer. Here, the X-axis is the height of sample tube from the bottom of 40 mm probe.

A pressure vessel manufactured by TEMCO was used in this work for all high pressure experiments. The main body of this pressure vessel was made with PEAK and was customized to fit the 40 mm probe and the compatible temperature control system. It has O.D. of 35 mm and I.D. of 22 mm. The total volume of its sample chamber is 82 mL.

Given the 4 cm sweet spot of the probe, the maximum oil sample volume would be ~ 15 mL. Consequently, the minimum volume inside the vessel for gas vapor is 67 mL. According to previously reported data (Mehrotra and Svrcek 1985a) and (Mehrotra and Svrcek 1985b) on two other bitumen samples (Peace River bitumen and Wabasca bitumen), the available vapor phase volume inside the vessel is much more than enough for saturating the 15 mL heavy oil sample in this work.

The heavy oil sample used in this work is Brookfield viscosity standard #B360000 (100% PAO oil), which has a viscosity of 361,700 cP at 25 °C. This is even more viscous than the Athabasca bitumen used in our previous work (Yang and Hirasaki 2008).

The three pure gases (CO_2, CH_4 and C_2H_6) used in this work are provided by Matheson Tri-Gas with product grade of Ultra High Purity.

3.3 Results

3.3.1 Characterization of Brookfield Oil at Different Temperatures

The same techniques we mentioned in Chapter 2 were employed to characterize the viscosity and NMR properties of the Brookfield oil at different temperatures.

3.3.1.1 Viscosity of Brookfield oil at Different Temperatures

The viscosity of Brookfield viscosity standard #B360000 at different temperature was measured by using the Brookfield viscometer LVDV-III+. The commercially available viscosity data of this Brookfield oil is provided by Brookfield Company, which is 361,700 cP at 25 °C.

The sample temperature was controlled by an oil bath (HAAKE K35) connected to the viscometer sample holder. The oil sample was measured from 10 °C to 90 °C. The measurement results are shown in Fig. 3.3.1 as below.

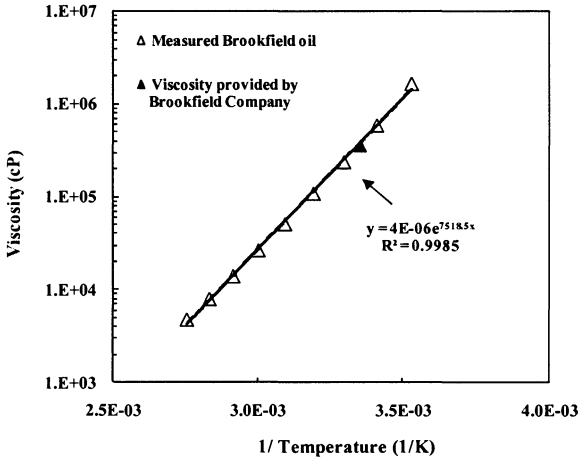

Figure 3.3.1 Viscosity of Brookfield oil at different temperatures

On the semi-logarithmic scale, the Brookfield oil closely follows a linear relationship between the viscosity and the reciprocal of sample temperature. Moreover, the viscosity value provided by the Brookfield Company at 25 °C (solid triangle symbol in Fig. 3.3.1) falls right on the fitting curve that derived from the experimental data. The fitted function is also shown in the plot.

3.3.1.2 NMR Measurement on Brookfield oil at Different Temperatures

The FID and CPMG measurements were performed on the Brookfield oil at different temperature. In this work, the same experimental methods as we used on Athabasca bitumen (Yang and Hirasaki 2008) were applied. In order to ensure that the sample temperature had no significant change during each NMR measurement, large sample volume was necessary to shorten the operation time.

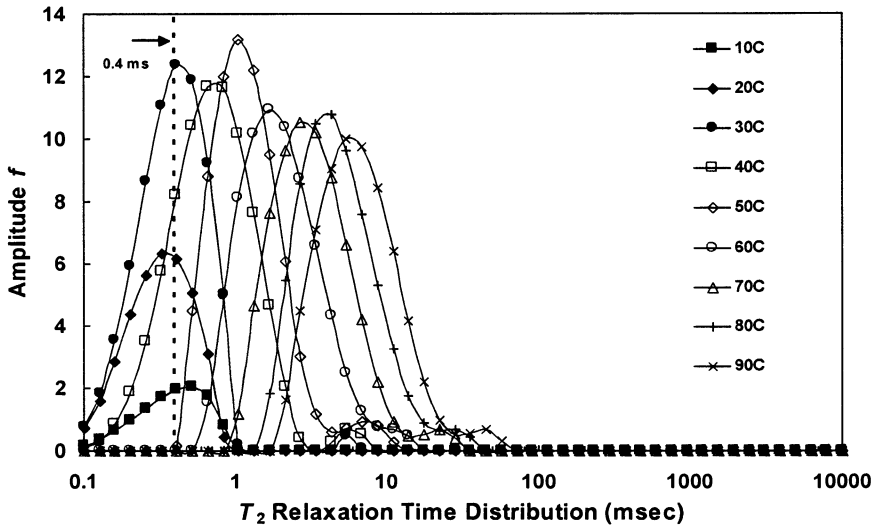

Figure 3.3.2 T_2 distribution of Brookfield oil at different temperatures. Here, the interpretation of CPMG data is without the specified M_0 and lognormal distribution model.

Therefore, the 50 mm probe instead of the 40 mm probe was employed to make the NMR measurements on the Brookfield oil sample at different temperatures. The sample volume is about 60 mL, resulting in ~4 cm in height. The applied echo spacing was 0.4 msec. The temperature of magnetic field was controlled at 30 °C with an error of ±0.1 °C for all measurements. The signal to noise ratio (SNR) was larger than 100. For

the Brookfield oil sample, the applied width of $\pi/2$ pulse was 8.6 μs and that of π pulse was 15.82 μs.

The NMR measurements (CPMG and FID) were performed on the Brookfield oil sample at temperature from 10 °C to 90 °C and were conducted with an interval of 10 °C at a time within the temperature range. At each temperature, the measurement was repeated for three times to ensure the reliability of experimental data.

The T_2 distribution of Brookfield oil at different temperature, which was interpreted from the regular CPMG data without specified M_0 and lognormal distribution model, is shown in Fig. 3.3.2. The 0.4 msec echo spacing is indicated by the vertical dashed line in the plot.

As shown in Fig. 3.3.2, the T_2 distribution of Brookfield oil is not entirely longer than the applied echo spacing until the sample temperature $\geq$ 50 °C. Therefore, for the cases at 10 °C to 40 °C, the M_0 obtained from the FID measurement at each temperature was imposed into the regular CPMG data and the lognormal distribution model (Yang and Hirasaki 2008) was employed to re-interpret the M_0 specified data as shown in Fig. 3.3.3.

Fig. 3.3.3(a) shows the extrapolated M_0 of Brookfield oil from FID at different temperatures. It is clear that, the extrapolated values closely follow the Curie's law (calculation based on M_0 from FID at 50 °C) within the entire temperature range. This is different from the results observed in the work on Athabasca bitumen (Chapter 2). This may be due to the much simpler composition of this synthetic oil sample. The Brookfield oil is a commercially available viscosity standard from Brookfield Company, which is made by 100% PAO, is much more pure than the crude Athabasca bitumen. Therefore, it

does not have many extremely fast relaxing components, which will result in significant FID information loss within dead time at low temperatures (Yang and Hirasaki 2008).

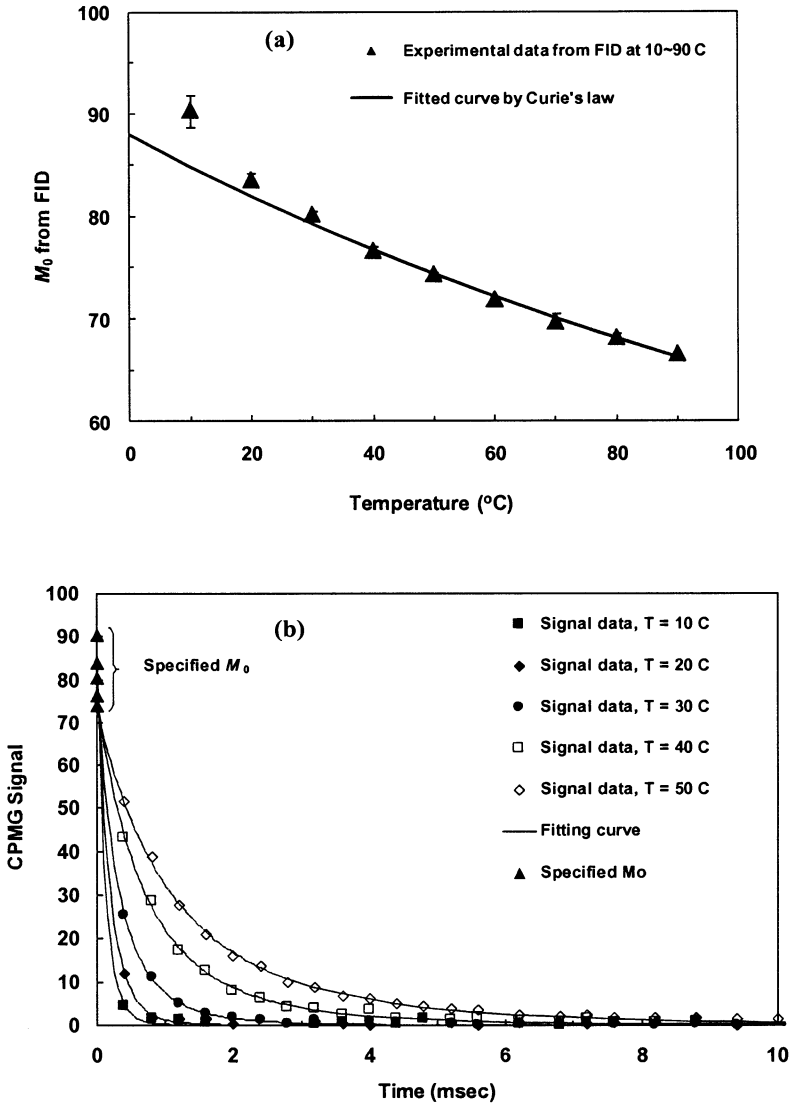

Figure 3.3.3 Interpretation of M_0 specified CPMG data of Brookfield oil by using lognormal distribution model. Here, (a) M_0 extrapolated from FID at different temperature; (b) fitting the supplemented CPMG data via lognormal distribution model

The fitted curve by Curie's law in Fig. 3.3.3(a) is calculated on the basis of the M_0 value obtained from FID at 50 °C. The FID measurement was repeated for at least three times at each temperature. The reason for the relatively large deviation of M_0 at 10 °C is unknown.

In order to verify that the regular method without specified M_0 and lognormal distribution model is able to correctly interpret the CPMG data of Brookfield oil at temperature ≥ 50 °C, the new interpretation was also applied to the 50 °C. It is clear that the lognormal distribution model fits these M_0 specified CPMG data very well. The T_2 distributions of Brookfield oil from the new interpretation at temperature of 10 °C to 50 °C are displayed in Fig. 3.3.4.

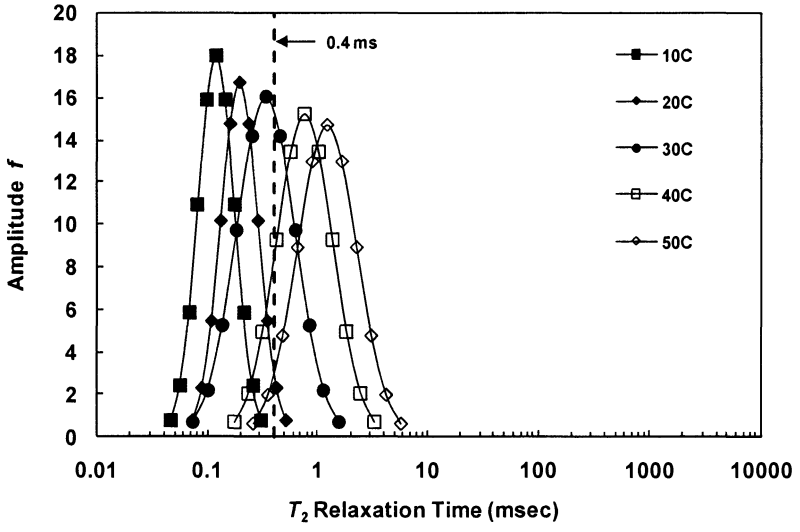

Figure 3.3.4 T_2 distribution of Brookfield oil from new interpretation. Here, the CPMG data was imposed with the specified M_0 from FID and the lognormal distribution model was applied.

Comparing Fig. 3.3.2 and Fig. 3.3.4, the logarithmic mean T_2 of Brookfield oil from two different interpretation methods at temperature of 10 °C to 50 °C is summarized in Table 3.3.1. It's clear that, when sample temperature < 50 °C, the T_2 of Brookfield oil from regular interpretation is significant larger than that from lognormal distribution model with specified M_0. The difference between the T_2 from two different interpretation methods decreases as temperature increases. This is similar to the observance in the investigation on Athabasca bitumen in Chapter 2.

Table 3.3.1 T_2 of Brookfield oil obtained from two different interpretations

Sample Temperature °C	T_2 from regular interpretation msec	T_2 from new interpretation msec
10	0.43	0.12
20	0.38	0.19
30	0.48	0.34
40	0.83	0.77
50	1.24	1.24

As the sample temperature reaches 50 °C, the T_2 value obtained from the lognormal distribution model is the same to that from the regular CPMG interpretation. This further verifies that regular method without specified M_0 and lognormal distribution model is able to correctly interpret the CPMG data of Brookfield oil at temperature ≥ 50 °C.

3.3.1.3 Relationship between Viscosity and T_2 for Dead Oil

The relationship between viscosity and T_2 is found to be linear on the log-log scale for both Brookfield oil and Athabasca bitumen, as shown in Fig. 3.3.5. This is similar to the observations on many other heavy oil samples reported previously (Dunn, Bergman and Latorraca 2002). However, from the fitted functions displayed in the plot for each correlation, the data trends of these two extremely viscous oils obviously don't follow those previously developed correlations, which were based on relatively lighter oils (Morriss, et al. 1997), (Zhang, et al. 1998), (Lo, et al. 2002). Here, in Fig. 3.3.5, the T_2 values for either Brookfield oil or Athabasca bitumen were from the new interpretation method (Yang and Hirasaki 2008) if regular CPMG interpretation was not able to obtain the T_2 value correctly at a certain temperature.

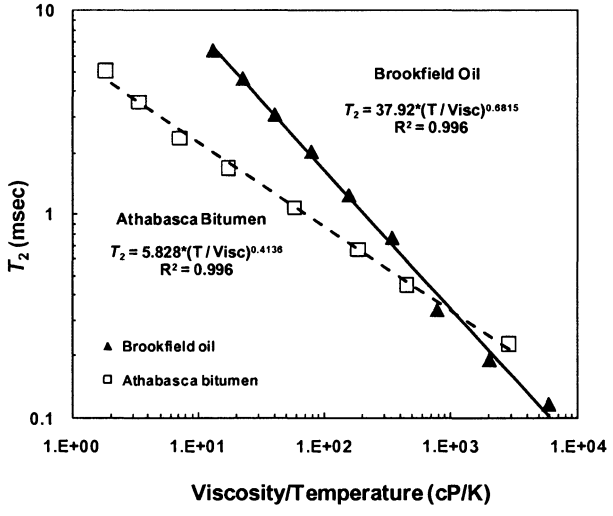

Figure 3.3.5 Relationship between T_2 and viscosity/temperature ratio for both Brookfield oil and Athabasca bitumen.

3.3.2 Investigations on Recombined Live Brookfield Oil

The investigations on the recombined live Brookfield oil were performed with three different reservoir gases, CO_2, CH_4, and C_2H_6. In each case, the measurements were conducted at different pressure levels.

During the experiments with each gas, the procedure was dived into two stages generally, the pressurization stage and the depressurization stage. First, the highly pressurized gas was introduced into the closed pressure vessel with certain amount of oil at bottom. After the gas-oil system reached equilibrium at the highest pressure level, the system pressure would be depressurized to several lower levels, step by step. At each lower pressure, the equilibrium was achieved as well.

During the entire process, NMR measurements were performed periodically to track the T_2 change. Proper number of scans (NS) was chosen to make the signal to noise ratio (SNR) equal to 100. Each measurement was repeated 6 times to ensure the reliability of experimental data. The system pressure inside the vessel was monitored by using a Senso-Metrics pressure transducer (Model 602008, Max. 5,000 psig).

3.3.2.1 Method for Calculating Gas Solubility at Different Pressures

The solubility of each gas in Brookfield oil needs to be calculated at different pressure levels in this work. The method for calculating the gas solubility from pressure data is described as follows:

(I) Pressurization Stage:

After the pressurization, the pressure inside the close system decreases first due to temperature change inside the vessel and then due to the dissolving of gas into the oil. In this stage, the starting pressure P_0 can be corrected by extrapolation in order to remove the influence of temperature change on the pressure reading. This will be discussed in details in the later sections. The equilibrium pressure P_{eq} is determined by the pressure reading when the system is considered to be equilibrated.

According to mass balance, the gas amount removed from the vapor phase equals to the gas amount transferred into the oil phase. In this manner, the gas solubility s_g in the oil can be calculated by the following equation:

$$s_g = \left(\frac{P_0 \cdot V_g}{z_0 \cdot R \cdot T} - \frac{P_{eq} \cdot V_g}{z_{eq} \cdot R \cdot T} \right) \Big/ V_{oil} \tag{3.1}$$

Here, V_g is the volume of vapor phase inside the pressure vessel. V_{oil} is the volume of oil sample inside the pressure vessel. Assuming the swelling effect of oil in this work is negligible, both V_g and V_{oil} are constant. P_0 and P_{eq} are the pressures at beginning and at equilibrium during the pressurization stage, respectively. z_0 and z_{eq} are the values of compressibility for each gas at beginning and at equilibrium during the pressurization stage, respectively.

(II) Depressurization Stage:

After each depressurization, the pressure inside the close system increases due to the release of dissolved gas from inside the oil into the gas vapor. In this stage, the starting pressure P_0 can be corrected by extrapolation in order to remove the influence of temperature change on the pressure reading. This will be discussed in details in the later

sections. The equilibrium pressure P_{eq} is determined by the pressure reading when the system is considered to be equilibrated.

According to mass balance, the gas amount transferred into the vapor phase after each depressurization equals to the gas amount removed from the oil phase. In this manner, the gas solubility s_g in the oil can be calculated by the following equation:

$$s_{g,i} = s_{g,i-1} - \left(\frac{P_{eq} \cdot V_g}{z_{eq} \cdot R \cdot T} - \frac{P_0 \cdot V_g}{z_0 \cdot R \cdot T} \right) \Big/ V_{oil} \tag{3.2}$$

Here, $s_{g,i}$ is the solubility at current pressure level. $s_{g,i-1}$ is the solubility at previous pressure level right before the depressurization. V_g is the volume of vapor phase inside the pressure vessel. V_{oil} is the volume of oil sample inside the pressure vessel. Assuming the swelling effect of oil in this work is negligible, both V_g and V_{oil} are constant. P_0 and P_{eq} are the pressure values at beginning and at equilibrium during the depressurization stage, respectively. z_0 and z_{eq} are the values of compressibility for each gas at beginning and at equilibrium during the depressurization stage, respectively.

3.3.2.2 Recombined Live Brookfield Oil with CO_2

The investigation on the recombined live Brookfield oil was first performed on the CO_2-Brookfield oil system. In this case, the gas pressure inside the vessel was initially raised to ~892 psia by injecting CO_2 from the top of the pressure vessel. Then, the gas source was cut off and no more gas was added into the system afterwards. The oil sample volume is ~ 16 mL.

The pressure vessel was vertically placed in the 30 °C air bath after the gas injection. In this manner, gas transferred into the oil due only to diffusion and natural convection (Haugen and Firoozabadi 2009), (Nasrabadi, Firoozabadi and Ahmed 2009). The T_2 distribution of CO_2 dissolved Brookfield oil was measured as a function of time. As displayed in Fig. 3.3.6, the oil T_2 peak markedly moves to larger values with time. It indicates that, the solution of CO_2 into the heavy oil simply via diffusion and natural convection was significant.

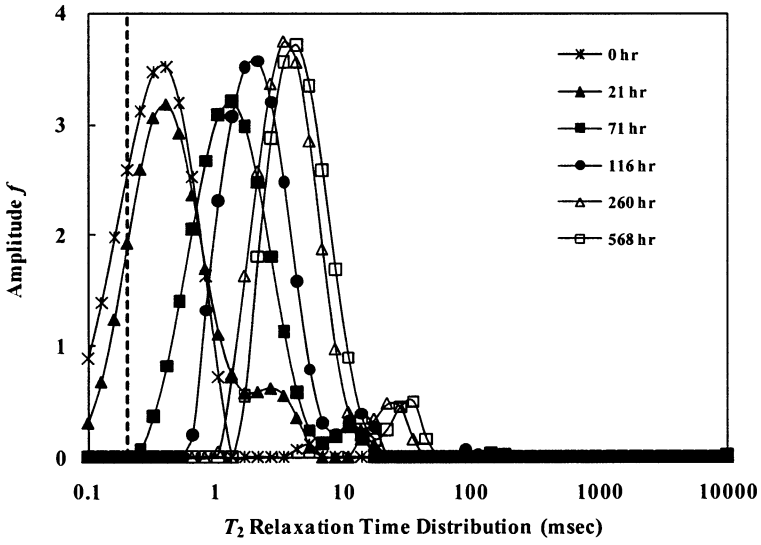

Figure 3.3.6 T_2 distribution of Brookfield oil with CO_2 as a function of time. Here, the sample temperature is 30 °C.

The recorded system pressure as well as the change of T_2 during the pressurization stage was displayed in Fig. 3.3.7. As CO_2 gradually dissolved into the oil, the pressure in the vapor phase kept decreasing. While, the oil T_2 with the dissolved CO_2

continuously increased. As shown in Fig. 3.3.7, after ~400 hours, the trends for both pressure and T_2 starts leveling out.

Theoretically, the ultimate pressure at equilibrium can be measured when the Brookfield oil is completely saturated with the CO_2. However, in practice, such a diffusion process may take an unreasonably long time to really reach the equilibrated state. Therefore, alternatively, we assumed the CO_2-Brookfield oil system reached quasi-equilibrium after 568 hours and then, moved to the next stage, depressurization.

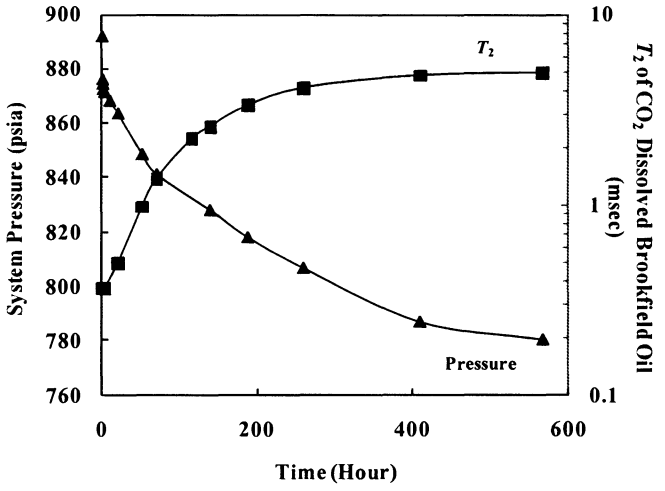

Figure 3.3.7 Pressure decay and T_2 change of CO_2-Brookfield oil system during pressurization stage.

The recorded pressure at 568 hours was 780.4 psia, while the T_2 of Brookfield oil saturated with CO_2 was 4.91 msec. Afterwards, the depressurization was conducted by decreasing the pressure by ~ 200 psi at a time till the pressure inside the vessel reached around 100 psia. The pressure vessel was kept vertical inside the 30 °C air bath during the

entire depressurization process. The changes of pressure and live oil T_2 were monitored in the similar way as we did during the pressurization

The NMR measurements and pressure recording lasted for at least extra two days after the CO_2 saturated oil first reached its equilibrated value at each pressure level. In this manner, the reliability of measured values for both T_2 and pressure at equilibrium can be ensured.

The change of T_2 and gas pressure for the CO_2 saturated Brookfield oil as a function of time at four different lower pressure levels are displayed in Fig. 3.3.8. The values of pressure and live oil T_2 at equilibrium are shown in each subplot, respectively. The time for the CO_2 saturated oil first reached its equilibrated value at each pressure level was indicated by the vertical dashed lines.

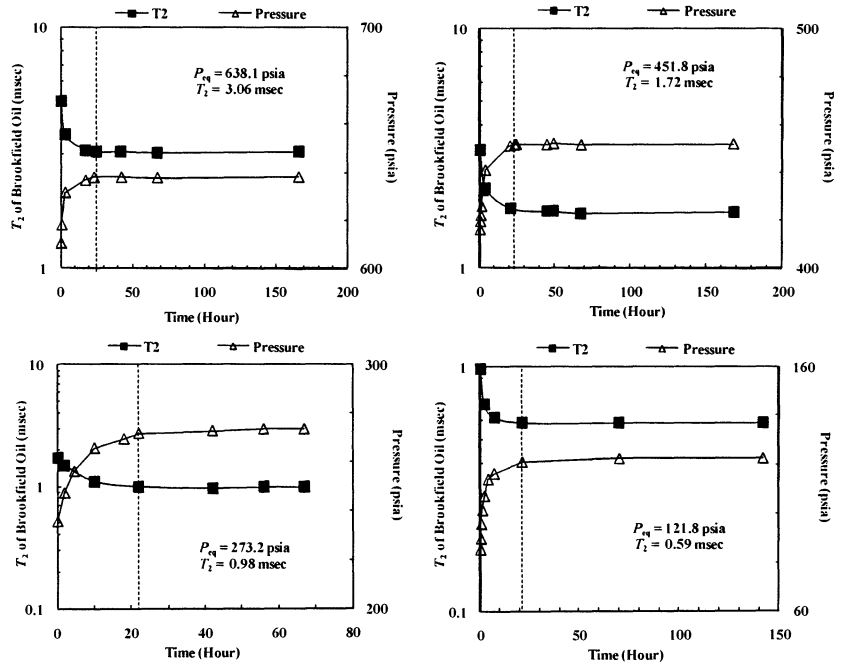

Figure 3.3.8 Change of T_2 and pressure for CO_2 saturated Brookfield oil as a function of time at different pressures during depressurization stage.

The change of T_2 distribution for the CO_2 saturated oil at different pressure from regular CPMG measurement is shown in Fig. 3.3.9. As the CO_2 depressurized from the ~780 psia to ~122 psia, the oil T_2 peak significantly shifted from the larger values to the smaller values. Moreover, even when the gas pressure is only ~122 psia, the T_2 of live oil is still markedly different from the oil without CO_2.

Given the pressure change, volume and temperature, the solubility of CO_2 in Brookfield oil at each pressure level can be calculated via the equation of state with the compressibility factor z for CO_2 (IUPAC 1973). The compressibility factor z of CO_2 at 30 ^{o}C is shown in Appendix B.

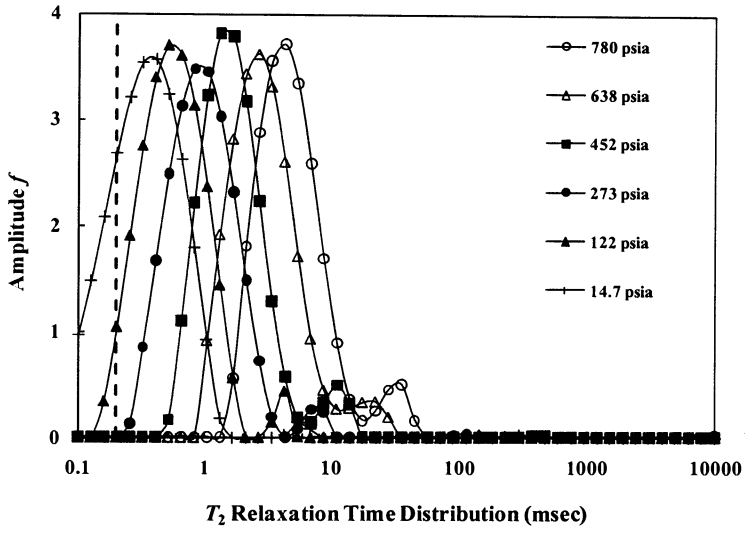

Figure 3.3.9 T_2 distribution of CO_2-Brookfield oil system at different pressure.

However, the big pressure change inside the pressure vessel within a relatively short time inevitable occurred at the beginning of each pressurization or depressurization. Consequently, the system would be either heated by the pressurization or cooled by the

depressurization temporarily, and then come back to the temperature of air bath (30 °C). In this manner, significant pressure fluctuation would be caused by the temperature change and display "unreal" P_0 for the solubility calculations. Therefore, the removal of the temperature influence on pressure reading at the start of each pressure level is necessary. In this work, extrapolation was employed to make the correction.

Fig. 3.3.10 shows the analysis and extrapolation of recorded pressure data for the pressurization stage of CO_2-Brookfield oil. The recorded data within the initial period, which were considered to be significantly influenced by temperature change, are shown by open triangles. The pressure data after this initial period are displayed by open rectangles and used for extrapolation.

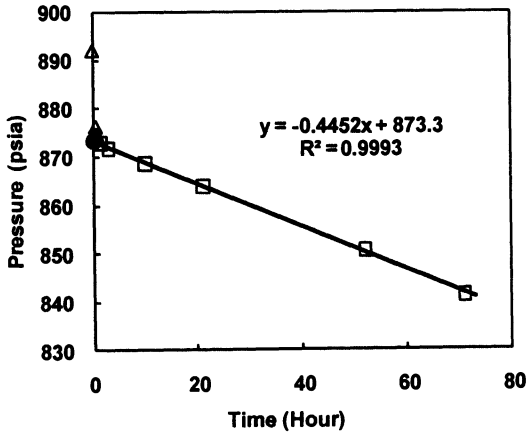

Figure 3.3.10 Extrapolation for the pressurization stage of CO_2-Brookfield oil.

The fitted function for extrapolation is displayed in Fig. 3.3.10. The estimated starting pressure P_0 from extrapolation (indicated by red solid dot) is 873.3 psia, which is

19 psi lower than the recorded pressure data right after the introduction of high pressure CO_2 (892.3 psia).

The similar analysis and extrapolation were also performed on the pressure data recorded in the stage of depressurization and shown in Fig. 3.3.11. The extrapolation is shown by solid line and the extrapolated value at each pressure level is highlighted by red solid dot in each subplot. The points excluded from extrapolation are indicated by arrows in each plot. The fitted functions and the R^2 values are also displayed.

It is clearly shown that, with the additional effect of temperature rise-up after each rapid depressurization, the pressure within the initial period (open triangles) increases significantly faster than those thereafter (open rectangles).

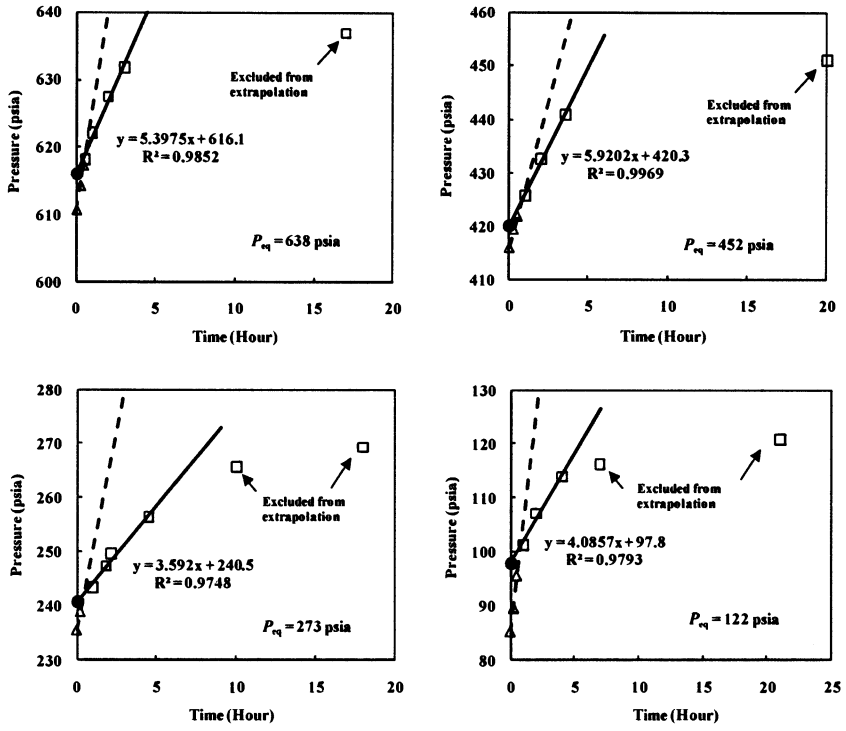

Figure 3.3.11 Extrapolations for the depressurization stage of CO_2-oil at different pressures

The solubility of CO_2 in Brookfield oil at each pressure level was calculated by using the corrected pressure data as shown in Fig. 3.3.10 and Fig. 3.3.11. The calculation methods for solubility, which is based on the mass balance, are shown in section 3.3.2.1.

The relationship between CO_2 solubility, which was calculated with either the corrected pressure data or the original recorded data, and its corresponding T_2 is plotted in Fig. 3.3.12. Here, the solubility of CO_2 in Brookfield oil is expressed in the unit of mole gas/ mL oil.

As displayed in Fig. 3.3.12, the calculated solubility of CO_2 in Brookfield oil by using the corrected pressure data is significantly smaller than that calculated from the originally recorded data at each pressure level. Apparently, the data trend calculated by using the corrected pressure values extrapolates closer to the dead oil T_2. The trend of solubility calculated from the originally recorded pressure is significantly more deviated.

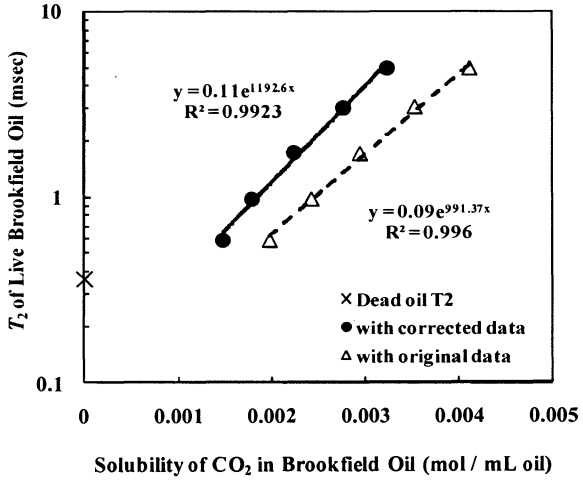

Figure 3.3.12 Relationship between the solubility of CO_2 in Brookfield oil and its corresponding T_2

3.3.2.3 Recombined Live Brookfield Oil with CH_4

In the case of CH_4-Brookfield oil, the gas pressure inside the vessel was initially raised to ~896 psia by injecting CH_4 from the top of the pressure vessel. Then, the gas source was cut off and no more gas was added into the system afterwards. The oil sample volume was ~ 15 mL.

The pressure vessel was vertically placed in the 30 °C air bath after the introduction of pressurized CH_4. In this manner, only diffusion occurred between the gas and oil. The T_2 distribution of Brookfield oil with CH_4 was measured as a function of time and the results are displayed in Fig. 3.3.13.

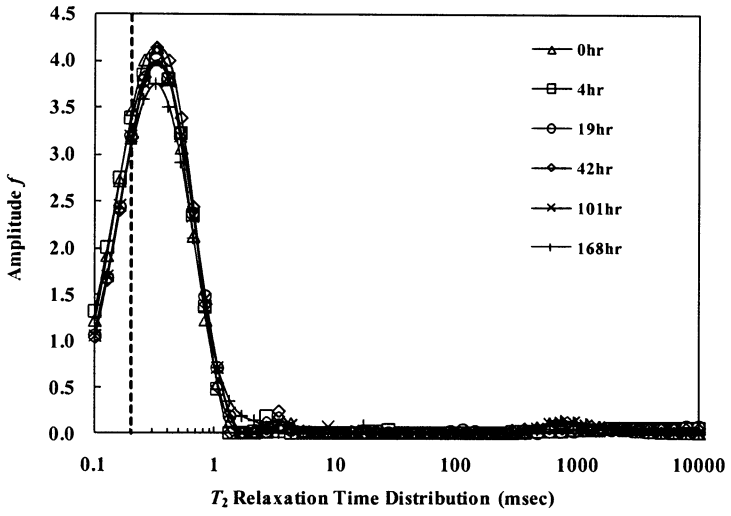

Figure 3.3.13 T_2 distribution of Brookfield oil with CH_4 as a function of time in diffusion. Here, the sample temperature is 30 °C.

As shown in Fig. 3.3.13, the position of live Brookfield oil peak does not significantly change during the entire measurement for 168 hours. The extremely slow dissolving of CH_4 is due to the small diffusivity of CH_4 into heavy oil (Zhang, Hyndman

and Maini 2000), (Upreti and Mehrotra 2002), (Tharanivasan, Yang and Gu 2006). In this manner, if only diffusion occurs between the oil and gas, the saturating of Brookfield oil with CH_4 would last for an unreasonable long time.

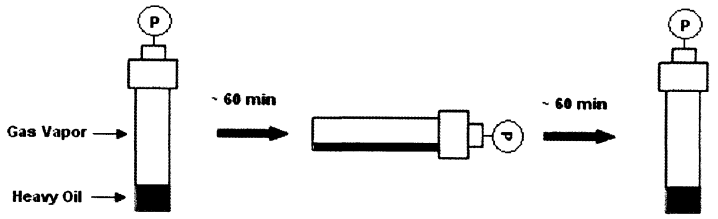

Figure 3.3.14 Demonstration of generating convection

Therefore, the generation of convection on the CH_4-oil system was in great necessity to boost the saturation process. In order to generate convection, the pressure vessel was placed on a support stand at room temperature and repeatedly turned from vertical to horizontal and then back to vertical, as shown in Fig. 3.3.14. The interval between each action (from vertical to horizontal, or from horizontal to vertical) was about 60 min.

The vessel was put back into the Maran every night and vertically placed in the 30 ^{o}C air bath for overnight. The system pressure and the T_2 of CH_4 dissolved oil were measured the next morning.

However, the generation of convection was not started immediately after the initial gas injection. Because, as stated in the previous section, the cool-down effect of the system temperature caused the pressure to decrease much more rapidly and significantly during the initial period after the introduction of pressurized gas. In order to

remove the temperature influence on pressure reading and find out the real starting pressure, the vessel was placed inside the 30 °C air bath first until the system temperature stabilized.

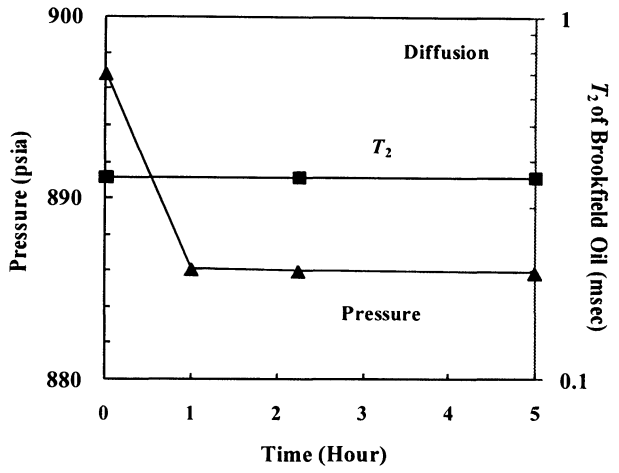

Figure 3.3.15 Measured pressure decay and T_2 of CH_4-Brookfield oil system during initial diffusion period

During this initial period, only diffusion occurred on the CH_4-Brookfield oil system. The change of pressure inside vessel and oil T_2 were recorded and displayed in Fig. 3.3.15. It's clear that recorded pressure reached plateau after the first hour, while the oil T_2 had no change during the first 5 hours.

The result from previous work has shown that, there is no significant dissolving of CH_4 via diffusion even after 168 hours. In this manner, the dissolving of CH_4 into oil during the first 5 hours can be neglected and the pressure reading right after the first 5 hours was considered as real starting pressure.

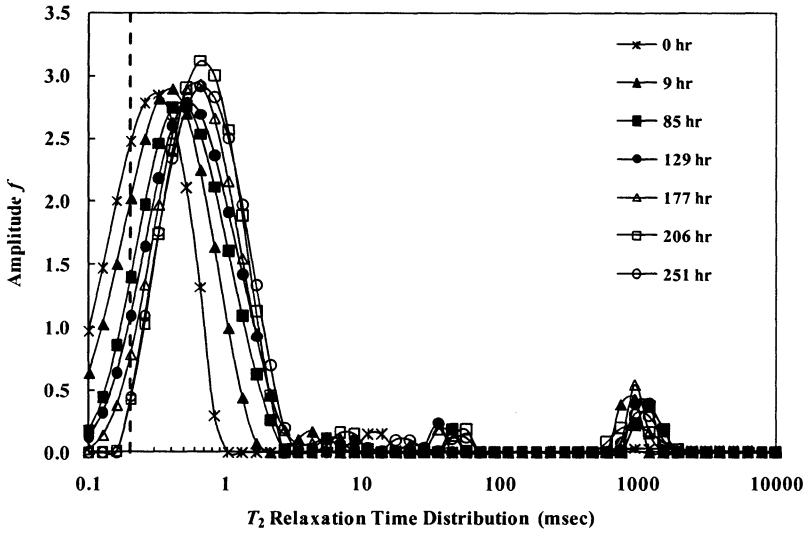

Figure 3.3.16 T_2 distribution of Brookfield oil with CH_4 as a function of time in convection. Here, the sample temperature is 30 °C.

The generation of convection on the CH_4-Brookfield oil (as shown in Fig. 3.3.14) started right after the first 5 hours. The T_2 distribution of CH_4 dissolved Brookfield oil was measured as a function of time in the period of convection and displayed in Fig. 3.3.16.

Different from the observance in Fig. 3.3.13, with the assist of convection, the position of oil T_2 peak shifts to the larger values. In Fig. 3.3.16, the T_2 distribution has a small peak at around 1 sec. This is believed to be from the response of high pressure CH_4 vapor inside the pressure vessel. The T_2 of pressurized CH_4 was found to be around 1 sec at ~1000 psia level (Private conversation with Dr. Arjun Kurup).

The recorded pressure and the measured oil T_2 during the convection period are summarized in Fig. 3.3.17. About 206 hours after the generation of convection, both the pressure and the T_2 of CH_4 dissolved oil reached plateau. The experiment continued for

extra two days and no significant changes for either pressure or T_2 was observed. Therefore, the system was considered to be equilibrated at that point. During the 206 hours, the generated convection made the pressure decrease by about 34 psi, from 886 psia to 852 psia. Correspondingly, the solution of CH_4 increased the oil T_2 from 0.36 msec to 0.69 msec.

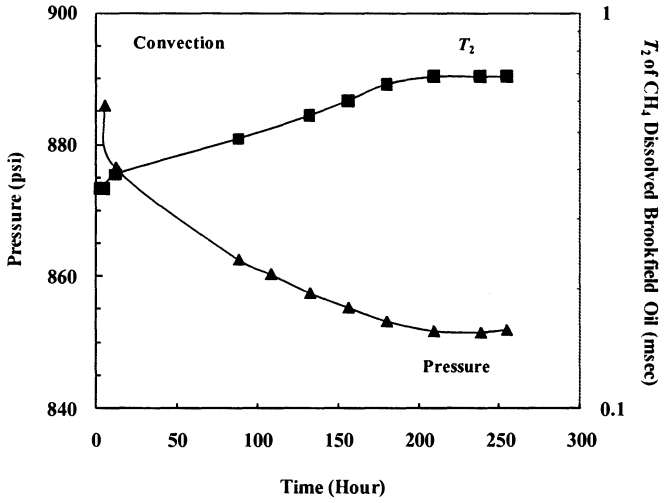

Figure 3.3.17 Pressure decay and T_2 change of CH_4-Brookfield oil system during pressurization stage.

Comparing with the observances in the case of CO_2-Brookfield oil, the solution of CH_4 produced much less increase in T_2 than CO_2 did. The T_2 rose from 0.36 msec to 0.69 msec at ~852 psia in the case of CH_4-oil, while the equilibrated T_2 was 4.91 msec at ~780 psia for CO_2-oil.

Therefore, in order to make enough difference in the measurement, we depressurized directly from ~852 psia to ~100 psia level in the CH_4 case. The same

experimental procedures as done in the CO_2 case were performed. The pressure change was recorded and the T_2 measurement was performed periodically.

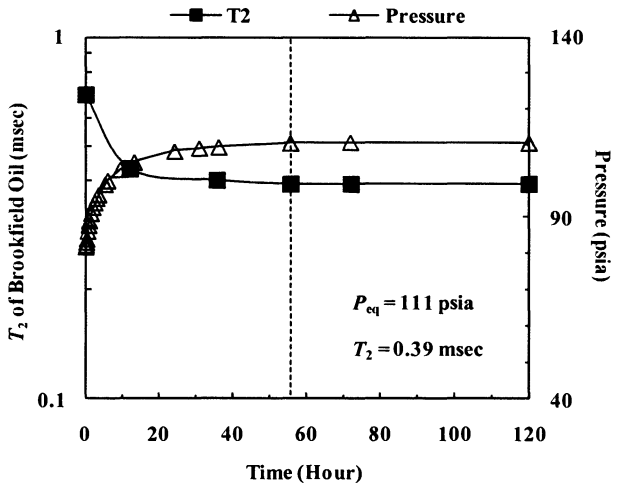

Figure 3.3.18 Change of T_2 and pressure for CH_4 saturated Brookfield oil as a function of time during depressurization stage.

The change of T_2 and the recorded pressure for the CH_4 saturated Brookfield oil at ~111 psia was displayed in Fig. 3.3.18. The equilibrated values for both pressure and live oil T_2 are also in the plot. The vertical dashed line indicates the time for the CH_4 saturated oil firstly reached its equilibrium.

The shift of live oil T_2 distribution at three different pressure levels is displayed in Fig. 3.3.19. As the CH_4 depressurized from the ~852 psia to ~111 psia, the T_2 peak significantly shifted to shorter values. However, the T_2 of CH_4 saturated Brookfield oil at ~111 psia still has remarkable difference from the T_2 of dead oil.

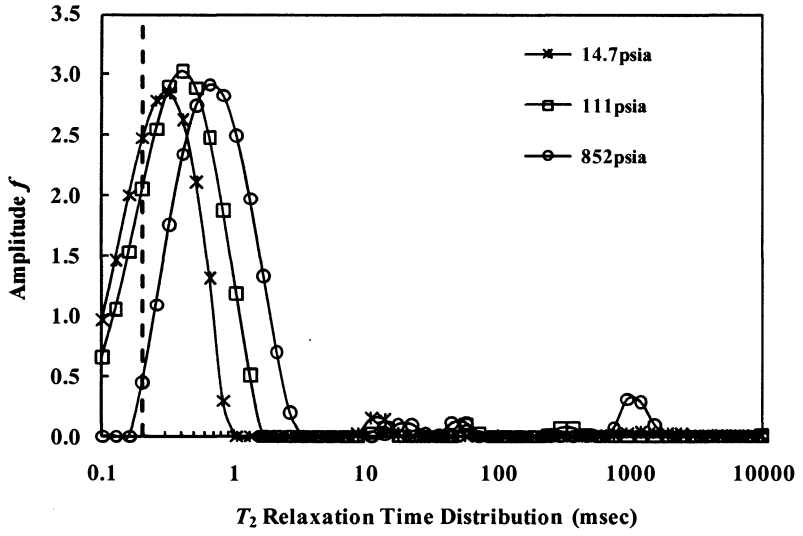

Figure 3.3.19 T_2 distribution of CH_4 saturated Brookfield oil at different pressure levels. Here, the sample temperature is 30 °C.

The heating effect resulting from the pressurization has been removed from the initial pressure reading as shown in Fig. 3.3.15. Extrapolation was used for the pressure correction in the stage of depressurization, as shown in Fig. 3.3.20.

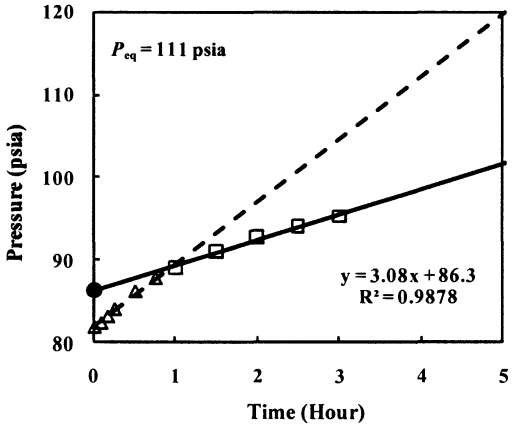

Figure 3.3.20 Extrapolation during depressurization stage for CH_4-Brookfield oil at lower pressure level.

The solubility of CH_4 in Brookfield oil at each pressure was calculated from the corrected pressure data by using the equation of state with compression factor z for CH_4 (NBS 1974). The relationship between the CH_4 solubility and its corresponding T_2 is plotted in Fig. 3.3.21, indicated by the solid dots and the solid fitted line. The open triangles represent the results calculated by using the originally recorded data. The T_2 of dead Brookfield oil is indicated by "X" symbol.

The solubilities calculated with uncorrected pressure obviously have more deviation from the trend extrapolating to the value of dead oil T_2 than the results calculated with corrected pressures. This is similar to the observations in the case of CO_2-Brookfield oil.

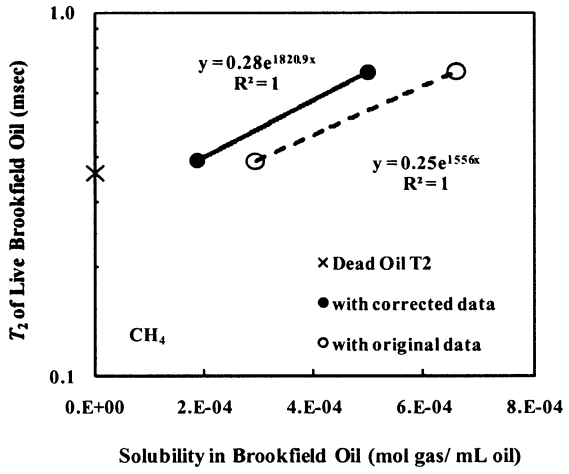

Figure 3.3.21 Relationship between the solubility of CH_4 in Brookfield oil and its corresponding T_2

3.3.2.3 Recombined Live Brookfield Oil with C_2H_6

In the case of C_2H_6-Brookfield oil, the gas pressure inside the vessel was first raised to ~551 psia by injecting C_2H_6 from the top of the pressure vessel. This pressure was less than the critical pressure of C_2H_6, which is 706.7 psia. The oil sample volume used in this case was ~ 13 mL.

After the initial pressurization, the gas source was cut off. The vessel was vertically placed inside the 30 °C air bath and the diffusion behavior of C_2H_6 was first investigated. The pressure decay was monitored by using the Senso-Metrics pressure transducer and the T_2 change as a function of time during the diffusion period was shown in Fig. 3.3.22.

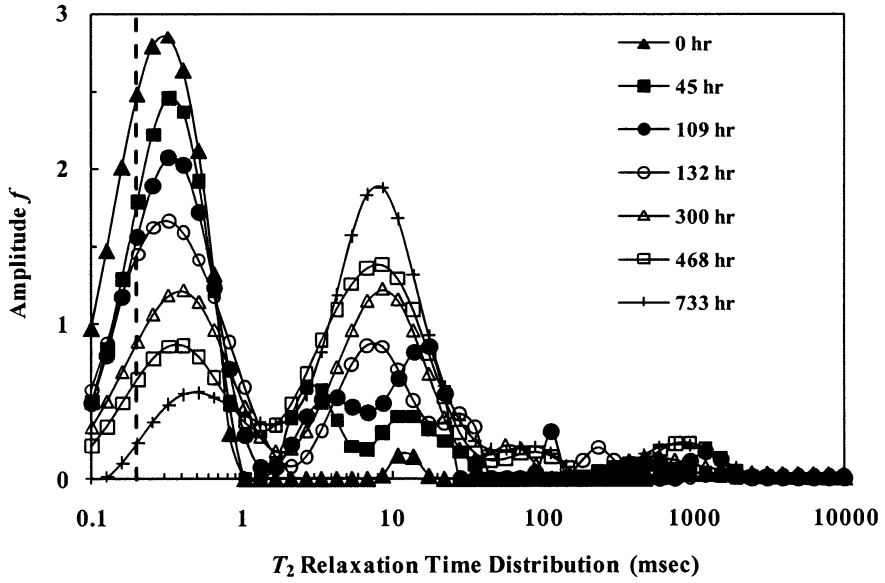

Figure 3.3.22 T_2 distribution of Brookfield oil with C_2H_6 as a function of time in diffusion. Here, the sample temperature is 30 °C.

An interesting finding in Fig. 3.3.22 is that, when C_2H_6 gradually dissolved into the oil, the T_2 distribution of the oil became bi-modal. This is because the dissolved C_2H_6 decreased the viscosity of oil, making the T_2 value of oil with C_2H_6 significantly larger (at ~10 msec). Meanwhile, the T_2 of oil without gas still remained its original value (< 1 msec). As more C_2H_6 dissolved into the Brookfield oil, the area of peak representing the C_2H_6 saturated oil increased while the area of peak for the oil without gas shrinks correspondingly.

The explanation to the bi-modal of T_2 distribution shown in Fig. 3.3.22 was verified by the static gradient CPMG measurement (slice measurement) on the oil sample with the 50-mm probe. The applied echo spacing was 0.4 msec. The sample volume in this case was ~13 mL, resulting in 3.4 cm in length in the pressure vessel. A regular CPMG measurement was made on the entire sample first. Afterwards, the slice measurements were performed at three different positions along the sample. The available slice thickness was about 1 cm.

The midline position of each slice was demonstrated in Fig. 3.3.23. Position #1: center of the entire sample; Position #2: 1.5 cm down from the sample center; and Position #3: 2.1 cm down from the sample center. In this manner, in slice #2, part of the slice at bottom was outside of the sample region. While, in slice #3, only a small part at the top of the slice was within the sample region. The results of the sliced T_2 measurements are displayed in Fig. 3.3.23, where the area for each peak approximately indicates the sample size involved in each slice measurement.

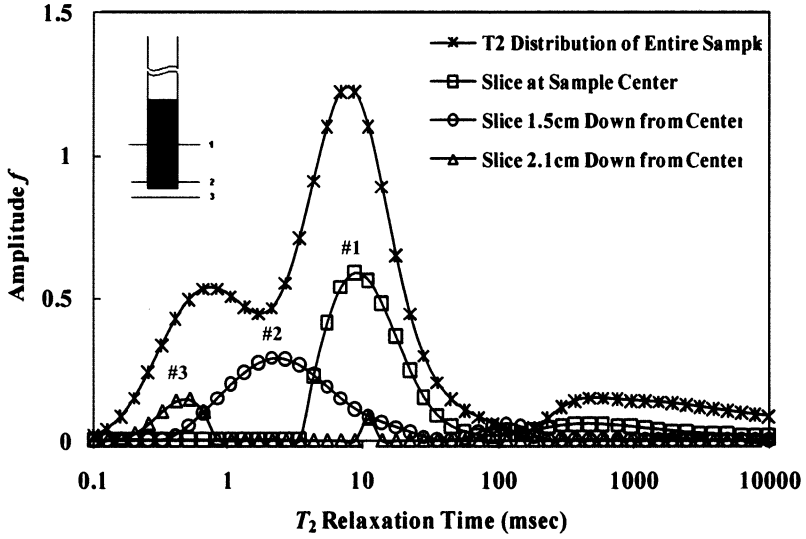

Figure 3.3.23 Static gradient T_2 measurements on C_2H_6 dissolved oil sample.

Comparing the T_2 distribution from each slice measurement with the T_2 distribution of the entire oil sample, it is clearly shown that the sample involved in slice #1 was the C_2H_6 saturated oil. While, the sample involve in slice #3 was the oil without C_2H_6. The T_2 distribution resulting from the slice #2 represents the combination of C_2H_6 saturated oil and dead oil.

After 733 hours for diffusion, the convection was introduced to the C_2H_6-Brookfield oil system by using the same method as used in the CH_4 case. The change of T_2 distribution as a function of time during the convection stage is displayed in Fig. 3.3.24. The last measurement made during diffusion, which was at 733 hours, was also plotted in Fig. 3.3.24 as a benchmark.

Comparing Fig. 3.3.22 and Fig. 3.3.24, we can find that the convection significantly boosted the dissolving of C_2H_6 into Brookfield oil. As shown in Fig. 3.3.24,

167 hours after the generation of convection (900 hours in total after the initial pressurization), the T_2 peak for the dead oil completely disappeared. The entire oil sample was saturated by C_2H_6. In both Fig. 3.3.22 and Fig. 3.3.24, the relatively small peaks showing up around 1 sec in the spectra are the T_2 response from the dissolved C_2H_6 inside the oil sample at the present pressure level. The T_2 of pressurized C_2H_6 was found to be ~10.4 sec at 560 psig and ~8.7 sec at 485 psig (private conversation with Dr. Arjun Kurup).

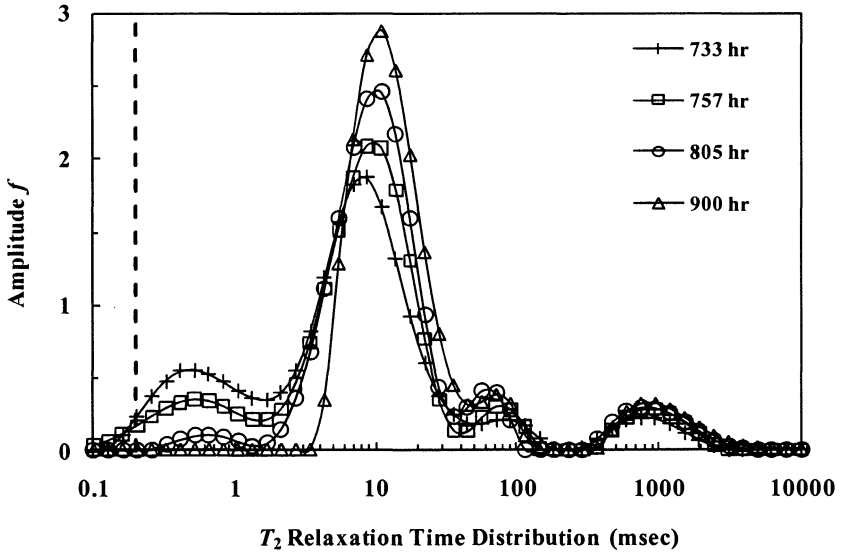

Figure 3.3.24 T_2 distribution of Brookfield oil with C_2H_6 as a function of time in convection. Here, the sample temperature is 30 °C.

The value of Repetition Delay (RD) in the NMR measurements was carefully selected so that, it is enough to allow the oil to be completely polarized but much less than what is needed for the free C_2H_6 to polarize. This is done to avoid the T_2 contribution from the C_2H_6 vapor on the spectra (Fig. 3.3.22 and Fig. 3.3.24). Also, the

smaller RD also significantly shortens the time for the entire measurement. The value of RD used in these measurements is 3 sec, which may not be enough for the complete polarization of the dissolved C_2H_6 inside the oil. Therefore, the peak area of the dissolved C_2H_6 as shown in Fig. 3.3.24 may be less than that corresponds to all the dissolved C_2H_6 inside oil.

The T_2 and pressure changes for C_2H_6- Brookfield oil during the entire process were summarized in Fig. 3.3.25. The pressure and the live oil T_2 reached plateau at about 900 hours. The experiment continued for another 96 hours and no significant change for either pressure or T_2 was observed. Therefore, the system was considered as equilibrated.

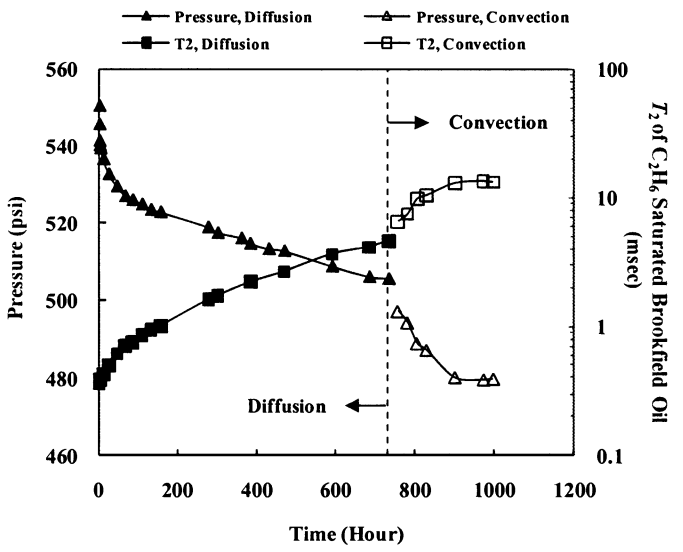

Figure 3.3.25 Pressure decay and T_2 change of C_2H_6-Brookfield oil system during pressurization stage.

The vertical dashed line shown in Fig. 3.3.25 is the border between diffusion and convection. During the diffusion period (0 ~ 733 hrs), pressure decreased from ~551 psia

to ~506 psia while oil T_2 increased from 0.36 msec to 4.59 msec. After the convection was generated, the pressure decreased by about 26 psi, from 506 psia to 480 psia and the oil T_2 dramatically increased from 4.59 msec to 13.40 msec within 167 hours.

After the Brookfield oil was saturated with C_2H_6 at ~480 psia, the depressurization was conducted by decreasing the pressure ~100 psi at a time till the pressure inside the vessel reached around 100 psia. The pressure vessel was kept vertically inside the 30 °C air bath during the entire depressurization process. The changes of pressure and live oil T_2 were monitored in the similar way as we did in the previous two cases.

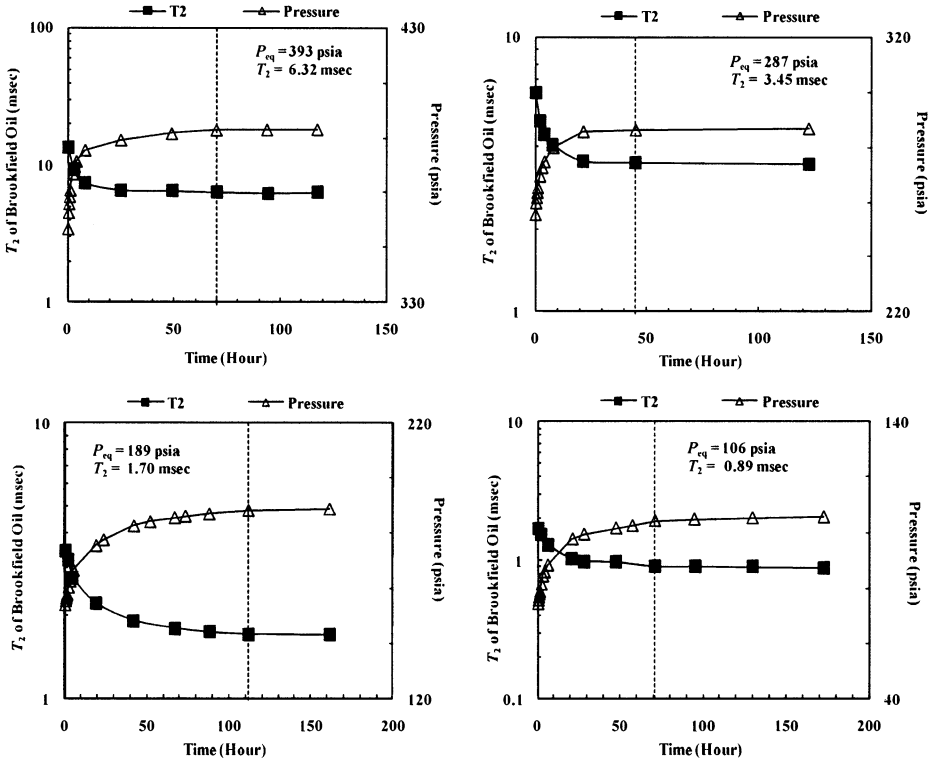

Figure 3.3.26 Changes of T_2 and pressure for C_2H_6 saturated Brookfield oil as a function of time at different pressures during depressurization stage.

The measured T_2 and recorded pressure change as a function of time for the C_2H_6 saturated Brookfield oil at four lower pressure levels were displayed in Fig. 3.3.26. The equilibrated values for both pressure and live oil T_2 at each pressure level are displayed in each subplot, respectively. The vertical dashed lines in Fig. 3.3.26 indicate the time for the C_2H_6 saturated oil firstly reached its equilibrium at each pressure level.

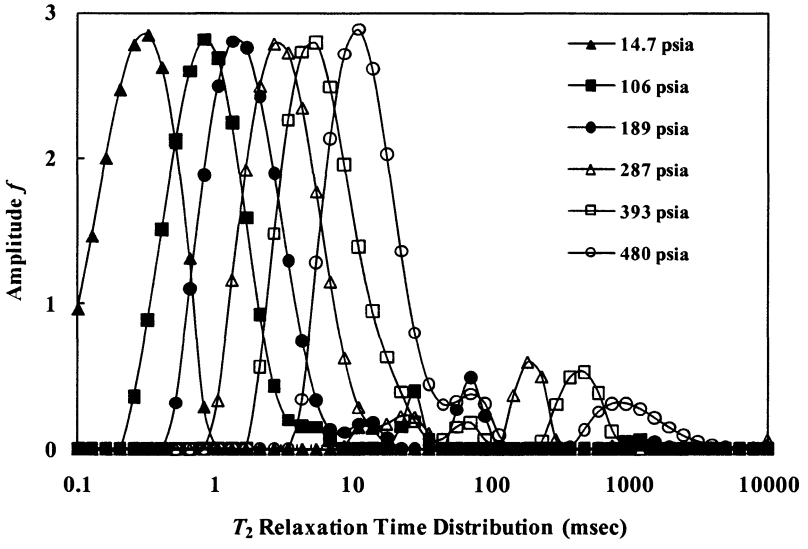

Figure 3.3.27 T_2 distribution of C_2H_6 saturated Brookfield oil at different pressure levels. Here, the sample temperature is 30 °C.

The T_2 peak shift of C_2H_6 saturated oil at different pressures is clearly shown in Fig. 3.3.27. As the C_2H_6 depressurized from the ~480 psia to ~106 psia, the T_2 peak significantly decreased. However, even when the equilibrium pressure was only ~106 psia, the C_2H_6 saturated Brookfield oil still had a T_2 value of 0.89 msec, which is markedly larger than the T_2 of dead oil (0.36 msec).

The T_2 peak from the response of dissolved C_2H_6, which is around 1 sec at ~480 psia, shifted to the smaller values as equilibrium pressure decreases (as shown in Fig. 3.3.27). Meanwhile, the area of the dissolved C_2H_6 T_2 peak shrinks as well, indicating the decrease of dissolved amount of C_2H_6 inside oil sample.

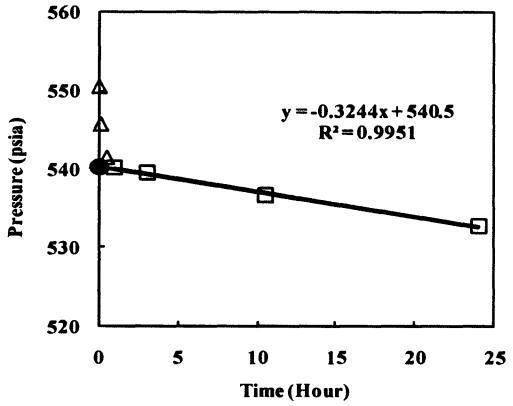

Figure 3.3.28 Extrapolation during pressurization stage for C_2H_6-oil.

The initial pressure P_0 at each pressure level was corrected by extrapolation. The analysis and extrapolation of recorded pressure data for C_2H_6-Brookfield oil during pressurization stage is shown in Fig. 3.3.28. The similar extrapolations for the pressure correction during depressurization stage are shown in Fig. 3.3.29. As shown in Fig. 3.3.28 and Fig. 3.3.29, the difference between the trend of pressure data within the initial period (open triangles) and the later part (open rectangles) is marked for both pressurization and depressurization. Due to the additional effect from temperature variation, the pressure within the initial period changes significantly faster than that thereafter.

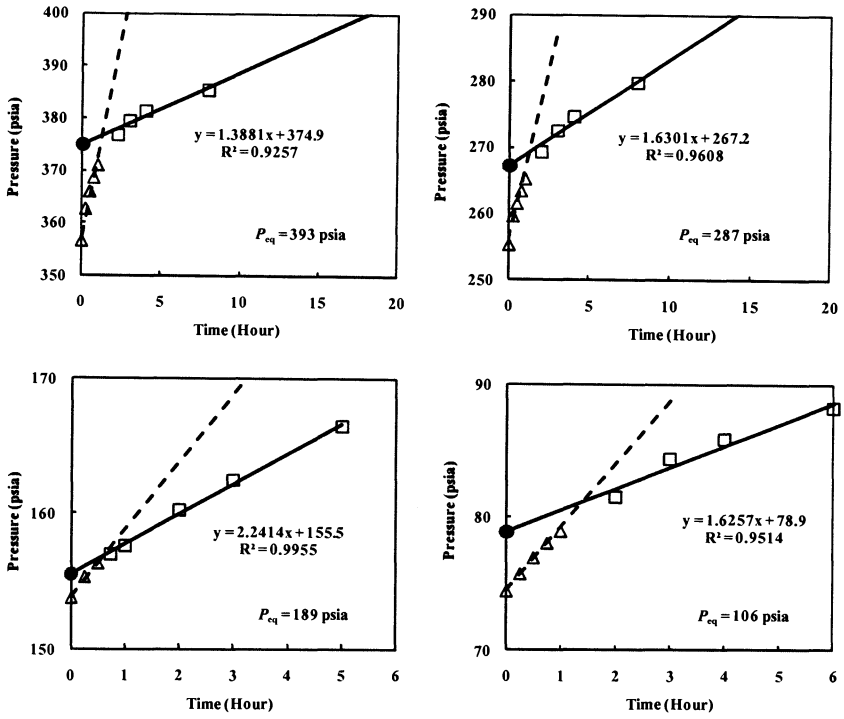

Figure 3.3.29 Extrapolations for the depressurization stage of C_2H_6-oil at different pressures

Given the proper pressure change, vapor phase volume and temperature, the amount of C_2H_6 dissolved into oil at each pressure level can be calculated based on mass balance (as shown in section 3.3.2.1). The equation of state with compressibility factor z for C_2H_6 (NBS 1976) is employed for the solubility calculation.

Fig. 3.3.30 shows the relationship between the solubility of C_2H_6 in oil, which was calculated with either the corrected pressure data or the original recorded data, and its corresponding T_2. The solid line is the fitted curve to the corrected data, while the dashed line is the fitted curve to the original data.

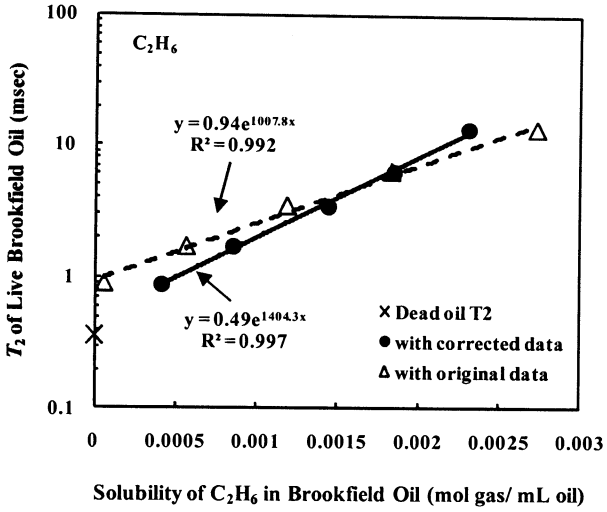

Figure 3.3.30 Relationship between the solubility of C_2H_6 in Brookfield oil and its corresponding T_2

As displayed in Fig. 3.3.30, the trend of C_2H_6 solubility calculated from the corrected data is much closer to the trend extrapolating to the position of the dead oil T_2. While, the trend of solubility calculated from the original pressure data is significantly deviated. Especially at 106 psia, the solubility calculated from the originally recorded pressure data is close to zero. However, as shown in Fig. 3.3.27, the C_2H_6 saturated oil T_2 is markedly larger than the dead oil T_2. This is unreasonable and also implies that the correction on the recorded pressure data is necessary.

3.3.2.4 Summary for NMR and PVT Measurements on Live Brookfield Oil with Different Gases

The logarithmic T_2 of live Brookfield oil at different pressures for three different reservoir gases is summarized in Fig. 3.3.31. The fitted equations and the corresponding

R^2 values are also displayed in the plot. As shown in Fig. 3.3.31, besides the case of CH_4-oil (has only 2 pressure levels), the R^2 values for both CO_2-oil and C_2H_6-oil are near unity, indicating that, although saturated by different gases, the change of live heavy oil T_2 at different pressure closely follows the exponential function.

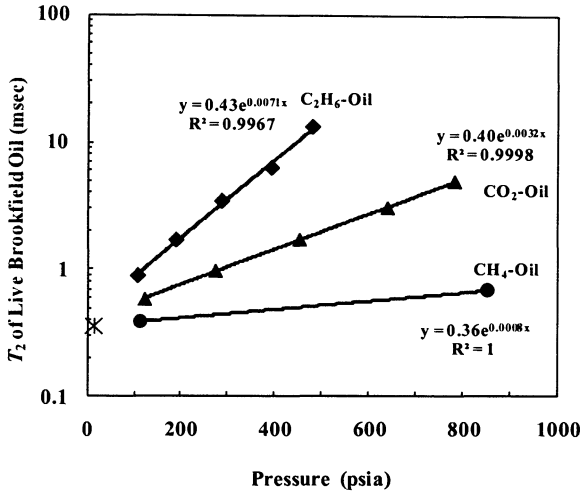

Figure 3.3.31 Relationship between equilibrium pressure and the corresponding live oil T_2 for different gases

As shown in Fig. 3.3.31, among the three gases, C_2H_6 has the most significant influence on the T_2 of Brookfield oil, while, CH_4 gives the least T_2 change at the same pressure level. The higher the equilibrium pressure, the larger the difference between the live oil T_2 caused by different gases. Moreover, the data trend from any of the three gases extrapolated well to the dead oil T_2 (indicated by "X" in the plot).

The relationship between the gas concentration in oil and the corresponding pressure at equilibrium is displayed in Fig. 3.3.32 for different gases. The calculation results are from the corrected pressure data. Henry's law is employed to fit the Pressure

vs. Gas Concentration data and the estimated Henry's constant for each gas in the Brookfield oil is displayed by the corresponding fitted function in the plot.

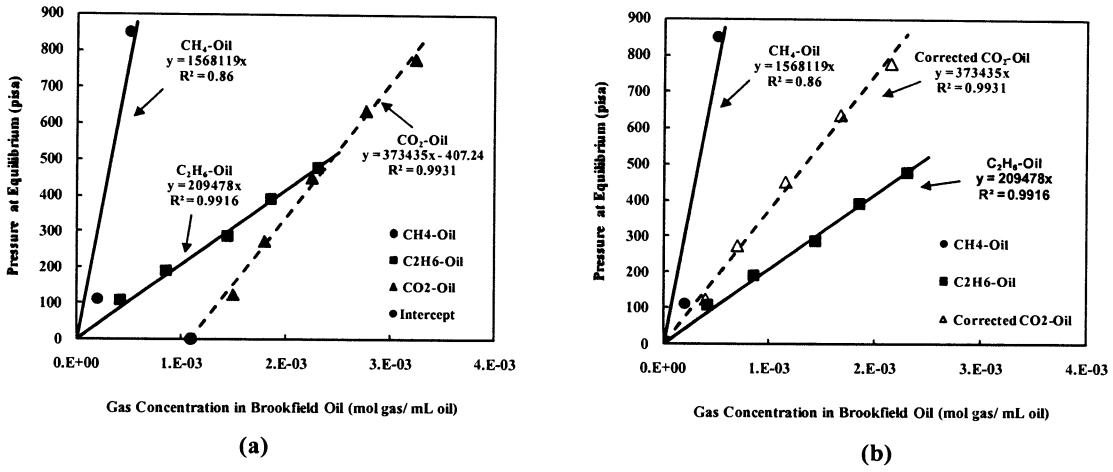

Figure 3.3.32 Relationship between the gas concentration in Brookfield oil and the equilibrated pressures. Here, (a) solubility data in the case of CO_2-Oil is deviated from Henry's law; (b) solubility data for CO_2-Oil is corrected to follow Henry's law.

As shown in Fig. 3.3.32(a), the calculated solubility values in the cases of C_2H_6-oil and CH_4-oil follow the Henry's law well. However, the originally calculated solubility of CO_2 is significantly deviated. The extrapolation of the CO_2 data does not pass the origin. Instead, at x-axis (y = 0), it has an intercept of 0.00109 mol gas/mL oil (indicated by the red solid dot).

The proposed explanation for this phenomenon is that, during the pressurization stage in the case of CO_2-oil (~800 psia at 30 °C), besides the original two phases (vapor CO_2 and liquid oil), a third phase, which is CO_2-rich liquid with presence of heavy-hydrocarbon components, may be formed inside the CO_2-heavy oil system. The L-L-V three-phase-equilibrium has been observed in both CO_2/Alkane system (Orr, Yu and Lien

1981), (Enick, Holder and Morsi 1985) and CO_2/Crude oil system (Orr, Yu and Lien 1981) (Syegh, et al. 1990) at near-critical condition. The extraction of heavy hydrocarbon components (as heavy as C_{24}) into CO_2-rich phase was reported by Orr et al. (Orr, Yu and Lien 1981). More importantly, the three phases coexisting was found to be able to form more easily with heavier component in the CO_2/oil binary mixture (Orr, Yu and Lien 1981).

During the pressurization stage of CO_2-oil system in this study, after the injection of the pressurized CO_2 was ceased, the stripping of hydrocarbons from the oil by CO_2 and the dissolving of CO_2 into oil occurred simultaneously. As more heavy-hydrocarbon components present in the CO_2 vapor phase, a CO_2-rich liquid phase could have gradually formed inside the pressure vessel. However, simply by monitoring the pressure change in vapor phase, we cannot tell the difference between the pressure decay from the dissolving of CO_2 into oil and the pressure decay caused by the condensation of CO_2 into the CO_2-rich liquid phase.

The recorded pressure decay due to the condensation of CO_2 in the second liquid phase was mistaken as that caused by the solution of CO_2 into the oil phase. As a result, the calculated solubility of CO_2 at the highest pressure level could be significantly larger than its "true" value.

Subsequently, as the pressure decreases, the CO_2-oil system moved away from the three phases coexisting region, and the data for the pressure difference at each lower pressure level could be obtained properly. However, based on the method for solubility calculation in this work (as shown in section 3.3.2.1), any impact on the solubility at the highest pressure will uniformly affect the calculation of solubility at each lower pressure.

Consequently, as shown in Figure 3.3.32(a), the calculated solubility of CO_2 in Brookfield oil appears to be overestimated with a constant value at each pressure level but still linearly correlates between the pressure at equilibrium and the solubility in the oil.

In order to correct the overestimation for the CO_2 solubility, we uniformly subtract the excess value at the intercept of x-axis from the originally calculated solubility at each pressure and re-plot the corrected CO_2 data in Figure 3.3.32(b). It is clear that, the corrected CO_2 data now follows the Henry's law well.

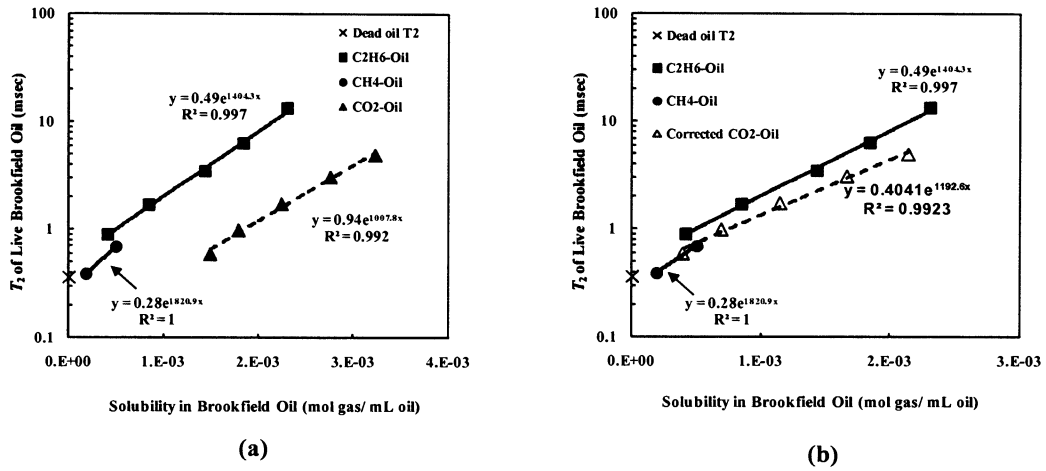

Figure 3.3.33 Relationship between the solubility of CO_2 in Brookfield oil and its corresponding T_2. Here, (a) data from CO_2-Oil is deviated from dead oil value; (b) corrected data for CO_2-Oil well extrapolates to dead oil value.

The corrected CO_2 data is also employed in the relationship of live oil T_2 and CO_2 solubility. As shown in Fig. 3.3.33(a), the originally calculated data from CO_2-oil significantly deviates from the dead oil value. However, as the solubility of CO_2 was corrected via the method as shown in Fig. 3.3.32, the data trend of T_2 vs. corrected

solubility of CO_2 now extrapolates to the dead oil value well. The relationship between the live oil T_2 and its corresponding gas solubility is closely linear on the semi-log scale for all three gases. Furthermore, an interesting finding in Fig. 3.3.33(b) is that, the relationship between the live oil T_2 and gas solubility appears to closely follow similar trend, regardless of the gas type used for saturation.

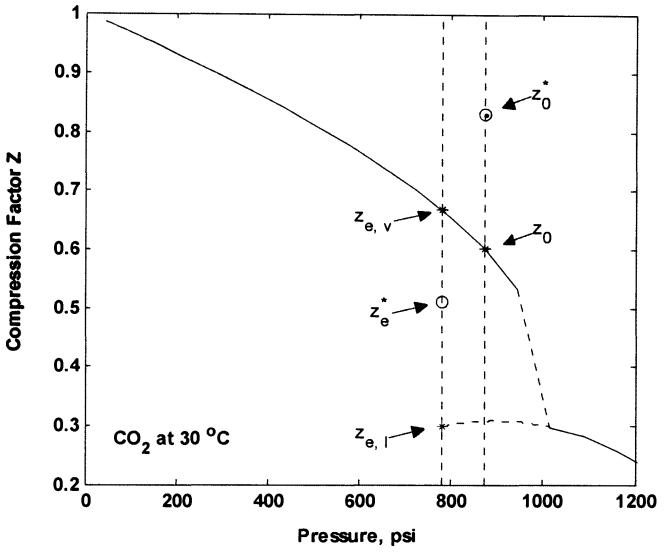

Figure 3.3.34 Analysis of compressibility factor z of CO_2 for adjusting the calculated solubility of CO_2 in Brookfield oil to follow Henry's law.

The gas solubility is calculated via equation of state with compressibility factor z, as shown in section 3.3.2.1. In order to remove the overestimation for CO_2 solubility, the compressibility factor z was re-adjusted to correct the Pressure vs. Solubility curve of CO_2 to follow the Henry's law (as shown in Fig. 3.3.32). The solubility calculation method during pressurization stage is expressed by Eq. [3.1]. The adjustment on z factor can be made on either z_0 (initial point) or z_{eq} (equilibrium point) to serve the purpose.

The adjustment on z_0 at the initial pressure was first performed and the re-evaluated value is indicated as z_0^* in Fig. 3.3.34. In order to correct the calculated solubility by changing the z factor at the initial pressure, the re-evaluated value needs to move up to a value of 0.83. This value is very unlikely for the compressibility factor of CO_2 at 873 psia.

The adjustment on z_e at the equilibrium pressure shows that, in order to correct the calculated solubility to follow Henry's law, the corrected z factor value needs to move down to a value of 0.51 (indicated as z_e^* in Fig. 3.3.34) at 780 psia.

As we discussed in previous paragraphs that, the proposed explanation to the deviation of CO_2 data from Henry's law is due to the coexisting of CO_2-rich liquid phase with the CO_2 vapor and oil phase. Therefore, the estimated value of z_e^* is contributed by both $z_{e,v}$ (z factor for CO_2 vapor phase) and $z_{e,l}$ (z factor for CO_2-rich liquid phase). As shown in Fig. 3.3.34, the extrapolated value of $z_{e,l}$ at 780 psia is highlighted by red asterisk, while $z_{e,v}$ is indicated by black asterisk. The z_e^* can be calculated by Eqs. [3.3] and [3.4].

$$z_e^* = z_{e,v} \cdot x_v + z_{e,l} \cdot x_l \tag{3.3}$$

Here,

x_v, mole fraction of CO_2 in vapor phase;

x_l, mole fraction of CO_2 in CO_2-rich liquid phase;

The sum of mole fraction of CO_2 in non-oil phase is considered as 1.

$$x_v + x_l = 1 \tag{3.4}$$

Given the values for all three z factors shown in Eq. [3.3] and combining Eq. [3.3] and Eq. [3.4], the mole fraction of CO_2 in vapor phase and CO_2 in CO_2-rich liquid phase can be calculated. The calculated mole fraction of CO_2 in vapor phase is 0.58, correspondingly, the mole fraction in CO_2-rich liquid phase is 0.42.

Here, on basis of the available data in the reference book (IUPAC 1973), the estimated density for CO_2 vapor is ~0.1431 g/mL and the density for CO_2-rich liquid is ~0.5421 g/mL. In this manner, the volume fraction of CO_2 in either vapor phase or CO_2-rich liquid phase is calculated to be 0.84 and 0.16, respectively.

3.3.2.5 Viscosity Measurements on Live Brookfield Oil

The viscosity of live Brookfield oil with different gases was measured at different pressures by using the capillary viscometer. All the measurements on the live oil were performed at room temperature (22 °C). The relationship between fluid viscosity and the flow rate, measured pressure drop and the tube dimension is governed by the *Hagen-Poiseuille* equation as below:

$$\mu = \frac{(P_0 - P_L) \cdot \pi \cdot R^4}{8 \cdot Q \cdot L} \tag{3.5}$$

Here, μ is oil viscosity, Q is flow rate, L is length of tube, R is inner radius of the tube.

The setup of the capillary viscometer used in this work is demonstrated in Fig. 3.3.35. The tubing used for measuring the viscosity is the Swagelok 1/8" stainless tubing, which has 14.9 cm in length and 0.175 cm in I.D. The transfer vessel at the bottom in the setup shown in Fig. 3.3.35 was manufactured by TEMCO. The ISCO pump was

employed to drive the fluid to flow. The pressure rating of the transducer used in this case is 200 psi

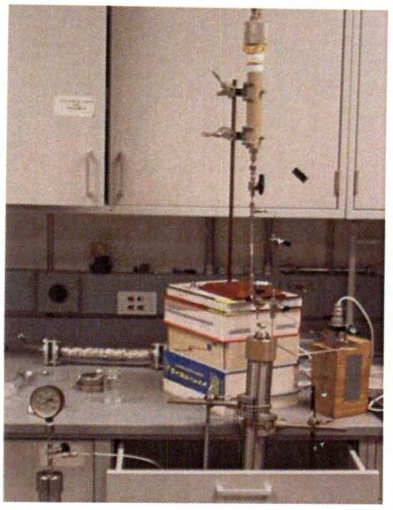

Figure 3.3.35 Setup of capillary viscometer.

The capillary viscometer was first tested with dead Brookfield oil at four different flow rates. The average value obtained by using the capillary viscometer was 468,996 cP at room temperature. Meanwhile, the viscosity measured by Brookfield viscometer at the same temperature was 481,000 cP, which had only ~2.5% difference from the average value from the capillary viscometer.

The viscosity of live Brookfield oil saturated by C_2H_6 was measured at five different pressure levels. Meanwhile, in the case of either CO_2-oil or CH_4 oil, the live oil viscosity measurement was performed at one pressure level for each. The measured viscosity values of Brookfield oil under different conditions are summarized in Table 3.3.2.

Table 3.3.2 Measured viscosity of Live Brookfield oil via capillary viscometer

Saturated Gas	Equilibrium Pressure (psia)	T_2 (msec)	Viscosity (cP)
CO_2	121	0.39	270,443
CH_4	227	0.29	332,914
C_2H_6	486	10.02	1,929
C_2H_6	391	4.57	4,918
C_2H_6	288	3.16	9,354
C_2H_6	208	1.32	43,106
C_2H_6	109	0.90	71,459

Fig. 3.3.36 displays T_2 vs Viscosity/Temperature ratio for the live Brookfield oil saturated with different gases. Each T_2 value of live oil shown in Table 3.3.2 and Fig. 3.3.26 was measured at room temperature. The data of dead oil viscosity at different temperatures are also plotted for comparison. It is clearly shown in Fig. 3.3.36 that, regardless of the gas type used for saturation, the live oil T_2 correlates with viscosity/temperature ratio on log-log scale. More importantly, as displayed in Fig. 3.3.36, the changes of T_2 and viscosity/temperature ratio caused by solution gas follows the same trend of those caused by temperature variations on the dead oil.

In this manner, given the proper T_2 value, the live heavy oil viscosity with different solution gases and at different pressure levels can be estimated through the T_2 vs. viscosity/temperature ratio correlation obtained from the measurements on the corresponding dead oil at different temperatures. This finding creates a new way for in-situ viscosity evaluation of heavy oil through NMR well logging.

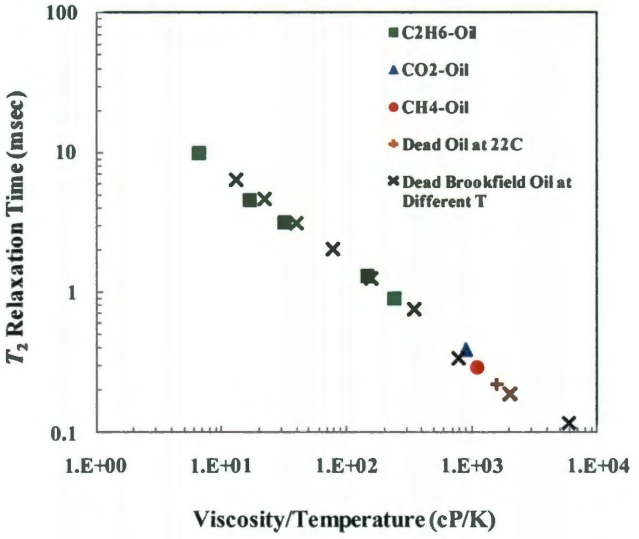

Figure 3.3.36 Relationship between the T_2 of Brookfield oil and the viscosity/temperature ratio

The viscosity and T_2 data of Brookfield oil obtained in this work are also employed for comparison with data from some other reference papers (Vinegar, et al. 1991), (LaTorraca, Dunn, et al. 1998), (MaCann, Vinegar and Hirasaki 1999), (Y. Zhang, PhD Thesis 2002). Also, data obtained in the case of Athabasca bitumen are included, indicated by the solid black rectangle symbols. All the T_2 and viscosity data are normalized with respect to 2 MHz (Y. Zhang, PhD Thesis 2002), (Hirasaki, Lo and Zhang 2003), (Yang and Hirasaki 2008), as expressed by Eq. [2.17] and Eq. [2.18], and shown in the form of Normalized Relaxation Time vs. Normalized Viscosity/Temperature ratio.

As shown in Fig. 3.3.37, the data of Athabasca bitumen follows the trend of those reference data from different crude oil samples well. However, although the T_2 vs. Viscosity data from the synthetic Brookfield oil are also linear on the log-log scale, the

trend is obviously deviated. This is due to the significant composition difference between the synthetic oil (100% for Brookfield oil) and those real crude oils.

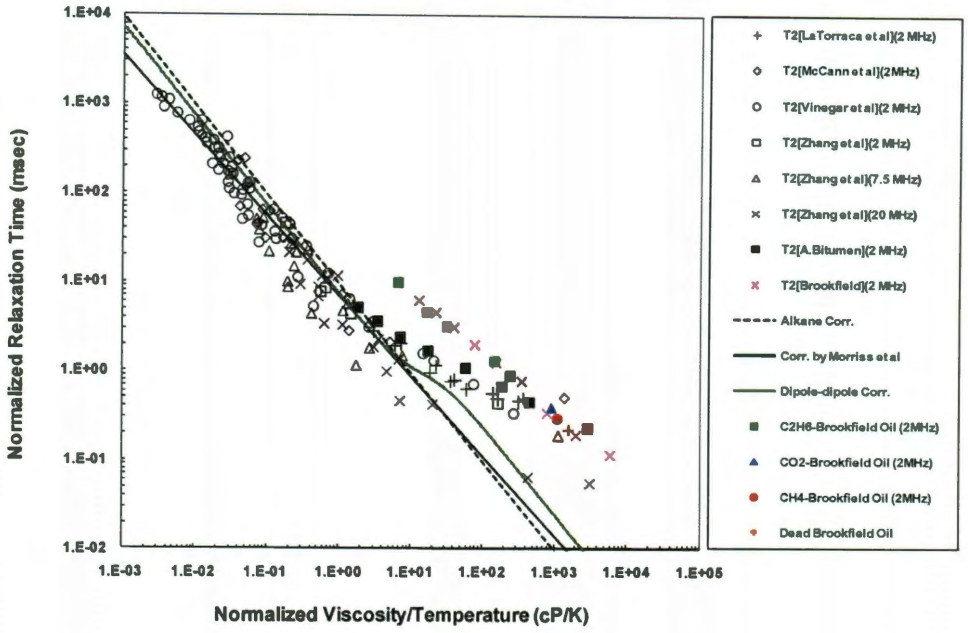

Figure 3.3.37 Relationship between normalized relaxation times and normalized viscosity/temperature ratio for Brookfield oil.

3.4 Conclusions

CO_2 has the largest mass transfer rate in Brookfield oil due to the unique natural convection. There was no significant dissolving of CH_4 observed via simply diffusion up to 168 hours at ~ 890 psia. The diffusion rate of C_2H_6 was found to be between the CO_2 and CH_4. The gradual diffusion of C_2H_6 into Brookfield oil from top to bottom was confirmed by the NMR slice measurement. The generated convection remarkably speeds up the gas dissolving rate.

The live oil T_2 is significantly larger than T_2 of dead oil, even at the lowest pressure level in this work (~100 psia). The relationship between the equilibrium pressure and the live oil T_2 is found to be closely linear on semi-log scale for all three reservoir gases.

The originally recorded pressure data for all the three gases (CO_2, CH_4 and C_2H_6) were analyzed. In order to remove the temperature influence on pressure reading and estimate the real starting pressure, extrapolation was employed to correct the recorded pressure data within the initial period after each pressurization or depressurization.

The solubility in Brookfield oil for all the three gases (CO_2, CH_4 and C_2H_6) were calculated by using the corrected pressure data. The dissolving of both CH_4 and C_2H_6 in Brookfield oil is found to follow the Henry's law well. However, the observed dissolving behavior of CO_2 in Brookfield oil is significantly deviated.

The relationship between the calculated gas solubility and the corresponding live oil T_2 is found to be closely linear on a semi-log scale for all three reservoir gases.

Regardless of the gas type used for saturation, the live oil T_2 correlates with viscosity/temperature ratio on log-log scale. Moreover, the changes of T_2 and viscosity/temperature ratio caused by solution gas follows the same trend of those caused by temperature variations on the dead oil. This creates a new way for in-situ viscosity evaluation of heavy oil through NMR well logging.

Chapter 4 NMR Measurement and Viscosity Evaluation of Live Bitumen

4.1 Introduction

The viscosity evaluation and the laboratory NMR measurements of the recombined live Brookfield oil have been discussed in Chapter 3. The effects of three major reservoir gases (CH_4, CO_2, and C_2H_6) on the changes of viscosity and T_2 of this synthetic oil were investigated under a series of saturation pressures. However, at the end of Chapter 3, Fig. 3.3.35 showed the deviation of the synthetic Brookfield oil data from the trend of those crude oil data due to the composition difference.

In this chapter, a new crude bitumen sample #10-19, provided by Shell E&P Company, was employed for all the investigations. Similar experimental procedures as mentioned in Chapter 3 were used for all the NMR, PVT and viscosity measurements on the bitumen #10-19 sample. The correlations among the saturation pressure, gas solubility, NMR T_2 and live bitumen viscosity for the bitumen are established in this chapter. Comparisons will be made between the data obtained from the investigations on bitumen sample and the results shown in the case of Brookfield oil.

4.2 Equipment and Experimental Procedures

The nuclear magnetic resonance (NMR) spectrometer (Maran-M), the NMR probes and the pressure vessel used in this work on bitumen #10-19 were the same as those employed for the Brookfield oil in Chapter 3.

The heavy oil sample used in this part of work is the bitumen sample #10-19, provided by the Shell Oil Company. The properties of this crude bitumen sample will be discussed in the following sections.

The three reservoir gases (CO_2, CH_4 and C_2H_6) used in this case are provided by Matheson Tri-Gas with product grade of Ultra High Purity.

4.3 Results

4.3.1 Characterization of Bitumen #10-19 at Different Temperatures

The same techniques we mentioned in Chapter 2 and Chapter 3 were employed to characterize the viscosity and NMR properties of the bitumen #10-19 sample at different temperatures.

4.3.1.1 Viscosity of Bitumen #10-19 at Different Temperatures

The viscosity of the bitumen #10-19 at different temperature was measured by using the Brookfield viscometer LVDV-III+. The sample temperature was controlled by an oil bath (HAAKE K35) connected to the viscometer sample holder. The oil sample was measured from 10 °C to 90 °C. The viscosity changes with temperature of Athabasca

bitumen and Brookfield oil are used to compare with the results from bitumen #10-19. The measurement results are shown in Fig. 4.3.1 as below.

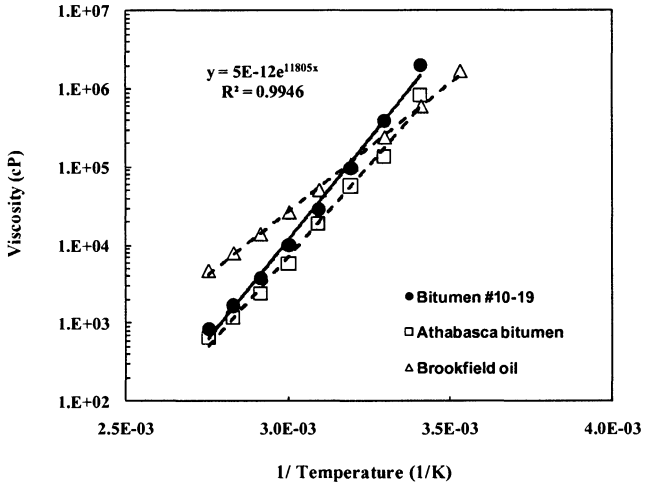

Figure 4.3.1 Viscosity of bitumen #10-19 at different temperatures

As shown in Fig. 4.3.1, on the semi-logarithmic scale, all the three heavy oils closely follow linear relationship between viscosity and reciprocal of sample temperature. The viscosity of bitumen #10-19 (indicated by solid dots) is generally higher than that of Athabasca bitumen at each temperature. The correlation equation for the result of bitumen #10-19 is displayed in the plot. It is clearly shown that, as crude oils, the experimental results of bitumen #10-19 and Athabasca bitumen follow the similar trend, while the results from Brookfield oil are apparently deviated.

Due to the limit of Brookfield viscometer LVDV-III+, the lowest temperature that the viscosity measurement can be performed on bitumen #10-19 was 20 °C. When the sample temperature was further lowered to 10 °C, the viscosity of the bitumen was

beyond the capability of Brookfield viscometer ($\leq 3.0 \times 10^6$ cP). By using the correlation shown in Fig 4.3.1, the estimated viscosity of bitumen #10-19 at 10 °C is ~6.4×10^6 cP.

4.3.1.2 NMR Measurement on Bitumen #10-19 at Different Temperatures

The same experimental methods as used in the cases of Athabasca bitumen and Brookfield oil were applied for the measurements on the bitumen #10-19 at different temperatures.

The total volume of bitumen sample used for NMR measurement was about 15 mL. The 40 mm probe was employed in this work and the applied echo spacing was 0.2 msec. The temperature of magnetic field was controlled at 30 °C with an error of ±0.1 °C for all measurements. For the bitumen #10-19 sample, the applied width of $\pi/2$ pulse was 8.28 μs and that of π pulse was 16.13 μs.

CPMG and FID measurement were performed on the bitumen sample at temperature from 10 °C to 90 °C and was conducted with an interval of 10 °C at a time within the temperature range. At each temperature, the measurement was repeated three times to ensure the reliability of experimental data.

The T_2 distribution of bitumen #10-19 at different temperature, which was interpreted using the regular CPMG data without specified M_0 and lognormal distribution model, is shown in Fig. 4.3.2. The 0.2 msec echo spacing is indicated by the vertical dashed line in the plot.

As shown in Fig. 4.3.2, within the entire temperature range, the bitumen sample always has certain fast relaxing components whose relaxation time is shorter than the applied echo spacing. Therefore, M_0 needs to be imposed into the CPMG data at each

temperature, and the lognormal distribution model needs to be employed for the re-interpretation of the M_0 specified data (Yang and Hirasaki 2008).

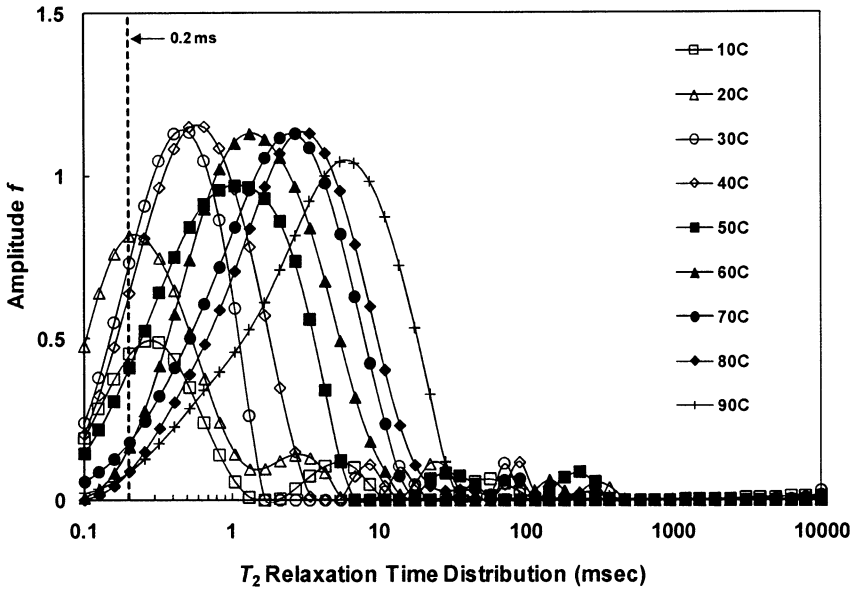

Figure 4.3.2 T_2 distribution of bitumen #10-19 at different temperatures. Here, the interpretation of CPMG data is without the specified M_0 and lognormal distribution model.

The small peaks to the right of the major oil peak on the T_2 spectra are from emulsified water inside the bitumen sample. The estimation from NMR measurement for water content in bitumen #10-19 is around 2%.

The FID measurement was performed at different temperatures and M_0 was estimated by extrapolation as shown in Fig. 4.3.3. The dead time for the 40-mm probe is 70 μsec. The extrapolated value for M_0 at different temperature is indicated as red asterisk at Time = 0.

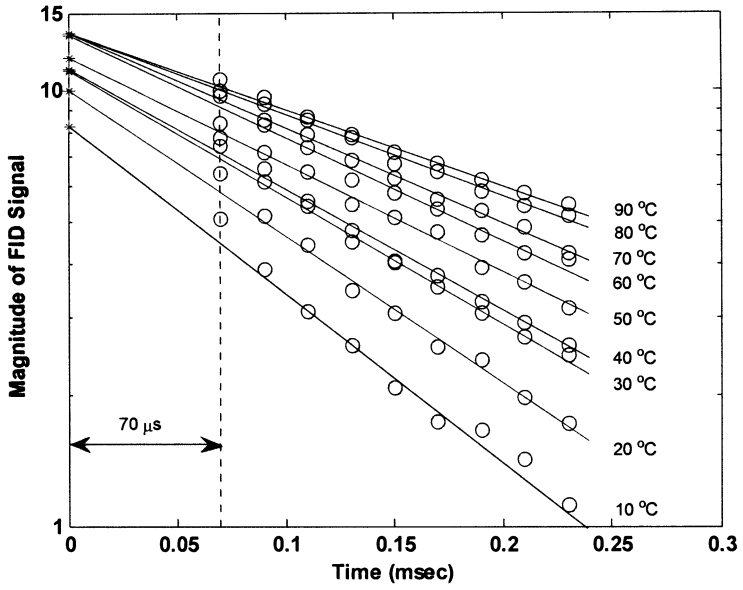

Figure 4.3.3 FID of bitumen #10-19 at different temperatures.

According to Curie's law, the value of M_0 should be inversely proportional to the sample temperature (Cowan 1997). However, as shown in Fig. 4.3.3, the extrapolated M_0 value increases with temperature. Similar phenomenon was also observed in the work on Athabasca bitumen (as shown in Chapter 2). This is due to the high viscosity of bitumen sample.

In this work, the FID information loss occurred within the 70 μsec dead time for most of the temperature range, which results from the extremely high viscosity of the bitumen sample. The extrapolated M_0 value keeps increasing with temperature until the sample temperature rises above 80 °C. In order to compensate for the FID loss, the same method as we developed in the work on Athabasca bitumen, which used the Curie's law

for the calibration, was employed to correct the M_0 of the bitumen #10-19 at each lower temperature.

The M_0 obtained from FID measurement at the highest sample temperature (90 °C in this work) is considered to be the real value at its corresponding temperature. The $M_{0,90^\circ C}$ of the bitumen #10-19 is 13.6. Based on this value, all the other M_0 at lower temperatures were evaluated by using the Curie's Law, as shown by Eq. [4.1].

$$M_{0,T} = M_{0,90^\circ C} \cdot \frac{363.15}{T} \tag{4.1}$$

The M_0 values of the bitumen calibrated by the Curie's law are summarized in Fig.4.3. 4 as a function of temperature. The M_0 values before correction, which are estimated through FID and CPMG, are also plotted for comparison.

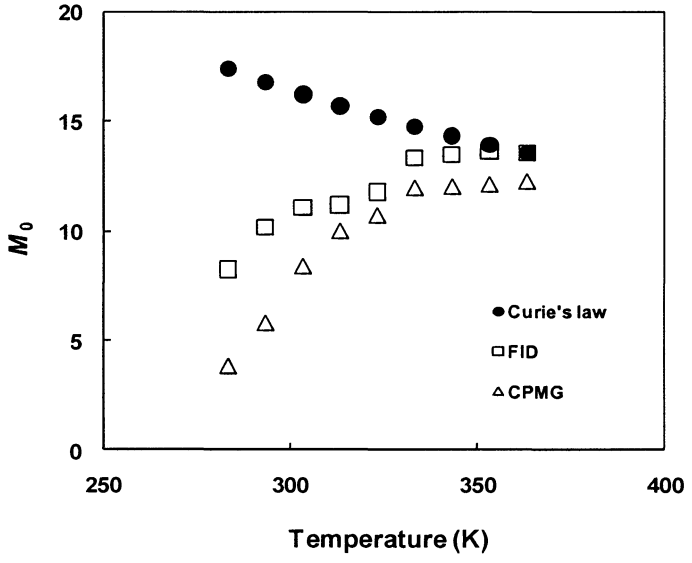

Figure 4.3.4 M_0 of the bitumen #10-19 at different temperatures estimated by using different methods.

The M_0 estimated from CPMG increases monotonically with temperature. This is due to the significant signal loss which is shorter than the applied echo spacing (0.2 msec). The lower the temperature, the higher the bitumen viscosity, the more the signal loss in CPMG measurement.

The M_0 evaluated from FID also increases with temperature until the sample temperature is above 80 °C. This is also resulting from the signal loss in FID measurement. However, because the dead time in FID (70 μsec) is much shorter than the echo spacing in CPMG (200 μsec), the estimated M_0 value at each temperature is always larger than that from CPMG.

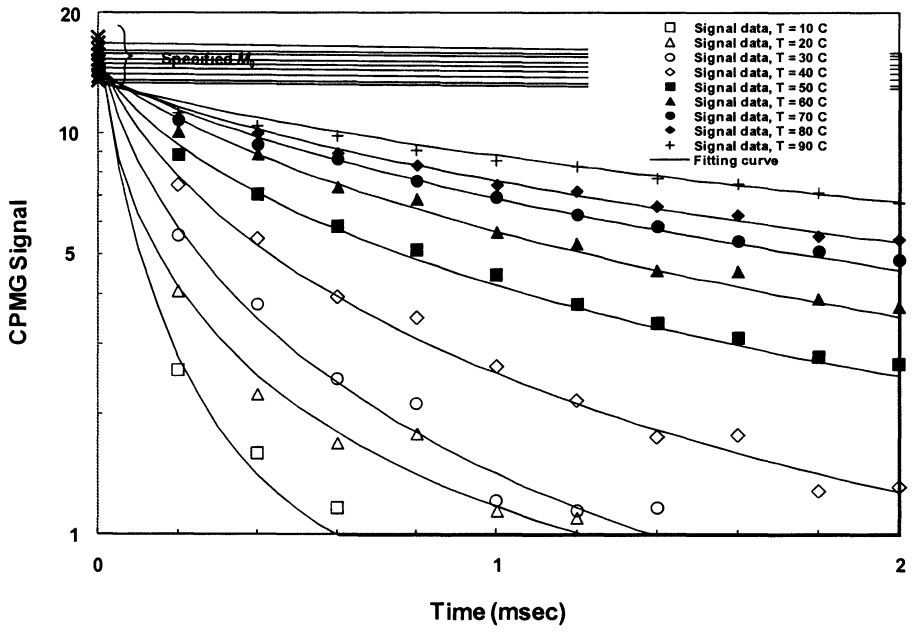

Figure 4.3.5 Fitting of M_0 specified CPMG data of bitumen #10-19 by using lognormal distribution model.

The new interpretations for the bitumen #10-19 via the lognormal distribution model (Yang and Hirasaki 2008) are shown in Fig. 4.3.5. The "X" symbols at Time = 0 are specified M_0 values from Curie's law for each temperature. As displayed in Fig. 4.3.5, the lognormal distribution model fits these M_0 specified CPMG data very well. The T_2 distribution of bitumen from the new interpretation at temperature of 10 °C ~ 90 °C is displayed in Fig. 4.3.6 as below.

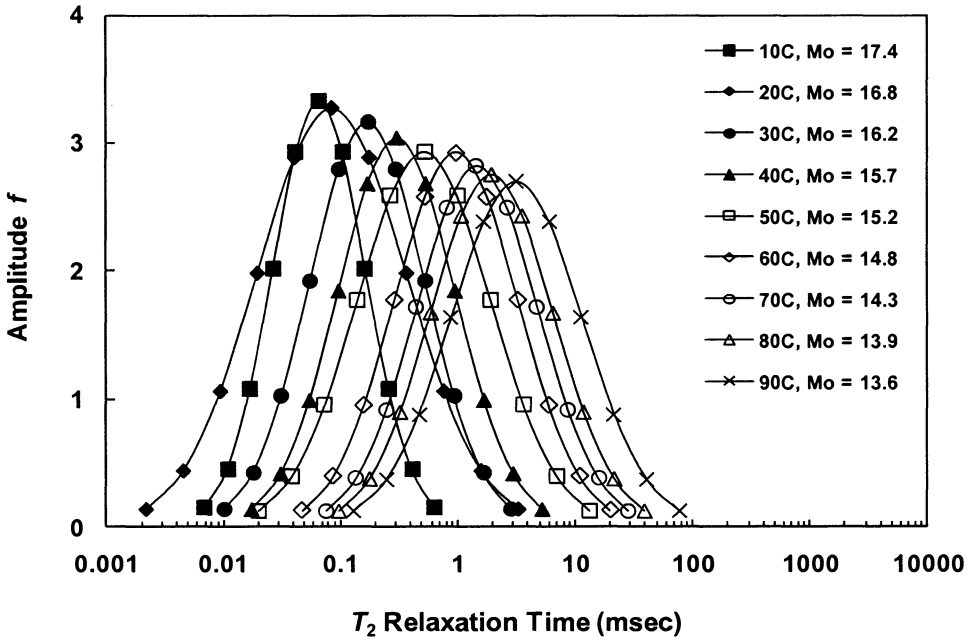

Figure 4.3.6 T_2 distribution of bitumen #10-19 from the new interpretation. Here, the CPMG data was imposed with the specified M_0 and the lognormal distribution model was applied.

Comparing Fig. 4.3.2 and Fig. 4.3.6, the logarithmic mean T_2 of the bitumen from two different interpretation methods at temperatures of 10 °C to 90 °C is summarized in

Fig. 4.3.7. The bitumen T_2 values from regular interpretation are generally larger than those from lognormal distribution model with specified M_0. The difference between the T_2 from the two different interpretation methods decreases as temperature increases. This is similar to the observance in the investigation on Athabasca bitumen, as shown in Chapter 2.

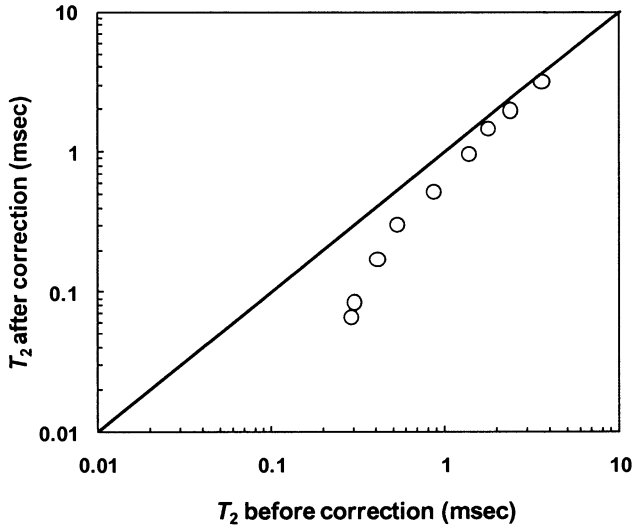

Figure 4.3.7 Comparison on bitumen T_2 obtained before and after the correction via lognormal distribution model.

4.3.1.3 Relationship between Viscosity and T_2 for Dead Bitumen

The relationship between the viscosity and T_2 for the bitumen #10-19 is found to be linear on the log-log scale. This is the same to the observations on the Brookfield oil and Athabasca bitumen, as well as many other heavy oil samples reported previously (Dunn, Bergman and Latorraca 2002). The fitted function for the bitumen data is

displayed in the plot. The goodness of the fitting is evaluated by the squared value of the correlation coefficient, R^2, which is close to unity in this case.

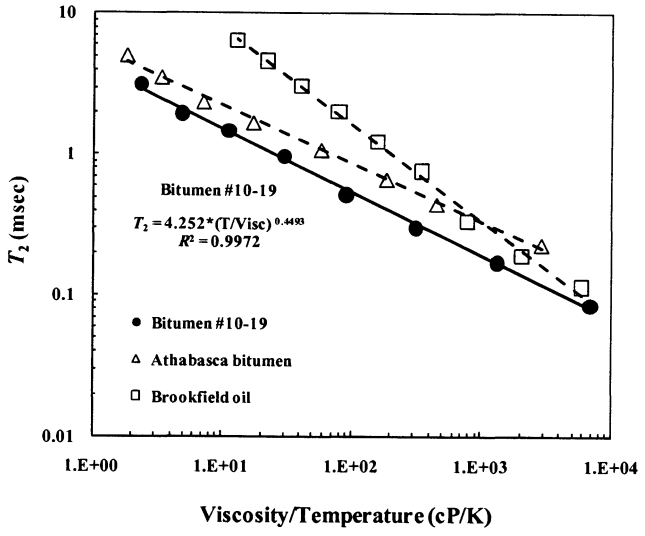

Figure 4.3.8 Relationship between T_2 and viscosity/temperature ratio for bitumen #10-19. Here, data from Brookfield oil and Athabasca bitumen are plotted for comparison.

As shown in Fig. 4.3.8, the T_2 of bitumen #10-19 is smaller than that of Athabasca bitumen, at similar viscosity/temperature ratio. In general, the data from the two crude bitumen samples follow the same trend, while the data from the synthetic Brookfield oil are deviated. Moreover, none of the data from the three heavy oils follow the correlations previously developed, basing on relatively lighter oils (Morriss, et al. 1997), (Zhang, et al. 1998), (Lo, et al. 2002). Here, in Fig. 4.3.8, all the T_2 values for three different oil samples were from the new interpretation method (Yang and Hirasaki 2008).

4.3.2 Investigations on Recombined Live Bitumen

The investigations on the recombined live bitumen were performed with three different reservoir gases, CO_2, CH_4, and C_2H_6. The measurements were conducted at different pressure levels for each gas.

The experimental procedures used in the work on bitumen are the same as those used in the case of Brookfield oil. For each gas, the procedure was divided into two stages, the pressurization stage and the depressurization stage. The highly pressurized gas was first introduced into the closed pressure vessel with bitumen at the bottom. After the gas-bitumen system reached equilibrium at the highest pressure level, the system pressure would be depressurized to a series of lower pressures. At each lower pressure, the equilibrium was achieved and the NMR measurements were performed.

During the NMR measurements in the work on bitumen, the number of scans (NS) was chosen to make the signal to noise ratio (SNR) equal to 100 in each case. Each measurement was repeated for 6 times so that the reliability of experimental data can be ensured. During the entire process, the system pressure inside the vessel was recorded as a function of time.

4.3.2.1 Calculation of Gas Solubility in Bitumen

The solubility of each gas in the bitumen #10-19 was calculated via the same method as mentioned in the work on Brookfield oil (section 3.3.2.1). Given the proper pressure data, the solubility can be calculated by using the equation of state with compression factor z for each gas.

4.3.2.2 Recombined Live Bitumen with C_2H_6

The investigation on the recombined bitumen was first performed with C_2H_6. The total dead bitumen sample volume used in this case was ~13 mL. The C_2H_6 was injected into the pressure vessel from the top. The gas pressure inside the vessel was monitored by using Senso-Metrics pressure transducer.

The total sample chamber volume of the pressure vessel is about 82 mL. Subtracting 13 mL for oil sample, the total space for gas is about 69 mL. The investigation on the estimation of pressure and gas volume for saturating the heavy oil in previous work shows that, for 13 mL heavy oil sample, the gas volume needed for saturation is about 28.6 mL at target pressure and temperature. Therefore, the total available gas is much more than enough for saturating the oil.

The critical temperature and pressure of C_2H_6 is 32.2 °C and 706.7 psia, respectively. The operation temperature in this work is 30 °C, which is close to the critical temperature of C_2H_6. Therefore, the highest pressure we can use for this C_2H_6-bitumen system should be lower than its critical pressure value.

In this manner, the gas pressure inside the vessel was first raised to ~531 psia. Right after the introduction of pressurized C_2H_6, the gas source was cut off and no more gas was added into the system afterwards. Due to the dissolving of C_2H_6 into the bitumen, the pressure inside the vessel will keep decreasing until it finally reaches the equilibrium.

4.3.2.2.1 Pressurization Stage of C_2H_6-Bitumen

During the initial period right after the gas injection was cut off, the pressure vessel containing bitumen and C_2H_6 was kept vertical in the 30 °C air bath of NMR spectrometer. In this manner, only diffusion occurred to the C_2H_6 dissolving into bitumen. The pressure change during the diffusion was recorded and would be used for extrapolation to remove the temperature effect on the initial pressure reading.

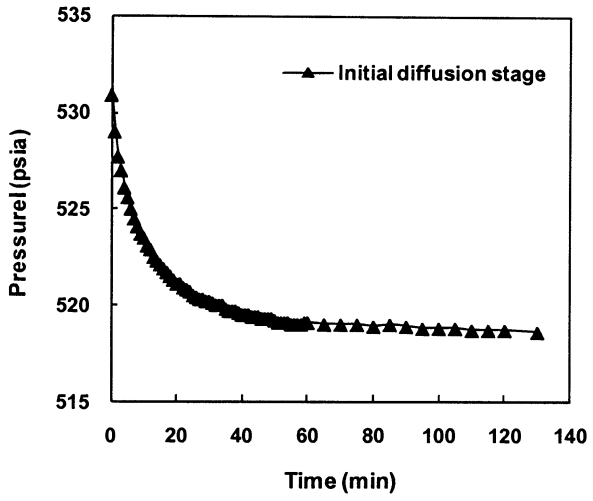

Figure 4.3.9 Recorded pressure change during diffusion in the case of C_2H_6- bitumen

As displayed in Figure 4.3.9, the recorded pressure decreased sharply within the initial 40 minutes. This is mainly due to the significant temperature change after pressurization. After the first hour, the system pressure started to level off and the recorded pressure decay markedly slowed down. During 130 minutes of diffusion, the recorded pressure inside the vessel decreased from 531 psia to 519 psia.

After the initial diffusion period, the pressure vessel was placed on the support stand at room temperature and repeatedly turned from vertical to horizontal and then

turning back to vertical, as shown in Fig. 3.3.14. In this manner, convection was introduced to the bitumen and C_2H_6 inside the vessel. Periodically, the vessel was put back into the 30 °C air bath and placed vertically for at least overnight. Then, the system pressure and the T_2 of C_2H_6 dissolved bitumen would be measured on the next morning.

The measured T_2 and pressure decay during the entire process are displayed in Fig. 4.3.10. The T_2 values in the plot are simply from the regular CPMG data interpretation. The newly interpreted T_2 values of the C_2H_6 saturated bitumen will be discussed in following sections.

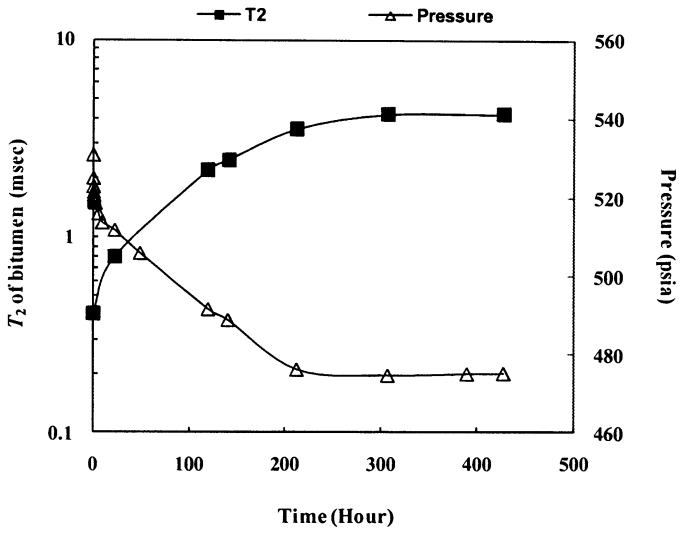

Figure 4.3.10 Pressure and T_2 change of C_2H_6- bitumen system

As shown in Fig. 4.3.10, both the recorded pressure and the measured T_2 started to level off after 200 hours and reached a plateau after ~300 hours. Afterwards, the experiment continued for an extra 129 hours and no significant changes for either pressure or oil T_2 were observed. Therefore, the system was considered as equilibrated at

that point. During the convection stage, the generated convection made the pressure decreased by about 44 psi, from 519 psia to 475 psia.

The response of C_2H_6 dissolved bitumen during the pressure decay process was monitored by NMR measurement. The measurement was taken as a function of time. Each NMR measurement was repeated at least 6 times to ensure the reliability of experimental data.

In this work, the applied echo spacing was 0.2 msec. The position of the first echo is indicated by a dashed vertical line shown in Fig. 4.3.11. The number of scans (NS) is 36 to reach SNR = 100. The operation temperature is controlled at 30 °C with an error of ±0.1 °C. The applied width of $\pi/2$ pulse and π pulse was tuned before each measurement.

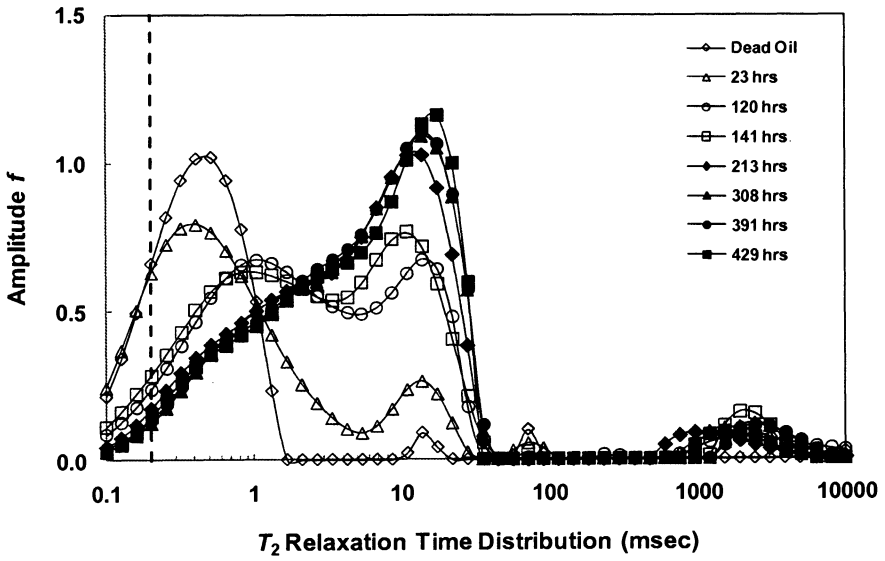

Figure 4.3.11 T_2 distribution of bitumen #10-19 with dissolved C_2H_6 during pressurization stage. Here, temperature is 30 °C.

The T_2 relaxation time distribution of C_2H_6 dissolved bitumen is shown in Fig. 4.3.11 as a function of time. Here, all the T_2 distributions are from regular CPMG data interpretations. The dashed line is the position of the first applied echo during the CPMG measurements. As displayed in Fig. 4.3.11, the T_2 distribution of the oil part become bi-modal as C_2H_6 gradually dissolves into the oil. The relatively small peaks showing up around 2 sec is the T_2 response from the dissolved C_2H_6 inside the bitumen sample at the present pressure level. These observations are similar to those obtained in the work on C_2H_6-Brookfield oil.

Because the dissolved gas decreased the viscosity of oil, the T_2 of oil with dissolved C_2H_6 becomes significantly larger (~ 10 msec). While, the T_2 of oil without gas still remained its original value (< 1 msec). Consequently, as more C_2H_6 dissolved into the bitumen, the area of peak representing the gas saturated bitumen increases and the area of peak for the bitumen without gas shrinks.

Different from the observances in the case of Brookfield oil, as shown in Fig. 4.3.11, the T_2 peak of C_2H_6 saturated bitumen is much broader. Moreover, even after the complete saturation of C_2H_6, the bitumen still has certain amount of components relaxing faster than the first applied echo spacing. This is because the bitumen #10-19 is a crude oil, which has much more complex components than the synthetic Brookfield oil, and the viscosity of this bitumen is even larger than that of Brookfield oil.

4.3.2.2.2 Depressurization Stage of C_2H_6-Bitumen

After the bitumen was saturated with C_2H_6 at ~475 psia, the depressurization was conducted by decreasing the pressure ~ 100 psi at a time till the pressure inside the vessel decreased to around 100 psia. The pressure vessel was kept vertical inside the 30 °C air bath of the NMR spectrometer during the entire depressurization process. The pressure change was recorded and the T_2 measurement was performed periodically.

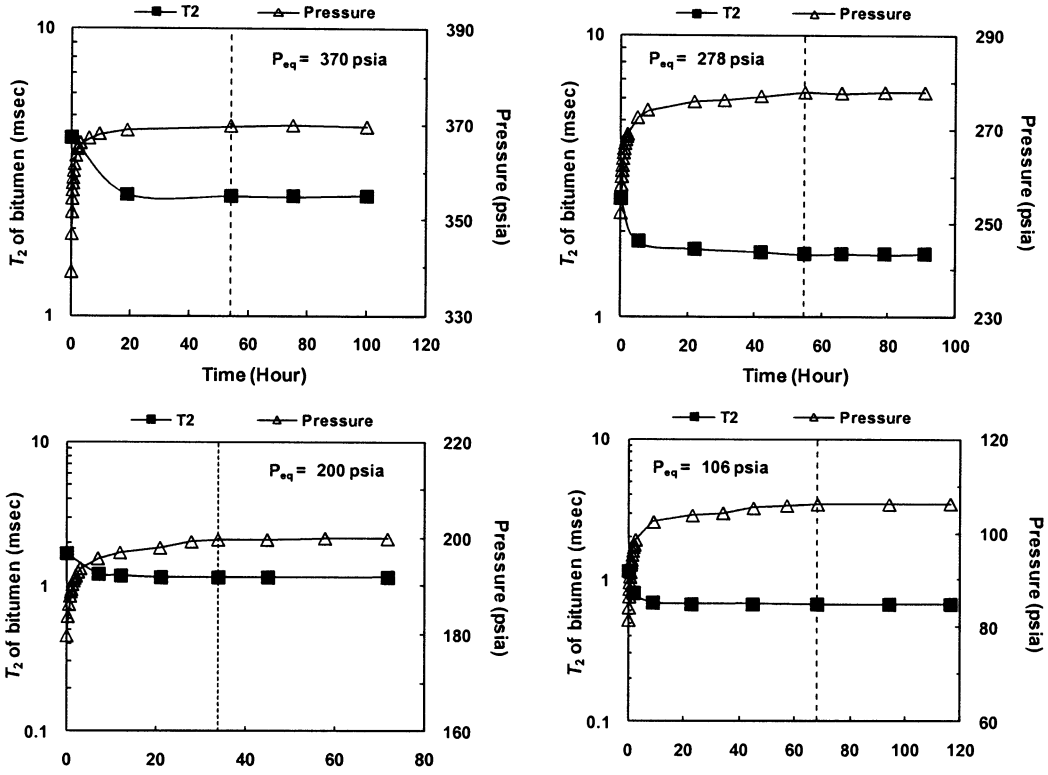

Figure 4.3.12 Change of T_2 and pressure for C_2H_6 saturated bitumen as a function of time at different pressure

All the measurements were performed at 30 °C. In order to ensure the reliability of experimental data, each NMR measurement was repeated 6 times. During the depressurization experiment, the measurement at each pressure level lasted for at least 2

more days after C_2H_6 saturated oil first reached its equilibrated value. In this manner, the reliability of measured values for T_2 and pressure at equilibrium can be ensured.

The change of the recorded pressure and T_2 for the C_2H_6 saturated bitumen at different pressure level was displayed in Fig. 4.3.12 as a function of time. The equilibrated pressure value is displayed in each subplot, respectively. The T_2 values shown in Fig. 4.3.12 are evaluated through the regular CPMG data without specified M_0 and lognormal distribution model. The new interpretation of the C_2H_6 saturated bitumen T_2 will be discussed in following sections. The vertical dashed lines in Fig. 4.3.12 indicate the time for the C_2H_6 saturated oil firstly reached its equilibrium at each pressure level.

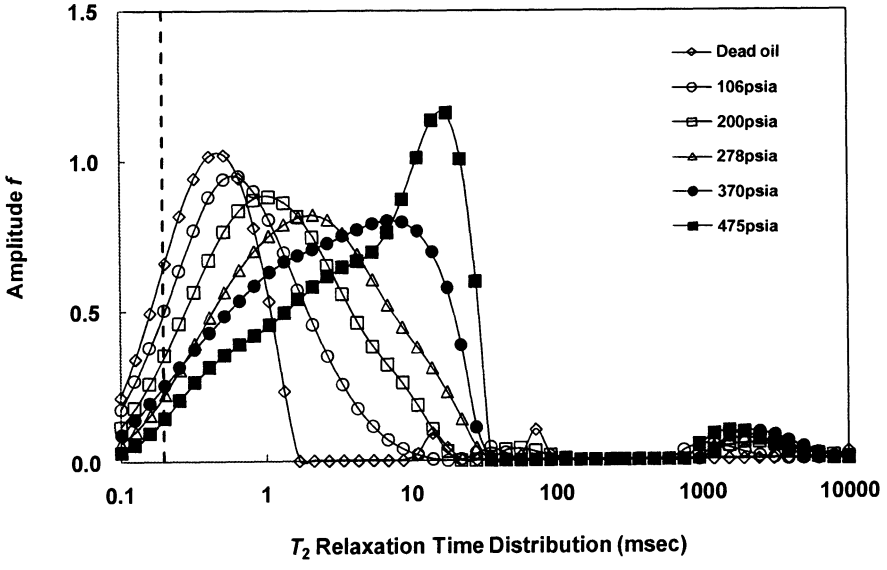

Figure 4.3.13 T_2 distribution of C_2H_6 saturated bitumen at different pressures.

The T_2 distributions of C_2H_6 saturated bitumen at different pressure levels are displayed in Fig. 4.3.13. Here, all the distributions in the plot are from the regular CPMG data interpretations. The major oil peaks on the T_2 spectra are much broader than those observed on synthetic Brookfield oil. This is because the bitumen is crude oil and has various components, which result in a broad range of T_2 responses. As mentioned in the case of C_2H_6-Brookfield oil in section 3.3.2.3, due to the specific selection of the RD value in this work, the small peaks around 2 sec as shown in Fig. 4.3.13 is not correctly proportional to the gas concentration in the bitumen.

4.3.2.2.3 New Interpretations of T_2 Distributions

As shown in Fig. 4.3.13, even saturated by C_2H_6 at the highest pressure level, the bitumen sample still has certain fast relaxing components whose relaxation time is shorter than the applied echo spacing. Therefore, M_0 needs to be imposed into the CPMG data at each equilibrated pressure level and the lognormal distribution model was employed to re-interpret the M_0 specified data (Yang and Hirasaki 2008).

As discussed in section 4.3.1.2, due to the extremely high viscosity of the bitumen sample, the value of M_0 directly extrapolated from FID has incorrect temperature dependence and needs to be corrected via Curie's law on the basis of the M_0 value obtained from FID at the highest temperature (90 °C). However, this technique for the M_0 estimation cannot be used on the bitumen sample inside the pressure vessel because the temperature rating of the vessel is only 40 °C.

Therefore, the M_0 of the dead bitumen sample inside the pressure vessel was estimated by the ratio of M_0 values obtained from regular CPMG measurements on the

two samples at same temperature (30 °C), as expressed by Eq. [4.1]. Because the M_0 value is proportional to the corresponding sample size, by using the ratio of M_0 values obtained from regular CPMG measurements, the sample volume inside the vessel can also be estimated. The M_0 of the original dead bitumen batch at 30 °C has been determined in section 4.3.1.2 and the volume of the original bitumen batch is known as ~15 mL.

$$\frac{M_{0,Curie,2}}{M_{0,Curie,1}} = \frac{M_{0,CPMG,2}}{M_{0,CPMG,1}} = \frac{V_2}{V_1} \tag{4.1}$$

Here,

Subscript 1, represents the original dead bitumen batch;

Subscript 2, represents the dead bitumen sample inside pressure vessel;

$M_{0,Curie,1}$, M_0 value of the original dead bitumen batch corrected by Curie's law;

$M_{0,Curie,2}$, M_0 value of the dead bitumen sample inside the pressure vessel corrected by Curie's law;

$M_{0,CPMG,1}$, M_0 value of the original dead bitumen batch estimated by regular CPMG measurement;

$M_{0,CPMG,2}$, M_0 value of the dead bitumen sample inside the pressure vessel estimated by regular CPMG measurement;

V_1, volume of the original dead bitumen batch, ~15 mL;

V_2, volume of the dead bitumen sample inside the pressure vessel;

In the NMR measurements on gas saturated live bitumen, the total M_0 value of the live bitumen sample is consist of two parts, response from dead bitumen and the detectable response from gas, as expressed by Eq. [4.2].

$$M_{0,T} = M_{0,b} + M_{0,g} \tag{4.2}$$

Here, $M_{0,b}$ is the response from dead bitumen and $M_{0,g}$ represents the detectable response from gas.

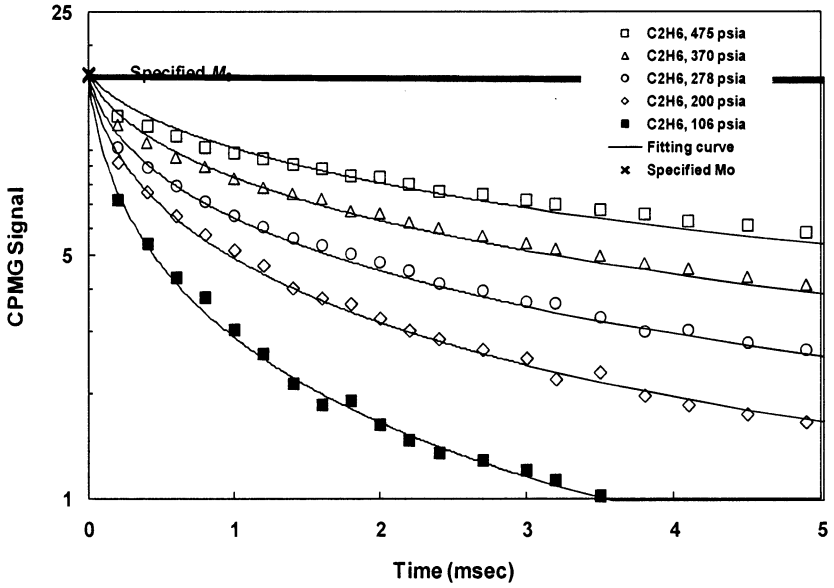

Figure 4.3.14 Interpretation of M_0 specified CPMG data of C_2H_6-bitumen by using lognormal distribution model

The method for estimating $M_{0,b}$ has been discussed in previous paragraphs. Among the three gases used in this work, the $M_{0,g}$ value of either C_2H_6 dissolved inside oil or CH_4 in vapor is calculated from its corresponding total response in the CPMG measurement because of their large T_2 relaxation time. CO_2 has no hydrogen in the

molecule thus, does not give response in the Maran spectrometer used in this work. Therefore, in the case of CO_2-bitumen, $M_{0,g}$ is 0.

The new interpretations for the C_2H_6-bitumen are displayed in Fig. 4.3.14. As shown in Fig. 4.3.14, the lognormal distribution model fits these M_0 specified CPMG data well. Note that the "X" at Time = 0, which represents the specified M_0, is not single value actually. The M_0 has different value at different pressure due to the change of $M_{0,g}$. However, in the case of C_2H_6-bitumen, the change of $M_{0,g}$ is at different pressure is not big enough to make significant difference for the total M_0 value on the logarithmic scale in Fig. 4.3.14.

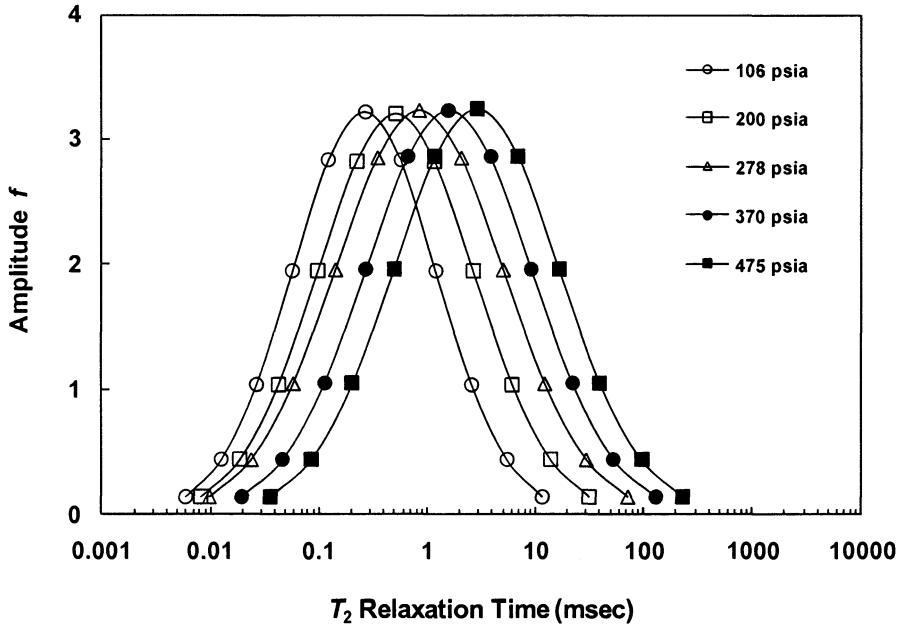

Figure 4.3.15 T_2 distribution of C_2H_6 saturated bitumen from new interpretation as a function of the equilibrium pressure

The T_2 distribution of C_2H_6 saturated bitumen from the new interpretation at each pressure level is displayed in Fig. 4.3.15. As the C_2H_6 depressurized from the ~475 psia to ~106 psia, the T_2 peak significantly shifted from the larger values to the smaller values.

The logarithmic mean T_2 of the C_2H_6 saturated bitumen from two different interpretation methods are compared in Fig. 4.3.16. The T_2 values of the live bitumen from regular interpretation are generally larger than those from lognormal distribution model with specified M_0. The difference between the T_2 values from two different interpretation methods decreases as saturation pressure increases.

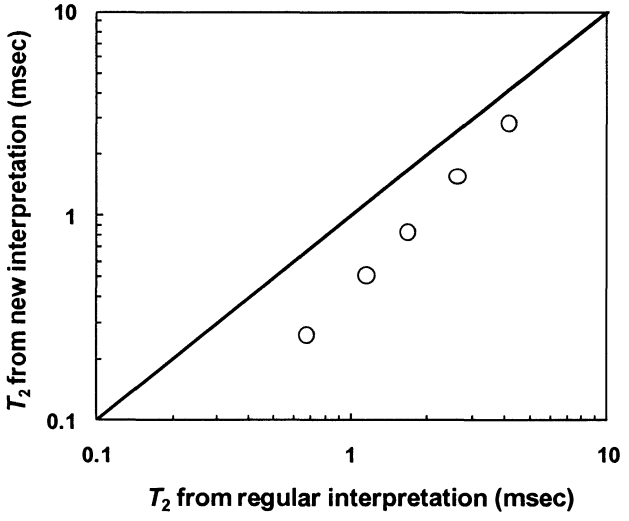

Figure 4.3.16 Comparison of C_2H_6 saturated bitumen T_2 at different pressure obtained before and after correction via lognormal distribution model.

The T_2 changes of C_2H_6 saturated oil as a function of the equilibrated pressure are displayed in Fig. 4.3.17. The rectangle symbols in Fig. 4.3.17 are the T_2 data obtained from regular interpretation at each pressure. The triangle symbols are the T_2 data obtained

from the new interpretation with lognormal distribution model. The solid lines are the fitted curves to the experimental data. The fitted functions are also shown in the plot.

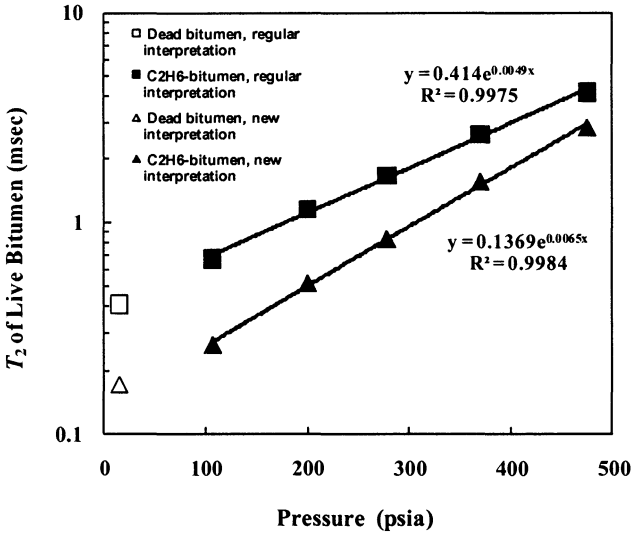

Figure 4.3.17 T_2 of C_2H_6 saturated bitumen at different pressure levels

An interesting finding from Fig. 4.3.17 is that, although the T_2 values from two different interpretations have significant discrepancy, the trends for them are both closely linear on the semi-log scale. Moreover, both of the two trends extrapolate well to their corresponding dead oil values, respectively. This proves that the T_2 differences between two interpretations are systematic, caused by the restriction of the applied echo spacing in this work.

As shown in Fig. 4.3.17, the R^2 value for two fitting curves are both near unity, indicating that the change of C_2H_6 saturated oil T_2 at different pressure closely follows the exponential function. This is similar to our observations in the work on gas-Brookfield oil systems.

4.3.2.2.4 Estimation of C_2H_6 Solubility in Bitumen

Given the pressure change, volume and temperature, the amount of C_2H_6 dissolved into bitumen at each pressure level can be calculated, as described in section 3.3.2.1. The compressibility factor z of C_2H_6 is from the NBS Technical Note 684 (NBS 1976). The plot for the z factor at 30 °C within the pressure range in this work is shown in Appendix B. The linear interpolation was used to calculate the value of compression factor z at any specific pressure, which is not directly shown by the reference book.

As mentioned in the work on Brookfield oil, the big pressure change inside the pressure vessel within a relatively short time inevitably occurred at the beginning of each pressurization or depressurization. Consequently, the significant temperature fluctuation was caused and the removal of the temperature influence on pressure reading at each pressure level is necessary.

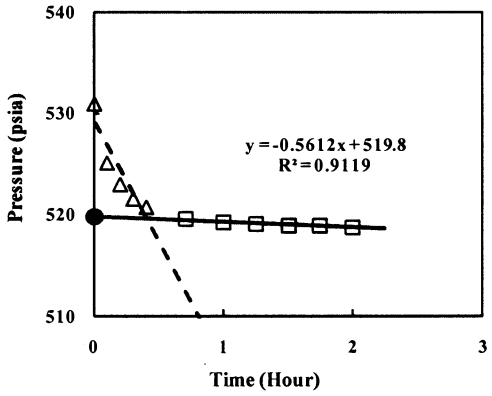

Figure 4.3.18 Extrapolation for the pressurization stage of C_2H_6-bitumen

Fig. 4.3.18 shows the analysis and extrapolation of recorded pressure data for the pressurization process of C_2H_6-bitumen. The recorded data within the initial period,

which were considered to be markedly influenced by temperature change, are shown by open triangles. The pressure data after this initial period are displayed by open rectangles and are used for extrapolation.

The extrapolation is indicated by solid line in Fig. 4.3.18. The estimated starting pressure P_0 from extrapolation is 519.8 psia, which is 11.1 psi lower than the recorded pressure data right after the introduction of high pressure C_2H_6 (530.9 psia). The similar work for depressurization is shown in Fig. 4.3.19.

In each subplot of Fig. 4.3.19, the extrapolation is shown by solid line and the extrapolated value at each pressure level is indicated by solid dot. The fitted functions and the R^2 values are also displayed.

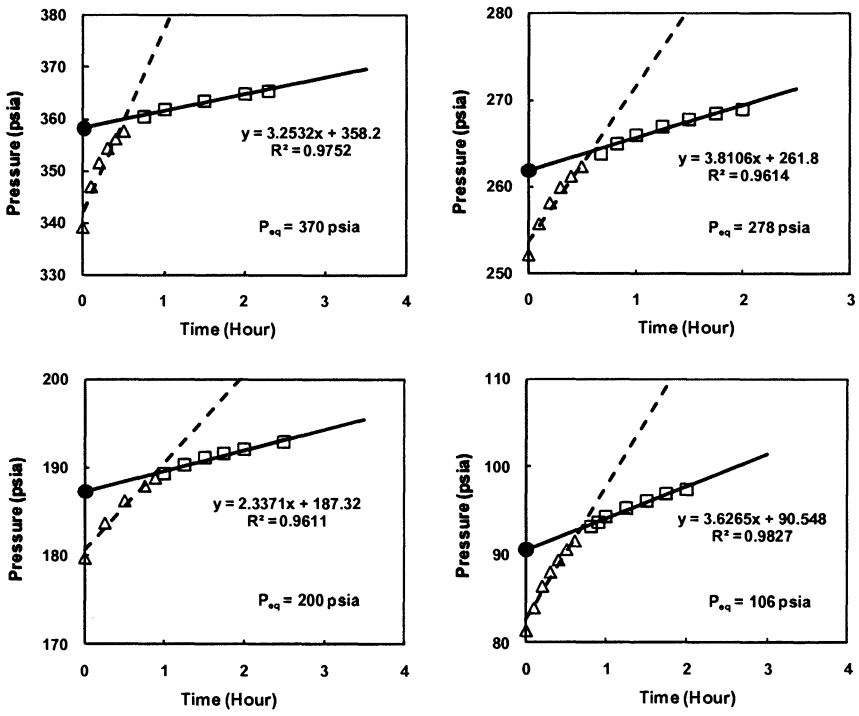

Figure 4.3.19 Extrapolations for the depressurization stage of C_2H_6- bitumen at different pressures

It is clearly shown that the difference between the trend of pressure data within the initial period (open triangles) and the later part (open rectangles) is marked. With the additional effect of temperature rise-up after each rapid depressurization, the reading pressure within the initial period increases significantly faster than those thereafter.

The estimated starting pressure P_0 at each different pressure level was summarized in Table 4.3.1. The solubility of C_2H_6 in bitumen at each pressure level was calculated by using these extrapolated starting pressure data

Table 4.3.1 Extrapolated pressure values for C_2H_6- bitumen

P_{eq} (psia)	Recorded P_0 (psia)	Extrapolated P_0 (psia)
475	530.9	519.7
370	339.1	358.2
278	252.1	261.8
200	179.7	187.3
106	81.4	90.5

The solubility of C_2H_6 in the bitumen #10-19 was calculated from the equation of state by using the extrapolated pressure data for different pressure levels. The relationship between the solubility of C_2H_6 in bitumen and its corresponding live bitumen T_2 is plotted in Fig. 4.3.20.

In Fig. 4.3.20, the solubility of C_2H_6 in bitumen is expressed in the unit of mole/mL oil. The T_2 values for the rectangle symbols are obtained from regular

interpretation and those for the triangle symbols are from the new interpretation. The solid lines are the fitted curves, whose fitted functions are shown in the plot as well.

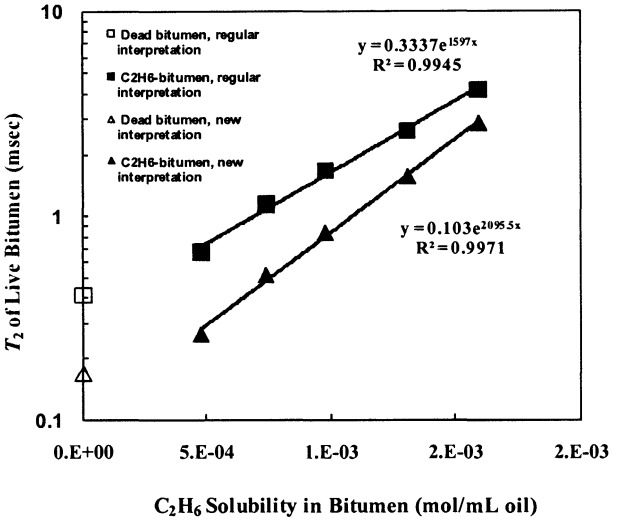

Figure 4.3.20 Relationship between the C_2H_6 solubility in bitumen and its corresponding live T_2

The similar finding can be obtained from Fig. 4.3.20 as what we had from Fig. 4.3.17. Although the T_2 values from two interpretations have significant difference, the trends for both of them are closely linear on the semi-log scale as a function of its corresponding solubility. Moreover, both of the two trends point to their corresponding dead oil values well.

The R^2 values for two fitting curves are both near unity, as shown in Fig. 4.3.20. This indicates that the exponential function is a good approximation for the relation between C_2H_6 saturated oil T_2 and its corresponding C_2H_6 solubility. This is similar to our observations on live Brookfield oil.

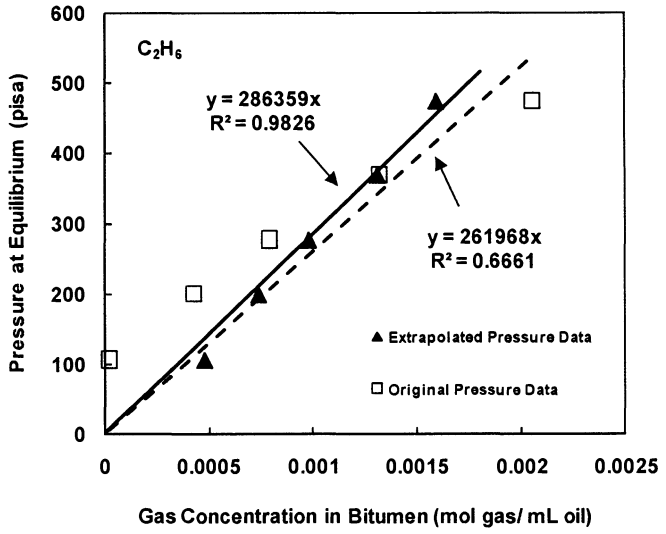

Figure 4.3.21 Relationship between the concentration of C_2H_6 in bitumen and equilibrated pressure

The relation between C_2H_6 concentration in bitumen, which was calculated with either the extrapolated pressure data or the originally recorded data, and its corresponding equilibrated pressure is plotted in Fig. 4.3.21. The solid triangles are calculations from extrapolated pressure data and are fitted by the solid line. The open rectangles represent the results by using the originally recorded data and are fitted by the dashed line.

As displayed in Fig. 4.3.21, the calculated solubility of C_2H_6 in bitumen by using the extrapolated pressure data is larger at the three lower pressure levels but smaller at the two larger equilibrium pressures, than those calculated from the originally recorded data. Especially, at 106 psia, the solubility calculated from the original pressure data is extremely low. Meanwhile, as shown in Fig. 4.3.13, the C_2H_6 saturated bitumen T_2 is significantly larger than the T_2 value of dead bitumen at 106 psia. This unreasonable result proves that correction on recorded pressure data is necessary.

Henry's law is employed to fit the Pressure vs. Gas Concentration data. The solid line is the fitted curve to the extrapolated data, while the dashed line is the fitted curve to the original data. The fitted functions for both two cases are displayed in the plot. As shown in Fig. 4.3.21, the calculated Pressure vs. Gas Concentration values with extrapolated pressure data closely follows the Henry's law. However, the calculation from the original data is badly deviated. The Henry's law constant of C_2H_6 in the bitumen #10-19 evaluated from the corrected pressure data is about 2.86 x 10^5 mL·psi/mol.

4.3.2.3 Recombined Live Bitumen with CO_2

The investigation on the CO_2 saturated bitumen was conducted with a total sample volume of ~9.5 mL. The total sample chamber volume of the pressure vessel is about 82 mL. Subtracting 9.5 mL for oil sample, the total space for gas is about 72.5 mL.

The gas pressure inside the vessel was first raised to ~760 psia by injecting CO_2 from the top of the pressure vessel. Then, the gas source was cut off and no more gas was added into the system afterwards. The gas pressure inside the vessel was monitored by using Senso-Metrics pressure transducer. Due to the dissolving of CO_2 into the bitumen, the pressure inside the vessel will keep decreasing until it finally reaches the equilibrium.

4.3.2.3.1 Pressurization Stage of CO_2-Bitumen

During the initial period right after the gas injection was cut off, the pressure vessel containing bitumen and CO_2 was kept vertical in the 30 °C air bath of NMR spectrometer. In this manner, only diffusion occurred to the CO_2 dissolving into bitumen.

The pressure change during the diffusion was recorded and would be used for extrapolation to remove the temperature effect on the initial pressure reading.

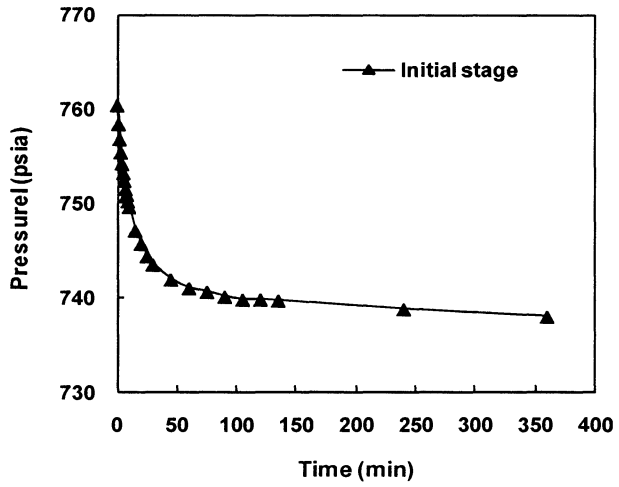

Figure 4.3.22 Recorded pressure change during diffusion in the case of CO_2- bitumen

As displayed in Figure 4.3.22, the recorded pressure decreased sharply within the initial 30 minutes. This is mainly due to the significant temperature change after the injection of the pressurized CO_2. After the first hour, the system pressure started to obviously slow down. The diffusion lasted for 6 hours (360 minutes), in which the pressure inside the vessel decreased from ~760 psia to ~738 psia.

After the initial diffusion period, the pressure vessel was placed on the support stand at room temperature and repeatedly turned from vertical to horizontal and then back to vertical, as shown in Fig.3.3.14. In this manner, convection was generated on the bitumen and CO_2 mixture inside the vessel. Periodically, the vessel was put back into the

30 °C air bath and placed vertically for at least overnight. The system pressure and the T_2 of CO_2 dissolved bitumen would be measured the next morning.

The measured T_2 and pressure decay during the entire process are displayed in Fig. 4.3.23. The T_2 values in the plot are simply from the regular CPMG data interpretation. The newly interpreted T_2 values of the CO_2 saturated bitumen will be discussed in following sections.

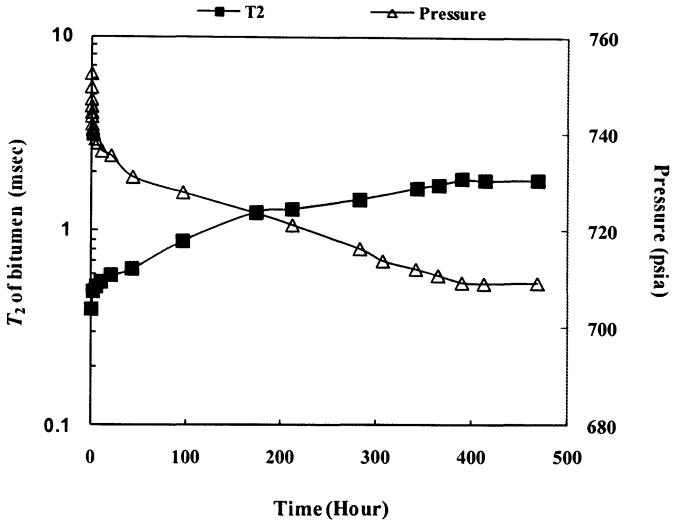

Figure 4.3.23 Pressure and T_2 change of CO_2- bitumen system

As shown in Fig. 4.3.23, the recorded pressure inside vessel and the measured T_2 of CO_2 dissolved bitumen firstly reached plateau at about 391 hours. The measurements continued for another 79 hours and no significant changes for either pressure or bitumen T_2 were observed. Therefore, the system was considered as equilibrated at that point. During the convection stage, the generated convection made the pressure decreased by about 29 psi, from ~738 psia to ~709 psia.

The response of CO_2 dissolved bitumen during the pressure decay process was monitored by NMR measurement as a function of time. Each NMR measurement was repeated for at least 6 times so that the reliability of experimental data can be ensured.

In this work, the applied echo spacing was 0.2 msec. The position of the first echo is indicated by a dashed vertical line shown in Fig. 4.3.24. The number of scans (NS) is adjusted accordingly to reach an SNR = 100. The operation temperature is controlled at 30 °C with an error of ±0.1 °C. The applied width of $\pi/2$ pulse and π pulse was tuned before each measurement.

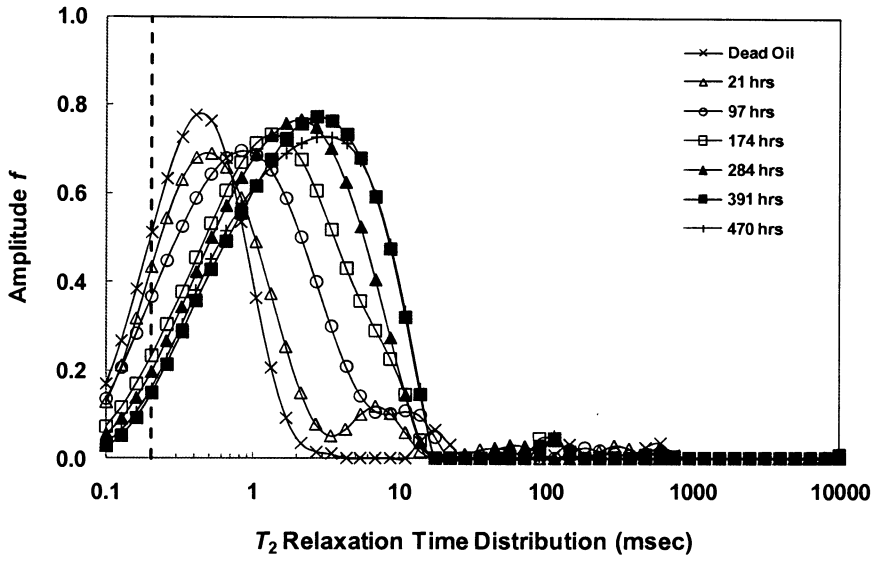

Figure 4.3.24 T_2 distribution of bitumen #10-19 with dissolved CO_2 during pressurization stage. Here, temperature is 30 °C.

The T_2 relaxation time distribution of CO_2 dissolved bitumen #10-19 is shown in Fig. 4.3.24 as a function of time. Here, all the T_2 distributions are from regular CPMG

data interpretations. The dashed line is the position of the first applied echo during the CPMG measurements. As more CO_2 dissolved into the bitumen, the oil T_2 peak gradually moves to the larger value side with time, as shown in Fig. 4.3.24.

Unlike the observations in C_2H_6-bitumen case, the bi-modal for the bitumen T_2 with CO_2 vanished much faster. After the initial 21 hours, no bi-peak was observed for the T_2 response during the rest of the CO_2 saturation process. This is due to the unique natural convection caused by the CO_2 dissolved oil (Haugen and Firoozabadi 2009), (Nasrabadi, Firoozabadi and Ahmed 2009). These observances are similar to those obtained in the work on the CO_2-Brookfield oil.

As shown in Fig. 4.3.24, the CO_2 inside bitumen reached saturation after ~391 hours. The gas dissolving experiment continued for an extra 79 hours thereafter and no significant change of T_2 distribution was observed. Different from the observances in the case of CO_2-Brookfield oil, the T_2 peak of CO_2 saturated bitumen is much broader. Moreover, even after the complete saturation of CO_2, the bitumen still has certain amount of components relaxing faster than the first applied echo spacing. Similar phenomenon was also observed in the work on C_2H_6- bitumen, as describe in the previous section.

4.3.2.3.2 Depressurization Stage of CO_2-Bitumen

After the bitumen sample was saturated with CO_2 at ~709 psia, the depressurization was conducted by decreasing the pressure ~ 150 psi at a time till the pressure inside the vessel decreases to around 100 psia. The pressure vessel was kept vertical inside the 30 °C air bath of the NMR spectrometer during the entire

depressurization process. The pressure change was recorded and the T_2 measurement was performed periodically.

All the measurements were performed at 30 °C. In order to ensure the reliability of experimental data, each NMR measurement was repeated 6 times. During the depressurization experiment, the measurement at each pressure level usually lasted for extra two more days after CO_2 saturated oil first reached its equilibrated value. In this manner, the reliability of measured values for T_2 and pressure at equilibrium can be ensured.

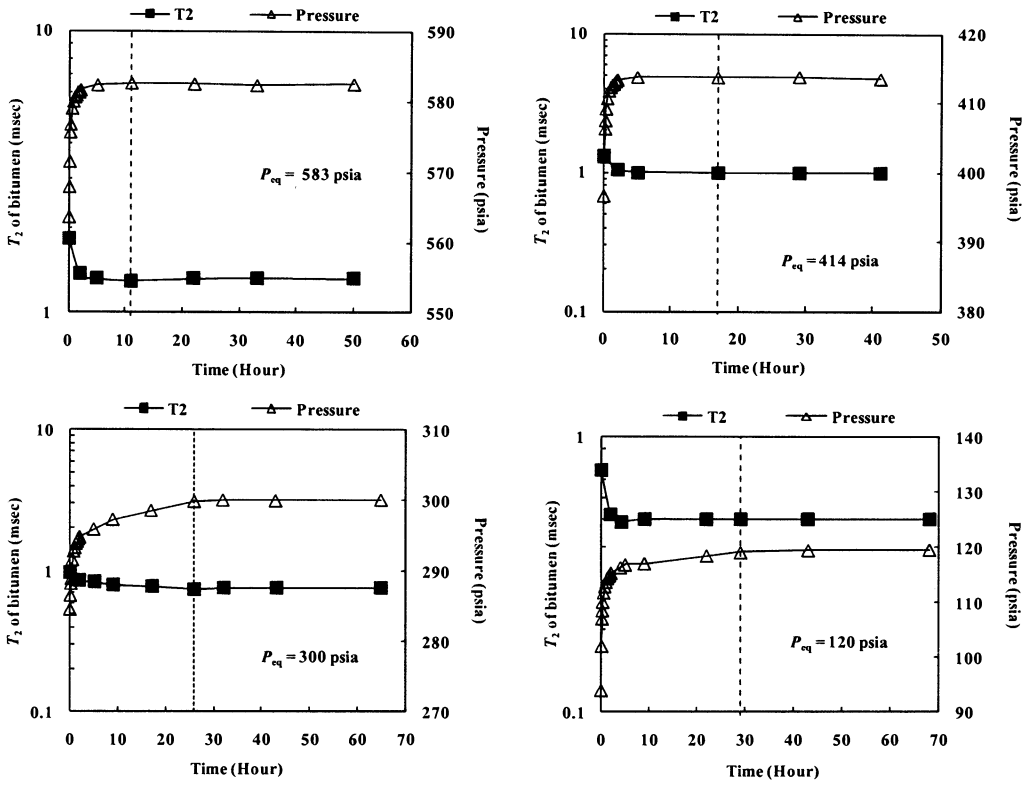

Figure 4.3.25 Change of T_2 and pressure for CO_2 saturated bitumen as a function of time at different pressure

The change of the recorded pressure and T_2 for the CO_2 saturated bitumen at different pressure level was displayed in Fig. 4.3.25 as a function of time. The equilibrated pressure value is displayed in each subplot. The T_2 values shown in Fig. 4.3.25 are evaluated through the regular CPMG data without specified M_0 and lognormal distribution model. The new interpretation of the CO_2 saturated bitumen T_2 with the lognormal distribution model will be discussed in following section. The vertical dashed lines in Fig. 4.3.25 indicate the time for the CO_2 saturated oil firstly reached its equilibrium at each pressure level.

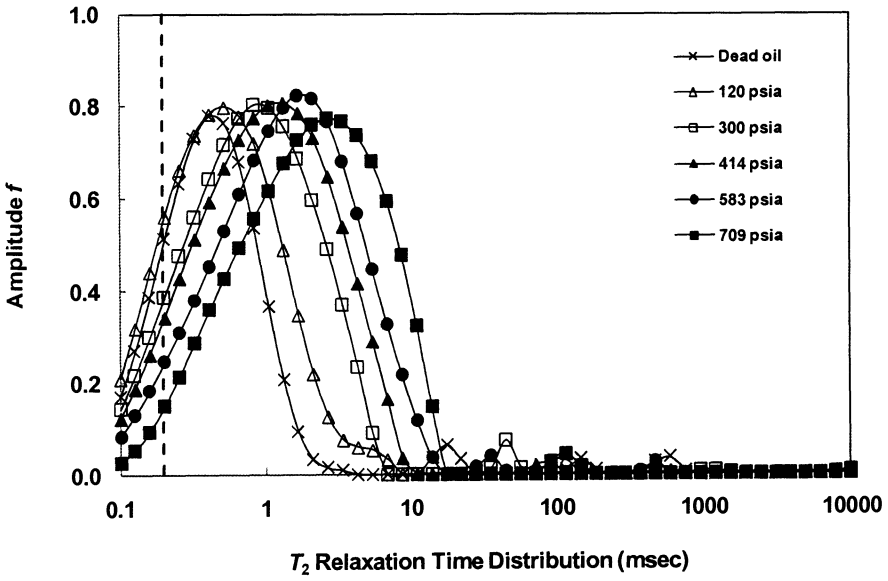

Figure 4.3.26 T_2 distribution of CO_2 saturated bitumen at different pressure level.

The T_2 distributions of CO_2 saturated bitumen at different pressure levels are displayed in Fig. 4.3.26. All the distributions shown in the plot are from regular CPMG

data interpretations. The major oil peaks on the T_2 spectra are much broader than those observed on synthetic Brookfield oil.

4.3.2.3.3 New Interpretations of T_2 Distributions

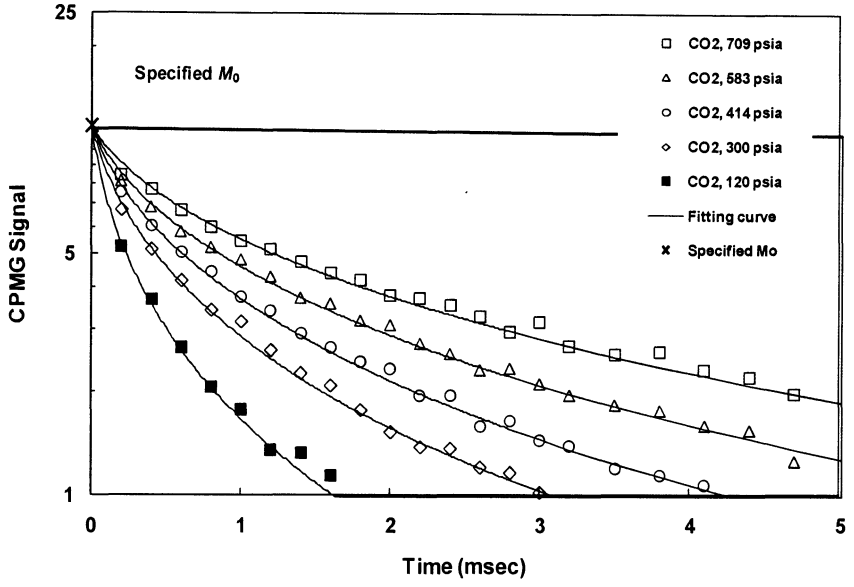

Figure 4.3.27 Interpretation of M_0 specified CPMG data of CO_2-bitumen by using lognormal distribution model

As shown in Fig. 4.3.26, even saturated by CO_2 at the highest pressure level, the bitumen sample still has certain fast relaxing components whose relaxation time is shorter than the applied echo spacing. Therefore, M_0 needs to be imposed into the CPMG data at each equilibrated pressure level and the lognormal distribution model was employed to re-interpret the M_0 specified data (Yang and Hirasaki 2008).

The new interpretations for the CO_2-bitumen are shown in Fig. 4.3.27. The "X" symbol at Time = 0 is the specified M_0 value. As mentioned in section 4.3.2.2.3, at constant temperature (30 °C), M_0 of the CO_2 saturated bitumen equals to the M_0 of dead bitumen and has a single value. The M_0 value used in Fig. 4.3.27 is estimated via the method discussed in section 4.3.2.2.3.

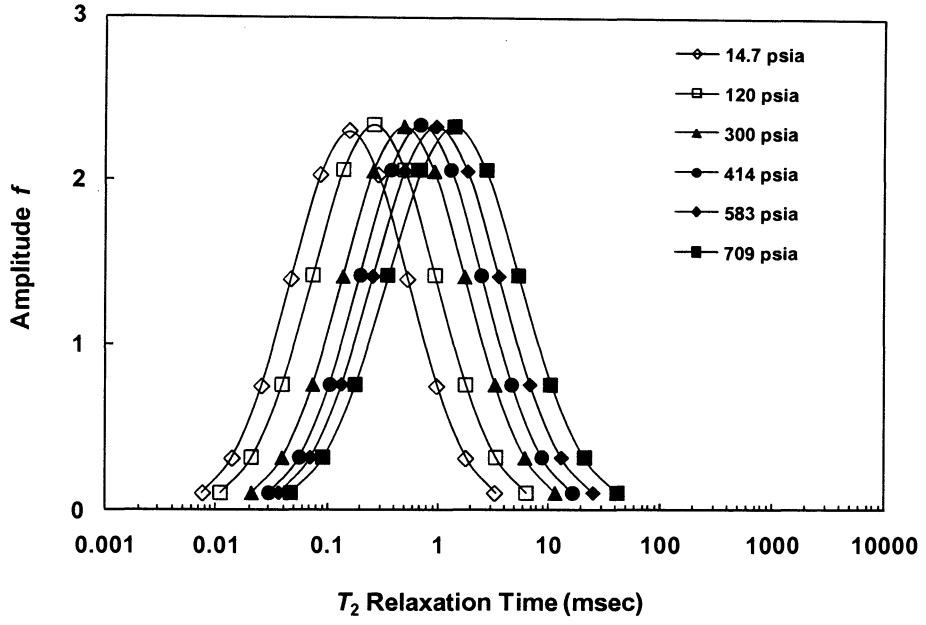

Figure 4.3.28 T_2 distribution of CO_2 saturated bitumen from new interpretation as a function of the equilibrium pressure

As displayed in Fig. 4.3.27, the lognormal distribution model fits these M_0 specified CPMG data well. The T_2 distribution of CO_2 saturated bitumen from the new interpretation at each pressure level is displayed in Fig. 4.3.28. As the CO_2 depressurized from the ~709 psia to ~120 psia, the T_2 peak significantly shifted from the larger to the smaller values.

The logarithmic mean T_2 of the CO_2 saturated bitumen from two different interpretation methods are compared in Fig. 4.3.29. Similar to the observations in the case of C_2H_6-bitumen, the T_2 values of the live bitumen from regular interpretation are generally larger than those from lognormal distribution model with specified M_0. The difference between the T_2 values from two different interpretation methods decreases as saturation pressure increases.

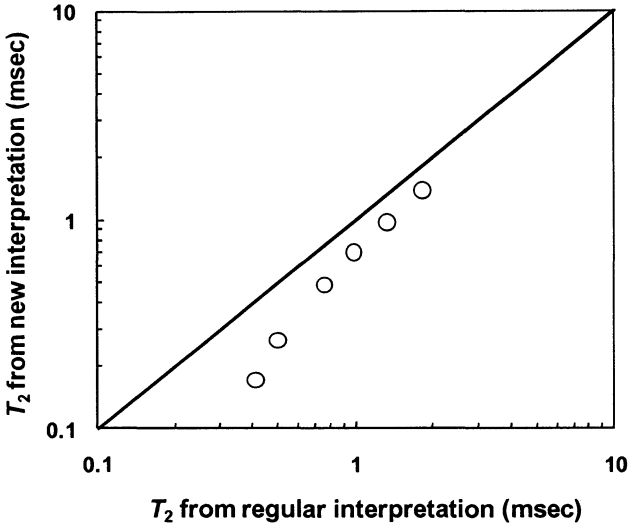

Figure 4.3.29 Comparison of CO_2 saturated bitumen T_2 at different pressure obtained before and after correction via lognormal distribution model.

The T_2 changes of CO_2 saturated oil as a function of the equilibrated pressure are displayed in Fig. 4.3.30. The rectangle symbols in Fig. 4.3.30 are the data for CO_2-bitumen. The triangle symbols are the results from C_2H_6-bitumen, used as comparison. Both the T_2 data shown in Fig. 4.3.30 are calculated from the new interpretation. The

solid lines are the fitted curves to the experimental data. The fitted functions are also shown in the plot.

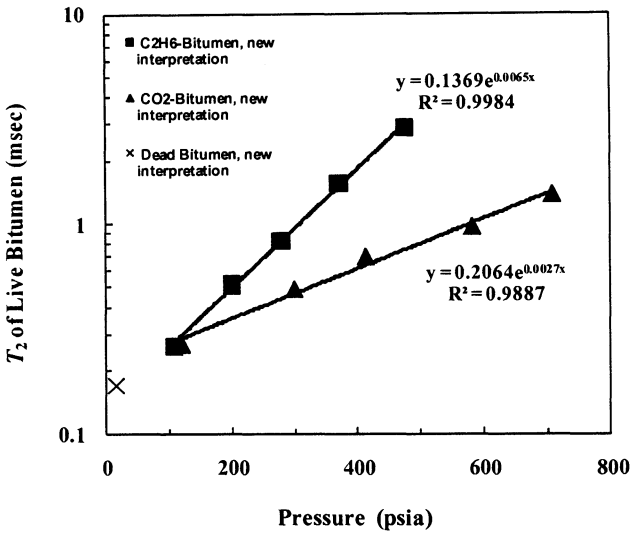

Figure 4.3.30 T_2 of CO_2 saturated bitumen at different pressure levels

It clearly shows that at the same pressure level, the T_2 change caused by C_2H_6 is generally larger than that caused by CO_2. Moreover, the higher the pressure level, the larger the difference in T_2 changes. As displayed in Fig. 4.3.30, the changes of T_2 data caused by two different gases are both closely linear on the semi-log scale and the two trends also well extrapolate to the dead bitumen value (indicated by "X"). The R^2 value for two fitting curves are both near unity, indicating that the live bitumen T_2 change caused by either C_2H_6 or CO_2 at different pressure closely follows the exponential function.

4.3.2.3.4 Estimation of CO_2 Solubility in Bitumen

Given the pressure change, volume and temperature, the amount of CO_2 dissolved into bitumen at each pressure level can be calculated, as described in section 3.3.2.1. In this case, the reference data for compression factor z of CO_2 is from the IUPAC International Thermodynamic Tables (IUPAC 1973). The linear interpolation was used to calculate the value of compression factor z at any specific pressure, which is not directly shown by the reference book.

In order to remove the temperature effects on the initial pressure reading, extrapolations were employed for the correction. Fig. 4.3.31 shows the analysis and extrapolation of recorded pressure data for CO_2-bitumen during the pressurization stage. The recorded data within the initial period, which were considered to be markedly influenced by temperature change, are shown by open triangles. The pressure data after this initial period are displayed by open rectangles and used for extrapolation.

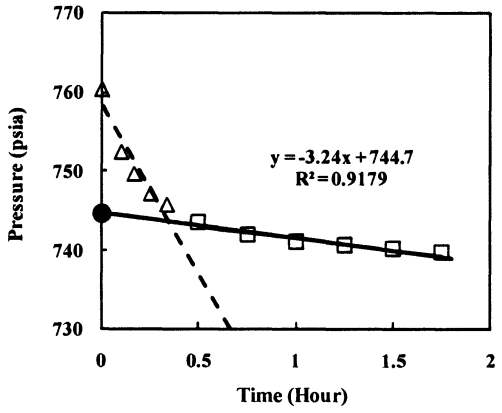

Figure 4.3.31 Extrapolation for the pressurization stage of CO_2-bitumen

The extrapolation is indicated by solid line in Fig. 4.3.31. The estimated starting pressure P_0 from extrapolation is 744.7 psia, which is 15.7 psi lower than the recorded pressure data right after the introduction of high pressure CO_2 (760.4 psia). The similar work for depressurization is shown in Fig. 4.3.32.

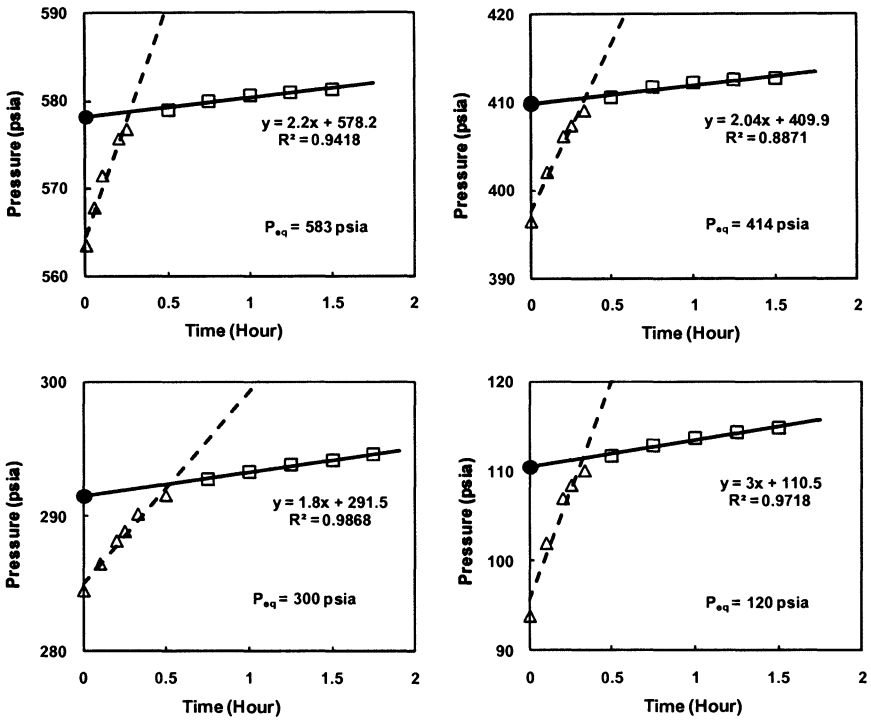

Figure 4.3.32 Extrapolations for the depressurization stage of CO_2-bitumen at different pressures

In each subplot of Fig. 4.3.32, the extrapolation is shown by solid line and the extrapolated value at each pressure level is indicated by solid dot. The fitted functions and the R^2 values are also displayed.

It clearly shows that, the difference between the trend of pressure data within the initial period (open triangles) and the later part (open rectangles) is marked. After being cooled by each rapid depressurization, the system temperature returns to the temperature of air bath. Due to the heating effect, the reading pressure within the initial period increases significantly faster than those thereafter.

The estimated starting pressure P_0 at each different pressure level was summarized in Table 4.3.2. The solubility of CO_2 in the bitumen #10-19 at each pressure level was calculated by using these extrapolated starting pressure data

Table 4.3.2 Extrapolated pressure value and solubility of CO_2 in the bitumen

P_{eq} (psia)	Recorded P_0 (psia)	Extrapolated P_0 (psia)	Solubility x 10^3 (mol gas/mL oil)
709	760.4	744.7	1.70
583	563.5	578.2	1.52
414	396.5	409.9	1.40
300	284.5	291.5	1.18
120	93.9	110.5	0.97

The solubility of CO_2 in bitumen #10-19 at different pressure level was calculated from the equation of state by using the extrapolated pressure data shown in Table 4.2. The corresponding solubilities are also shown in Table 4.3.2. The relationship between the solubility of CO_2 in bitumen and its corresponding live bitumen T_2 is plotted in Fig. 4.3.33.

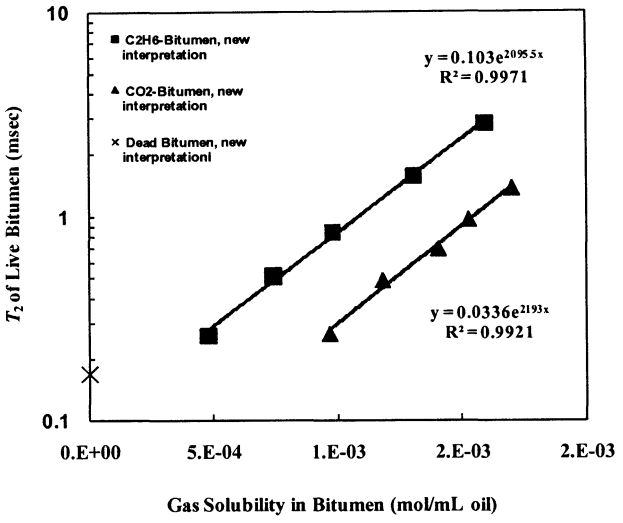

Figure 4.3.33 Relationship between the CO_2 solubility in bitumen and its corresponding live T_2

In Fig. 4.3.33, the solubility of C_2H_6 in bitumen is used to compare with the calculations in the case of CO_2-bitumen. The gas solubility is expressed in the unit of mole gas/mL oil. The T_2 values for both cases are corrected. The solid lines are the fitted curves, whose fitted functions are shown in the plot as well.

The relationship between the T_2 of CO_2 saturated bitumen and its corresponding gas solubility is closely linear on the semi-log scale. This is the same to results from C_2H_6-bitumen. However, as displayed in Fig. 4.3.33, the extrapolation of the CO_2-bitumen data is significantly deviated from the T_2 value of dead bitumen at solubility equals zero. This is the same to the observations in case of CO_2-Brookfield oil.

The relation between the CO_2 concentration in bitumen, which was calculated with the extrapolated pressure data, and its corresponding equilibrated pressure is plotted in Fig. 4.3.34. The open triangles are calculations for CO_2-bitumen. The solid rectangles

represent the results from measurements on C_2H_6-bitumen, which are used for comparison.

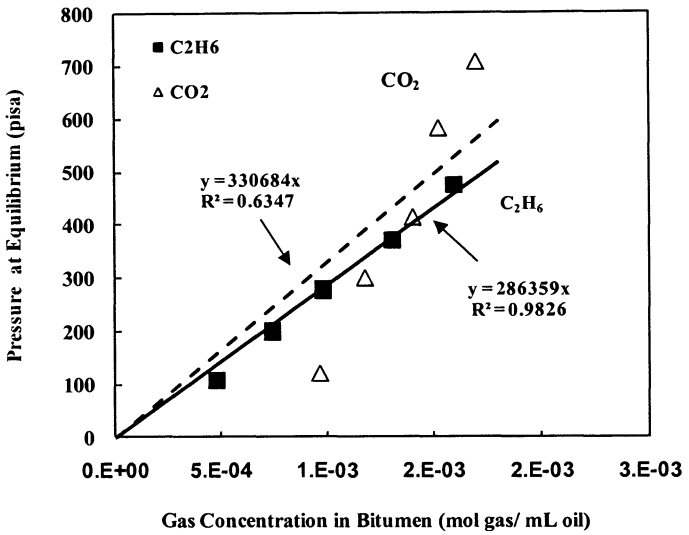

Figure 4.3.34 Relationship between the concentration of different gases in bitumen and equilibrated pressure

Henry's law is employed to fit the Pressure vs. Gas Concentration data for both cases. The solid line is the fitted curve to the C_2H_6-bitumen data, while the dashed line is the fitted curve to CO_2-bitumen data. The fitted functions for both two cases are displayed in the plot.

Similar to the observance in Fig. 4.3.33, the data from CO_2-bitumen has a marked discrepancy from the Henry's law. The calculated solubilities for CO_2 in bitumen appear not to be extrapolated to zero. This is similar to the observations on CO_2-Brookfield oil. The estimated Henry's law constant of CO_2 is about 3.54×10^5 mL·psi/mol.

4.3.2.3.5 T_1 Measurements of CO_2 Saturated Bitumen

T_1 measurements were performed on the CO_2 saturated bitumen at each corresponding pressure shown in Fig. 4.3.26. The Inversion Recovery sequence with 20 different recovery times logarithmically spaced between 30 μsec and 5 sec was employed. The interpreted T_1 distributions for the live bitumen at each equilibrated pressure level are displayed in Fig. 4.3.35.

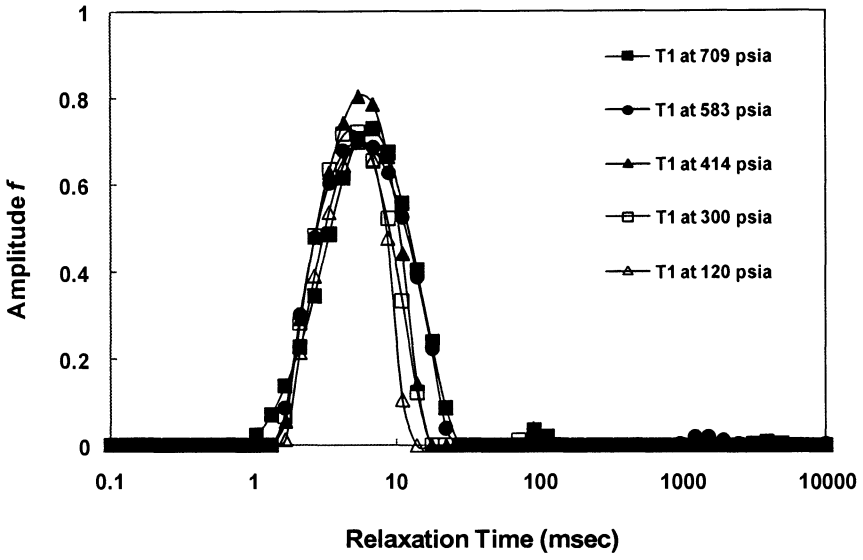

Figure 4.3.35 T_1 distribution of CO_2 saturated bitumen at different pressure levels

The change of T_1 distribution with pressure is much less significant, comparing to the corresponding T_2 change of live bitumen as shown in Fig. 4.3.26. In other words, the change of bitumen viscosity (caused by the change of CO_2 solubility at different pressure) has much more effect on the T_2 response rather than T_1. This observance accords the results obtained by our group in previous work on other heavy oil samples

(Hirasaki, Lo and Zhang 2003) and the results recently reported by some other researchers (Zielinski, et al. 2010).

4.3.2.4 Recombined Live Bitumen with CH_4

Due to the extremely high viscosity of bitumen, the sample volume was inevitably lost during the previous measurements. In the investigation on the CH_4-bitumen, the total volume of bitumen was ~7.6 mL. The total sample chamber volume of the pressure vessel is about 82 mL. Subtracting 9.5 mL for oil sample, the total space for gas is about 74.4 mL.

The gas pressure inside the vessel was firstly raised to ~946 psia by injecting CH_4 from the top of the pressure vessel. Then, the gas source was cut off and no more gas was added into the system afterwards. The gas pressure inside the vessel was monitored by using Senso-Metrics pressure transducer during the entire process until the gas-bitumen system finally reached equilibrium.

4.3.2.4.1 Pressurization Stage of CH_4-Bitumen

During the initial period right after the gas injection was cut off, the pressure vessel containing bitumen and CH_4 was kept vertical in the 30 °C air bath of NMR spectrometer. In this manner, only diffusion occurred to the CH_4 dissolving into bitumen. The pressure change during the diffusion was recorded and would be used for extrapolation to remove the temperature effect on the initial pressure reading.

Unlike the observation in the case of CH_4-Brookfield oil, the methane was found to be easier to dissolve into the bitumen than the Brookfield oil simply via diffusion. The

pressure decay inside the vessel was detectable through the Senso-Metrics pressure transducer during the diffusion period. Therefore, the method used in CH_4-Brookfield (as shown in Fig. 3.3.14) for correcting the initial pressure reading during the pressurization stage cannot be used in this case. Instead, the same method used in the cases of C_2H_6-bitumen and CO_2-bitumen was employed.

As displayed in Figure 4.3.36, the pressure decreased sharply within the first half of an hour. This is mainly due to the significant temperature decrease inside the vessel after the heating caused by the pressurization. The determination of the actual initial pressure by extrapolation will be discussed in the later section. The system pressure started slowing down obviously afterwards. During the initial 4 hours, the recorded pressure inside the vessel decreased from ~946 psia to ~926 psia.

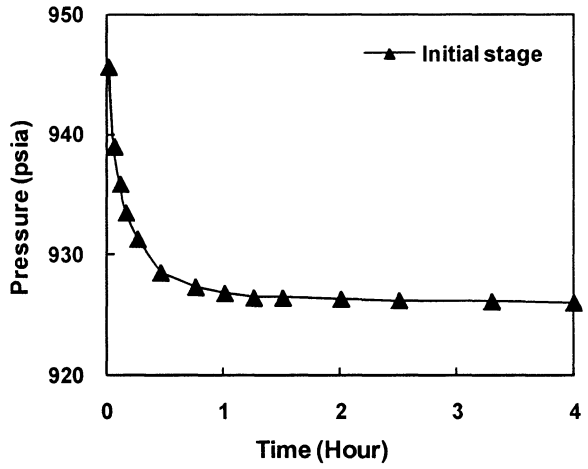

Figure 4.3.36 Recorded pressure change during diffusion in the case of CH_4- bitumen

After the initial diffusion period, the pressure vessel was placed on the support stand at room temperature and repeatedly turned from vertical to horizontal and then turning back to vertical, as shown in Fig. 3.3.14. In this manner, convection was introduced to the bitumen and CH_4 mixture inside the vessel. Periodically, the vessel was put back into the 30 °C air bath and placed vertically for at least overnight. The system pressure and the T_2 of C_2H_6 dissolved bitumen would be measured the next morning.

The measured T_2 and pressure decay during the entire process are displayed in Fig. 4.3.37. The T_2 values in the plot are simply from the regular CPMG data interpretation. The newly interpreted T_2 values of the C_2H_6 saturated bitumen will be discussed in following sections.

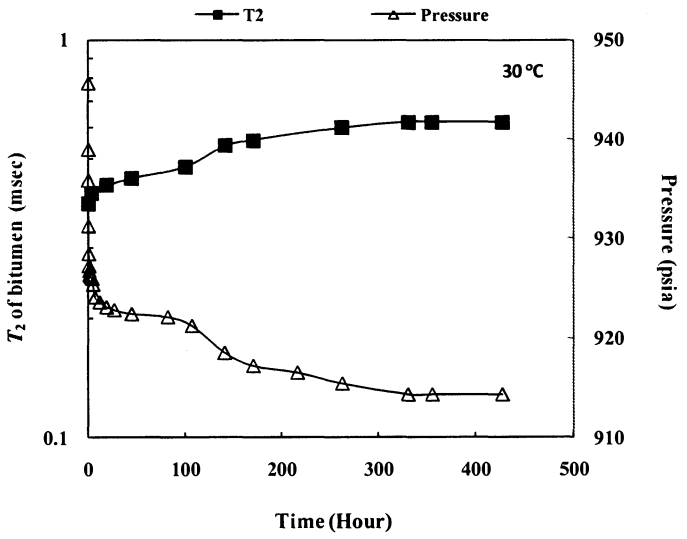

Figure 4.3.37 Pressure and T_2 change of CH_4- bitumen system

As shown in Fig. 4.3.37, the recorded pressure inside vessel and the measured T_2 of CH_4 dissolved bitumen firstly reached plateau after ~331 hours. The measurements

continued for another 97 hours and no significant changes for either pressure or bitumen T_2 were observed. Therefore, the system was considered as equilibrated at that point. During the convection stage, the generated convection made the pressure decreased by about 29 psi, from ~926 psia to ~914 psia.

The response of CH_4 dissolved bitumen during the pressure decay process was monitored by NMR measurement as a function of time. Each NMR measurement was repeated for at least 6 times so that the reliability of experimental data can be ensured.

In this work, the applied echo spacing was 0.2 msec. The position of the first echo is indicated by a dashed vertical line shown in Fig. 4.3.38. The number of scans (NS) is adjusted accordingly to reach SNR = 100. The operation temperature is controlled at 30 °C with an error of ±0.1 °C. The applied width of $\pi/2$ pulse and π pulse was tuned before each measurement.

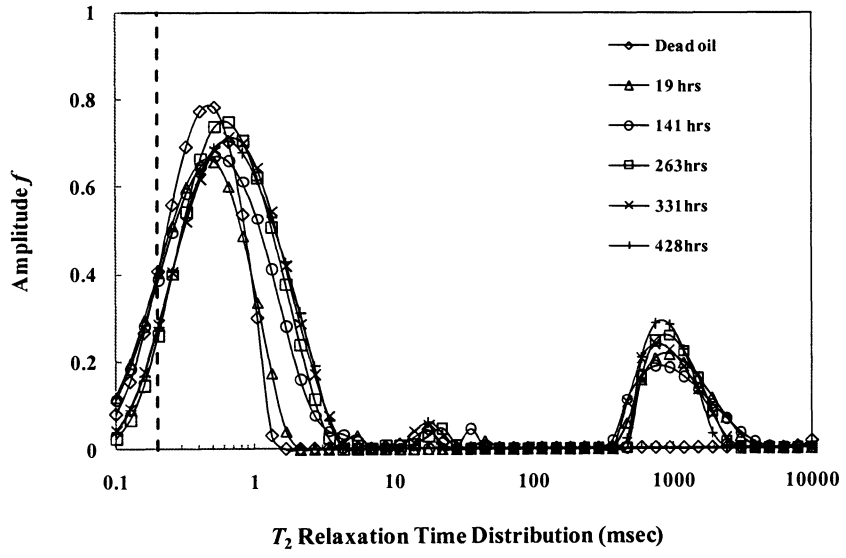

Figure 4.3.38 T_2 distribution of bitumen #10-19 with dissolved CH_4 during pressurization stage. Here, temperature is 30 °C.

The T_2 relaxation time distribution of CH_4 dissolved bitumen is shown in Fig. 4.3.38 as a function of time. Here, all the T_2 distributions are from regular CPMG data interpretations. The dashed line is the position of the first applied echo during the CPMG measurements. As more CH_4 dissolved into the bitumen, consequently as shown in Fig. 4.3.38, the oil T_2 peak gradually moves to larger values with time. Moreover, unlike the observation in C_2H_6-bitumen case, a bimodal distribution was not observed for the T_2 response during the entire CH_4 saturation process. As mentioned in the CH_4-Brookfield oil, the smaller peaks locate around 1 sec are from the CH_4 vapor inside the vessel.

As shown in Fig. 4.3.37 and Fig. 4.3.38, the CH_4 bitumen reached saturation in bitumen after ~331 hours. The gas dissolving experiment continued for an extra 97 hours thereafter and no significant changes were observed for both T_2 distribution and system pressure.

4.3.2.4.2 Depressurization Stage of CH_4-Bitumen

The depressurization was performed after the bitumen sample was saturated with CH_4 at ~914 psia. Due to the much smaller solubility of CH_4, the depressurization in this case was only conducted at two lower pressures so that enough difference can be obtained between each pressure level.

The pressure was decreased by ~ 400 psi at a time till the pressure inside the vessel decreases to around 100 psia. The pressure vessel was kept vertical inside the 30 ^{o}C air bath of the NMR spectrometer during the entire depressurization process. The pressure change was recorded and the T_2 measurement was performed periodically.

All the measurements were performed at 30 °C. In order to ensure the reliability of experimental data, each NMR measurement was repeated 6 times. During the depressurization experiment, the measurement at each pressure level usually lasted for extra two more days after CH_4 saturated oil first reached its equilibrated value. In this manner, the reliability of measured values for T_2 and pressure at equilibrium can be ensured.

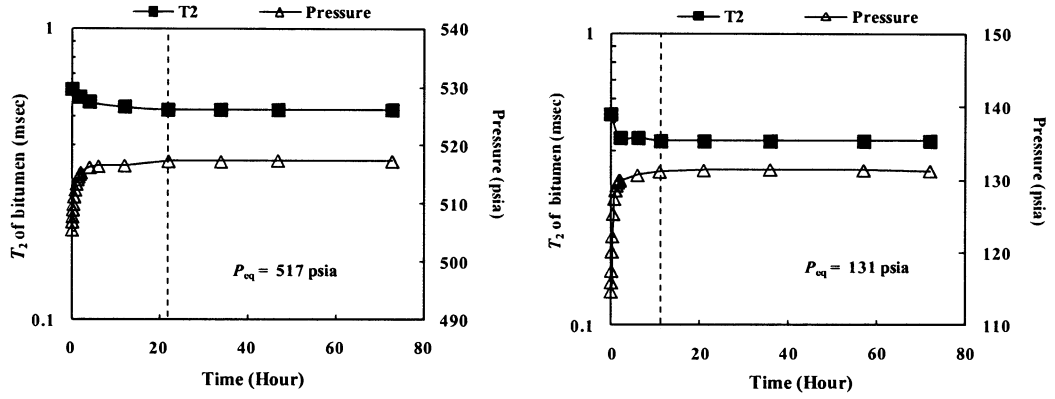

Figure 4.3.39 Change of T_2 and pressure for CH_4 saturated bitumen as a function of time at different pressure

In order to ensure the reliability of experimental data, each NMR measurement was repeated for 6 times. During the depressurization experiment, the measurement at each pressure level usually lasted for at least extra two more days after CH_4 saturated oil first reached its equilibrated value. In this manner, the reliability of measured values for T_2 and pressure at equilibrium can be ensured.

The change of the recorded pressure and T_2 for the CH_4 saturated bitumen at different pressure level was displayed in Fig. 4.3.39 as a function of time. The

equilibrated pressure value is displayed in each subplot, respectively. The T_2 values shown in Fig. 4.3.39 are evaluated through the regular CPMG data without specified M_0 and lognormal distribution model. The vertical dashed lines in Fig. 4.3.39 indicate the time for the CH_4 saturated oil firstly reached its equilibrium at each pressure level.

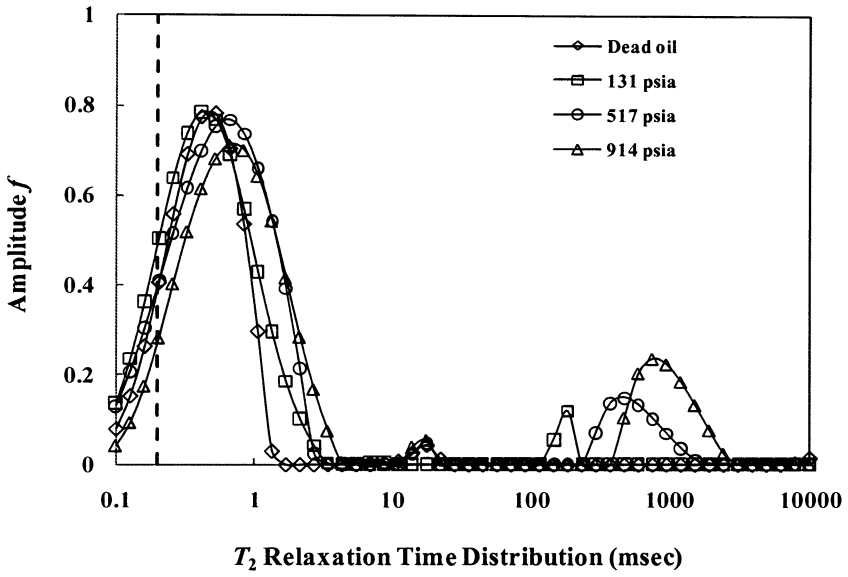

Figure 4.3.40 T_2 distribution of CH_4 saturated bitumen at different pressure level.

The T_2 distributions of CH_4 saturated bitumen at different pressure levels are displayed in Fig. 4.3.40. All the distributions shown in the plot are from regular CPMG data interpretations. The oil T_2 change resulting from the saturation of CH_4 is obviously less significant than that observed in the case of CO_2 or C_2H_6. This indicates that the much less solubility of CH_4 in the bitumen. The minor peaks between 100 msec and 1000

msec in Fig. 4.3.40 are from free CH_4 in the vapor phase. As the system pressure decreases, the gas peak moves to the smaller values and peak area shrinks.

4.3.2.4.3 New Interpretations of T_2 Distributions

As shown in Fig. 4.3.40, even saturated by CH_4 at the highest pressure level, the bitumen sample still has certain fast relaxing components whose relaxation time is shorter than the applied echo spacing. Therefore, the M_0 need to be imposed into the CPMG data at each equilibrated pressure level and the lognormal distribution model was employed to re-interpret the M_0 specified data (Yang and Hirasaki 2008).

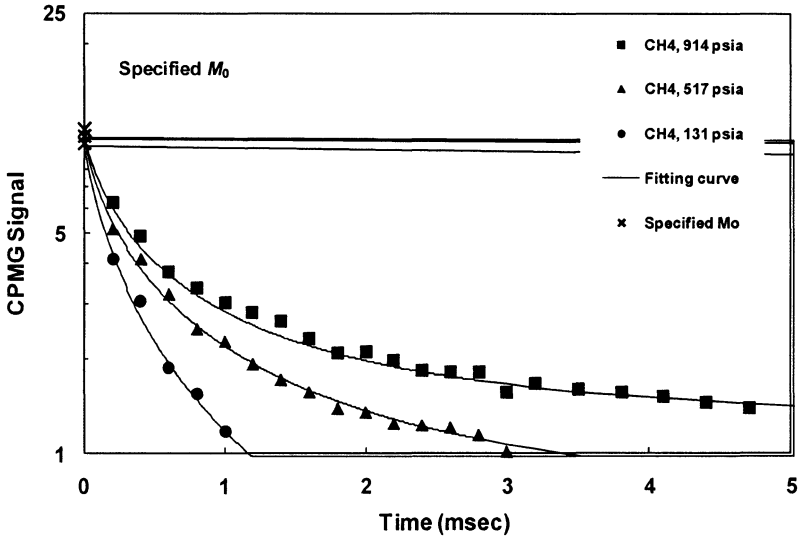

Figure 4.3.41 Fitting of M_0 specified CPMG data of live bitumen with CH_4 by using lognormal distribution model

The new interpretations for the live bitumen with CH_4 are shown in Fig. 4.3.41. The "X" symbols at Time = 0 are the specified M_0 values, which are estimated via the method discussed in section 4.3.2.2.3.

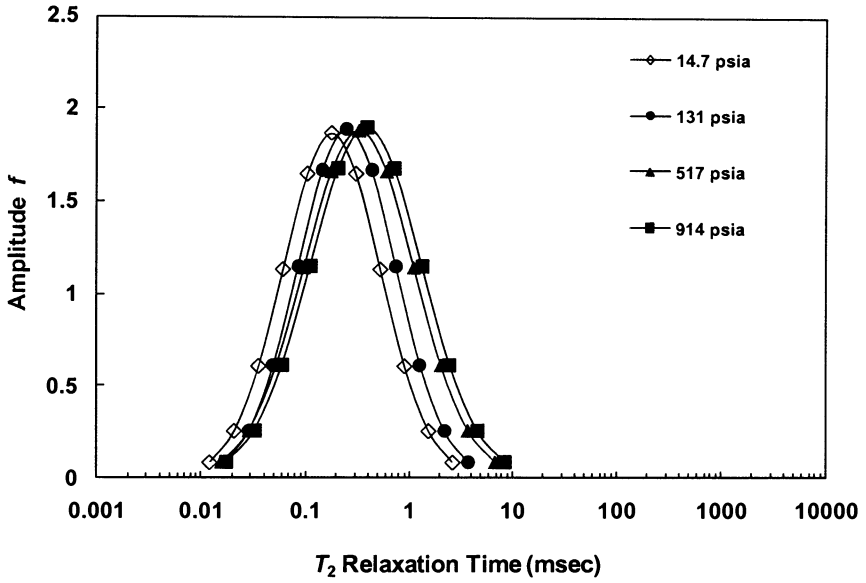

Figure 4.3.42 T_2 distribution of CH_4 saturated bitumen from new interpretation as a function of gas pressure

As displayed in Fig. 4.3.41, the lognormal distribution model fits these M_0 specified CPMG data well. The T_2 distribution of CH_4 saturated bitumen from the new interpretation at each pressure level is displayed in Fig. 4.3.42. As the CH_4 depressurized from the ~914 psia to ~131 psia, the T_2 peak shifted from the larger to the smaller values. However, due to the much smaller solubility of CH_4, the T_2 change shown in Fig. 4.3.42 is much less significant than those in the case of either C_2H_6-bitumen or CO_2-bitumen.

The logarithmic mean T_2 of bitumen from two different interpretation methods at different pressure levels are compared in Fig. 4.3.43. The T_2 values of bitumen from regular interpretation are generally larger than those from lognormal distribution model with specified M_0. The percentage difference between the T_2 from two different interpretation methods decreases as saturation pressure increases.

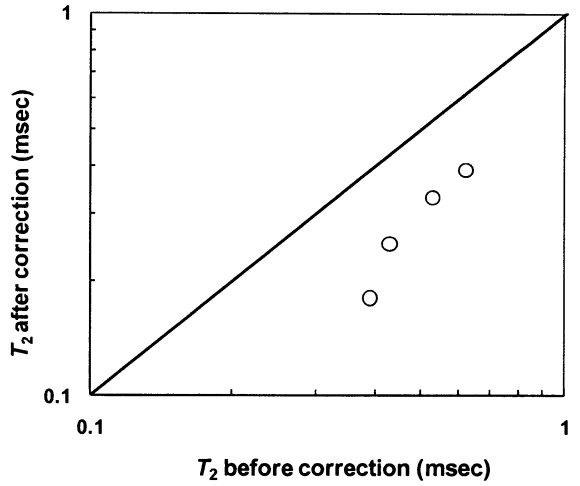

Figure 4.3.43 Comparison of bitumen T_2 at different pressure obtained before and after correction of lognormal distribution model.

The T_2 changes of live oil as a function of the equilibrated pressure for all three gases are summarized in Fig. 4.3.44. The solid dot symbols in Fig. 4.3.44 are the data for CH_4-bitumen. While the rectangle and triangle symbols are the results from CO_2-bitumen and C_2H_6-bitumen, respectively. Here, all T_2 data are calculated by using the new interpretation (Yang and Hirasaki 2008). The solid lines are the fitted curves to each experimental data. The fitted functions are shown in the plot.

It clearly shows that, at the same pressure level, C_2H_6 generally caused the largest T_2 change while CH_4 did the least. Moreover, the higher the pressure level, the larger the difference in T_2 changes for the three gases. This is similar to our observation on gas-Brookfield oil system in previous work.

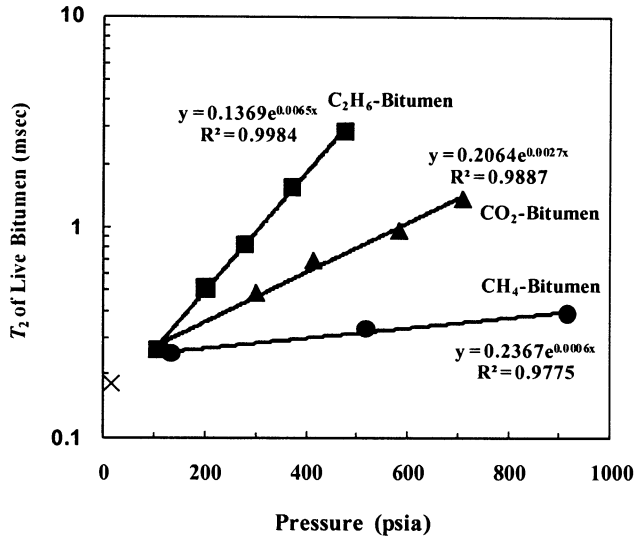

Figure 4.3.44 Live bitumen T_2 saturated by three different gases at different pressure levels

As displayed in Fig. 4.3.44, the changes of T_2 data caused by three different gases are both closely linear on the semi-log scale and the three trends also extrapolate to the dead oil value closely. The R^2 value for the three fitting curves are both nearly unity, indicating that the live oil T_2 change caused by any of these three gases at different pressure closely follows the exponential function. In this manner, the T_2 of bitumen saturated with each of the three gases at any other pressure within the pressure range in this work can be estimated.

4.3.2.4.4 Estimation of CH_4 Solubility in Bitumen

Given the pressure change, volume and temperature, the amount of CH_4 dissolved into bitumen at each pressure level can be calculated, as described in section 3.3.2.1. The reference data for compression factor z of CO_2 is from the NBS Technical Note 653 (NBS 1974). The linear interpolation was used to calculate the value of compression factor z at any specific pressure, which is not directly shown by the reference book.

In order to remove the temperature effects on the initial pressure reading, extrapolations were employed for the correction. Fig. 4.3.45 shows the analysis and extrapolation of recorded pressure data for CO_2-bitumen during the pressurization stage. The recorded data within the initial period, which were considered to be markedly influenced by temperature change, are shown by open triangles. The pressure data after this initial period are displayed by open rectangles and used for extrapolation.

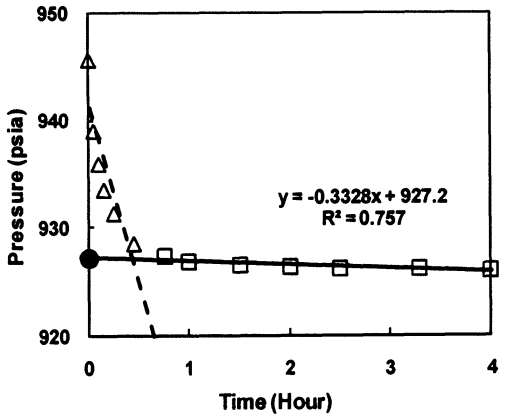

Figure 4.3.45 Extrapolation for the pressurization stage of CH_4-bitumen

The extrapolation is indicated by solid line in Fig. 4.3.45. The estimated starting pressure P_0 from extrapolation is 927.2 psia, which is 18.5 psi lower than the recorded pressure data right after the introduction of high pressure CH_4 (945.7 psia). The similar work for depressurization is shown in Fig. 4.3.46.

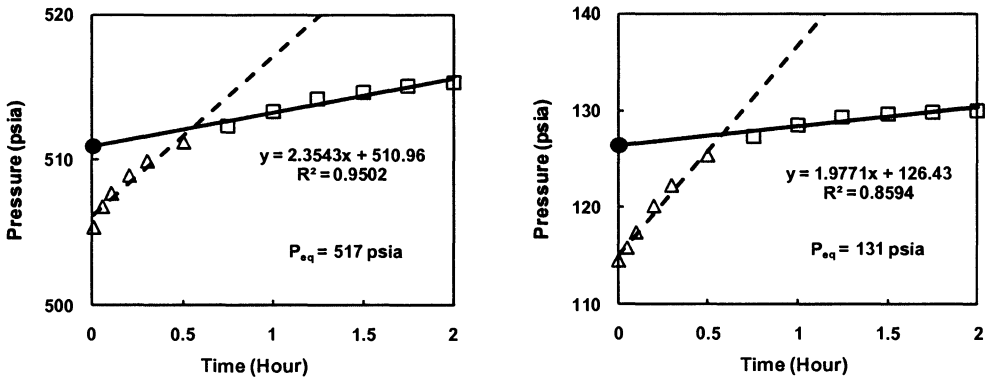

Figure 4.3.46 Extrapolations for the depressurization stage of CH_4-bitumen at different pressures

In each subplot of Fig. 4.3.46, the extrapolation is shown by solid line and the extrapolated value at each pressure level is indicated by solid dot. The fitted functions and the R^2 values are also displayed. The difference between the trend of pressure data within the initial period (open triangles) and the later part (open rectangles) is remarkable. After being cooled by each rapid depressurization, the system temperature intends to go back to the temperature of air bath. With the heating effect, the reading pressure within the initial period increases significantly faster than those thereafter.

The estimated starting pressure P_0 values for both pressurization stage and depressurization stage were summarized in Table 4.3.3. The solubility of CH_4 in the

bitumen #10-19 at each pressure level was calculated by using these extrapolated starting pressure data

Table 4.3.3 Extrapolated pressure value and solubility of CH_4 in the bitumen

Stage	P_{eq} (psia)	Recorded P_0 (psia)	Extrapolated P_0 (psia)	Solubility x 10^3 (mol gas/mL oil)
Pressurization	914	945.7	927.2	0.42
Depressurization	517	505.4	511.0	0.23
	131	114.5	126.4	0.09

The relationship between gas concentration in bitumen, which was calculated with the extrapolated pressure data, and its corresponding equilibrated pressure is plotted in Fig. 4.3.47. The dots are the calculations for CH_4-bitumen. The results obtained from C_2H_6 and CO_2 are also plotted for comparison. The rectangles represent the results from measurements on C_2H_6-bitumen and the triangles are from CO_2-bitumen.

Henry's law is employed to fit the Pressure vs. Gas Concentration data for all three gases. The two solid lines are the fitted curves to the C_2H_6-bitumen and CH_4-bitumen data, respectively. The dashed line is the fitting to the CO_2-bitumen data. The fitted functions are displayed in the plot.

As shown in Fig. 4.3.47(a), the calculated values of Gas Concentration vs. Pressure closely follow the Henry's law for the cases of C_2H_6 and CH_4. However, the data for the case of CO_2-bitumen has marked discrepancy from the Henry's law. The calculated solubility for CO_2 in bitumen appears not to extrapolate to zero when pressure becomes zero. Instead, it has an intercept of 0.00082 mol gas/mL oil at x-axis (indicated

by the red solid dot). This is similar to the observations in the work on CO_2-Brookfield oil.

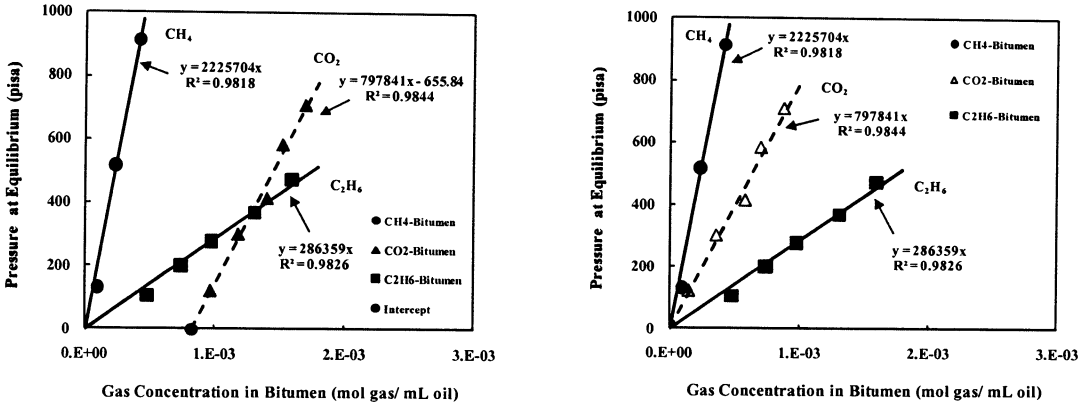

Figure 4.3.47 Relationship between the gas concentration in bitumen and the equilibrated pressures. Here, (a) solubility data in the case of CO_2-bitumen is deviated from Henry's law; (b) solubility data for CO_2-bitumen is corrected to follow Henry's law.

The proposed explanation for this phenomenon has been discussed in section 3.3.2.4. In order to correct the overestimation for the calculated CO_2 solubility in bitumen, we uniformly subtract the excess value at the intercept of x-axis from the originally calculated solubility at each pressure and re-plot the corrected CO_2 data in Figure 4.3.47(b). It is clear that, the corrected CO_2 data follows the Henry's law well.

The corrected CO_2 data is also employed in the relationship of live bitumen T_2 and CO_2 solubility. As shown in Fig. 4.3.48(a), the originally calculated data from CO_2-oil significantly deviates from the dead oil value. However, as the solubility of CO_2 was corrected via the method as shown in Fig. 4.3.47, the data trend of T_2 vs. corrected solubility of CO_2 extrapolates to the dead oil value well. The relationship between the

live bitumen T_2 and its corresponding gas solubility is closely linear on the semi-log scale for all three gases. Furthermore, similar to the observations in CO_2-Brookfield oil, the relationship between the live oil T_2 and gas solubility shown in Fig. 4.3.48(b) appears to closely follow similar trend, regardless of the gas type used for saturation.

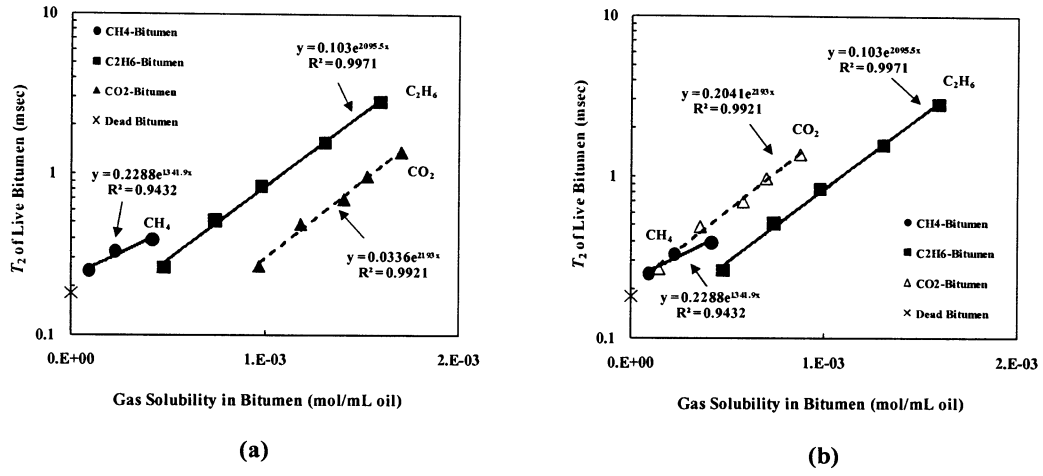

Figure 4.3.48 Relationship between the gas solubility in bitumen and its corresponding T_2. Here, (a) data from CO_2-bitumen is deviated from dead oil value; (b) corrected data for CO_2-bitumen well extrapolates to dead oil value.

The gas solubility is calculated via equation of state with compressibility factor z, as shown in section 3.3.2.1. In order to remove the overestimation for CO_2 solubility, the compressibility factor z was re-adjusted to correct the Pressure vs. Solubility curve of CO_2 to follow the Henry's law (as shown in Fig. 4.3.47). The solubility calculation method during pressurization stage is expressed by Eq. [3.1]. The adjustment on z factor can be made on either z_0 (initial point) or z_{eq} (equilibrium point) to serve the purpose.

Adjusting z_0 at the initial pressure to follow Henry's law gives the re-evaluated value z_0^* (as shown in Fig. 4.3.49) to be 0.96. This value is very unlikely for the compressibility factor of CO_2 at 745 psia.

The adjustment on z_e shows that, in order to correct the calculated solubility to follow Henry's law, the corrected z factor value needs to move down to a value of 0.55 (indicated as z_e^* in Fig. 4.3.49) at 709 psia.

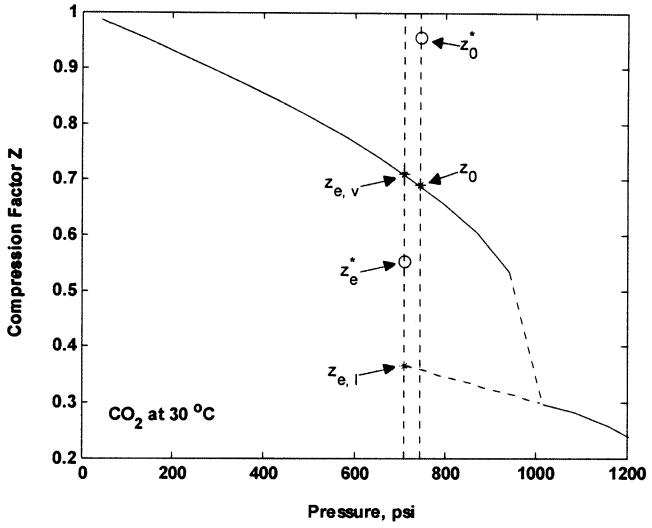

Figure 4.3.49 Analysis of compressibility factor z of CO_2 for adjusting the calculated solubility of CO_2 in bitumen #10-19 to follow Henry's law.

As we discussed in section 3.3.2.4, the estimated value of z_e^* is contributed by both $z_{e,v}$ (z factor for CO_2 vapor phase) and $z_{e,l}$ (z factor for CO_2-rich liquid phase). As shown in Fig. 4.3.49, the extrapolated value of $z_{e,l}$ at 709 psia is highlighted by red asterisk, while $z_{e,v}$ is indicated by black asterisk.

Given the values for all three z factors shown in Eq. [3.3] and combining Eq. [3.3] and Eq. [3.4], the mole fraction of CO_2 in vapor phase and CO_2 in CO_2-rich liquid phase can be calculated. The calculated mole fraction of CO_2 in vapor phase is 0.540, correspondingly, the mole fraction in CO_2-rich liquid phase is 0.460.

In this case, based on the available data in the reference book (IUPAC 1973), the estimated density for CO_2 vapor is ~0.1223 g/mL and the density for CO_2-rich liquid is ~0.4586 g/mL. In this manner, the volume fraction of CO_2 in either vapor phase or CO_2-rich liquid phase is calculated to be 0.815 and 0.185, respectively. These values are close to the calculations in the case of CO_2-Brookfield oil in Chapter 3.

4.3.2.5 Viscosity Measurements on Live Bitumen

The viscosity of live bitumen with different gases was measured at room temperature (22 °C in the cases of C_2H_6-bitumen and CO_2-bitumen, 23 °C in the case of CH_4-bitumen) via the same method as we used in the work on Brookfield oil. The viscosity measurements on the C_2H_6 saturated bitumen were performed at three pressure levels. However, due to the limited volume of available bitumen sample, the viscosity of live bitumen saturated by either CH_4 or CO_2 was only measured at one pressure level, respectively. The measured viscosity values of the bitumen #10-19 with three different gases and under different conditions are summarized in Table 4.3.4. Noted that, the T_2 value of live bitumen listed in Table 4.3.4 was re-evaluated from the NMR measurement at the same temperature as that used for viscosity measurement in each case.

Table 4.3.4 Measured viscosity and T_2 for bitumen at different temperature and pressure

Sample	Temp (°C)	P_{eq} (psia)	T_2 (msec)	Viscosity (cP)
Dead Bitumen	20	14.7	0.08	2,010,000
Dead Bitumen	30	14.7	0.17	396,000
Dead Bitumen	40	14.7	0.30	96,819
Dead Bitumen	50	14.7	0.52	29,046
Dead Bitumen	60	14.7	0.97	9,994
Dead Bitumen	70	14.7	1.46	3,818
Dead Bitumen	80	14.7	1.96	1,693
Dead Bitumen	90	14.7	3.16	844
C_2H_6-Bitumen	22	411	1.95	2,122
C_2H_6- Bitumen	22	260	0.84	10,351
C_2H_6- Bitumen	22	108	0.24	148,703
CO_2- Bitumen	22	670	0.46	44,457
CH_4- Bitumen	23	929	0.18	293,935

Comparing Fig. 4.3.50 with Fig. 3.3.36, we can find that, although the crude bitumen sample is totally different from the synthetic Brookfield oil, the live oil T_2 still correlates with viscosity/temperature ratio on log-log scale, regardless of the gas type used for saturation. Same as the observations in the case of Brookfield oil, the changes of T_2 and viscosity/temperature ratio caused by solution gas follows the same trend of those caused by temperature variations on the dead bitumen.

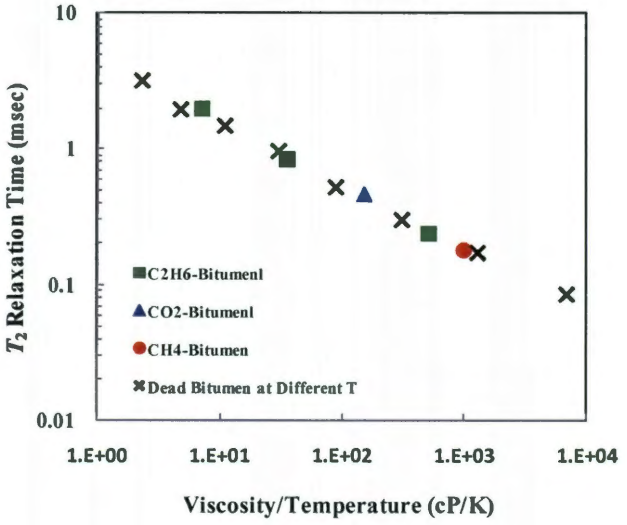

Figure 4.3.50 Relationship between the live bitumen T_2 and the viscosity/temperature ratio for all three gases

In this manner, given the proper T_2 value, the live bitumen viscosity with different solution gases and at different pressure levels can be estimated through the T_2 vs. viscosity/temperature ratio correlation obtained from the investigation on dead bitumen(as shown in Fig. 4.3.8). Data from other reference papers (Vinegar, et al. 1991), (LaTorraca, Dunn, et al. 1998), (McCann, Vinegar and Hirasaki 1999), (Y. Zhang, PhD Thesis 2002) are employed to compare with the bitumen and Brookfield oil data obtained in this work and shown in Fig. 4.3.51. Here, the relaxation time and viscosity/temperature ratio are normalized with respect to 2 MHz, as expressed by Eq. [2.17] and Eq. [2.18].

As displayed in Fig. 4.3.51, all the results of bitumen are highlighted in red. While, the data obtained from Brookfield oil are highlighted in blue. As shown in Figure 18, although the data trend of synthetic Brookfield oil is deviated from others, both T_2

and T_1 data obtained in the work on bitumen #10-19 well follow the trend of reference data from other crude oils, respectively.

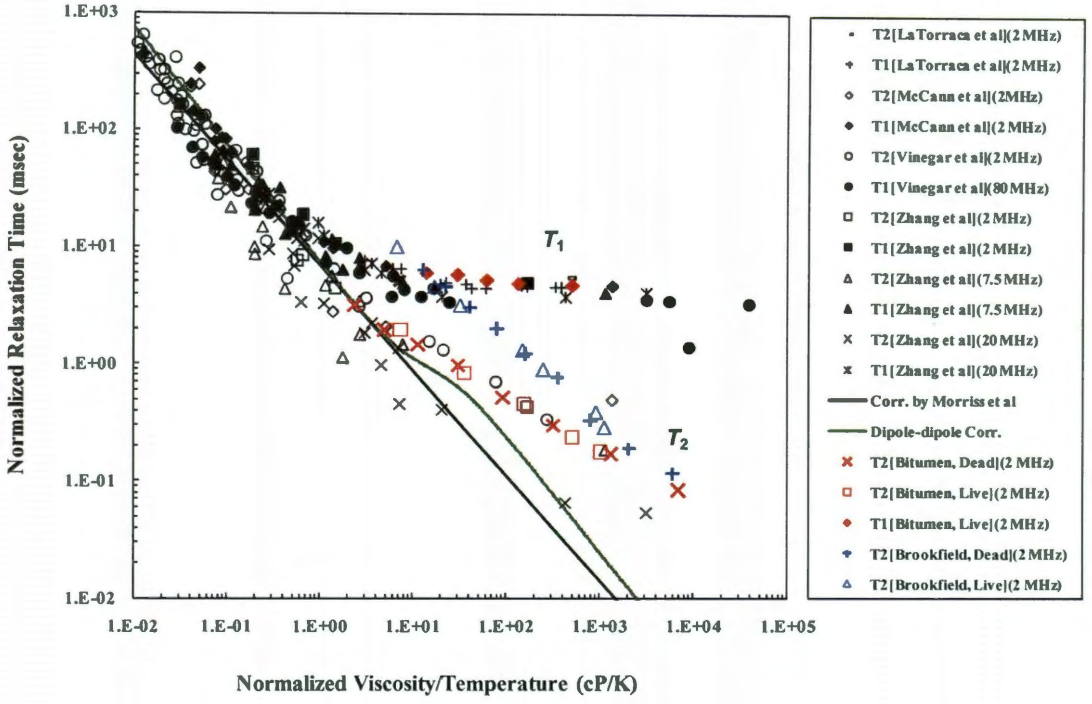

Figure 4.3.51 Relationship between the normalized relaxation time and the normalized viscosity/temperature ratio for bitumen #10-19 and other oil samples

4.4 Conclusions

The T_2 of live bitumen is significantly larger than the T_2 of dead bitumen, even at the lowest pressure level in this work (~100 psia). The relationship between the equilibrium pressure and the live oil T_2 of the bitumen sample is found to be closely linear on semi-log scale for all three reservoir gases. C_2H_6 has the most significant influence on the T_2, while, CH_4 gives the least T_2 change at the same pressure level.

Moreover, the data trend from any of the three gases extrapolated well to the dead bitumen T_2. All these findings are similar to the observations in the work on Brookfield oil.

The dissolving of both CH_4 and C_2H_6 in the bitumen sample follows the Henry's law well. However, the behavior of CO_2 significantly deviates from Henry's Law. Similar results were also noticed in the case of CO_2-Brookfield oil. The relationship between the calculated gas solubility and the corresponding live oil T_2 is found to be closely linear on a semi-log scale for all three gases. Deviation was also found for CO_2. The deviations in the case of CO_2 are possibly due to unexpected phase behavior temporarily occurring at the highest pressure level in this work, resulting in the overestimation of the pressure difference data used in the calculation of solubility. This proposed explanation needs to be verified in the future work.

In the viscosity measurements, we found that, regardless of the gas type used for saturation, the live bitumen T_2 correlates with the viscosity/temperature ratio on log-log scale. Moreover, both the T_2 and T_1 data obtained from the measurements on bitumen follow the trend of reference data from other crude oils. Furthermore, changes of T_2 and the viscosity/temperature ratio caused by solution gas follow the same trend of those caused by temperature variations on the dead oil and holds true for both crude bitumen and synthetic Brookfield oil. This creates a new way for in-situ viscosity evaluation of heavy oil through NMR well logging.

Chapter 5 Conclusions and Future Work

5.1 Conclusions of This Study

The echo spacing restriction of regular CPMG measurement on highly viscous bitumen can be overcome by specifying the initial magnetization M_0 in CPMG raw data and assuming lognormal distribution for bitumen during the interpretation.

The apparent M_0 of Athabasca bitumen from FID at low temperatures (< 60 °C) has incorrect dependence on temperature due to the loss of FID signal within the instrument's dead time. This incorrect temperature dependence can be corrected by applying the Curie's Law. Given a correct M_0 value at a certain temperature, the M_0 of the same sample at any other temperatures can be predicted by the Curie's Law.

As discussed in Chapter 2, given the Curie's Law corrected M_0 and proper cut-off between oil and water, the hydrogen index (HI) and water saturation (S_w) of bitumen sample can be evaluated by applying the method introduced in this work. The estimated HI of Athabasca bitumen is 0.82.

The T_1 and T_2 of Athabasca bitumen follow the trend of previous literature data in the relationship between the normalized relaxation time and the normalized viscosity/temperature ratio. The existing T_2 vs. viscosity correlations, which are good for the oil with relatively low viscosity, are not suitable for the samples with extremely high viscosity like Canadian bitumen.

In Chapter 3, the measurements performed on the live Brookfield oil illustrate that, CO_2 has the largest mass transfer rate in the Brookfield oil due to the unique natural

convection. There was no significant dissolving of CH_4 observed simply via diffusion up to 168 hours at ~ 890 psia. The diffusion rate of C_2H_6 was found to be between the CO_2 and CH_4. The gradual diffusion of C_2H_6 into Brookfield oil from top to bottom was confirmed by the NMR slice measurement. The convection generated by changing the orientation of the pressure vessel markedly boosts the gas dissolving rate.

The live oil T_2 is significantly larger than the T_2 value of dead oil, even at the lowest pressure level in this work (~100 psia). The relationship between the equilibrium pressure and the live oil T_2 is found to be closely linear on semi-log scale for all three reservoir gases (CO_2, CH_4 and C_2H_6).

Based on the mass balance of gas inside the closed pressure vessel, the equation of state with compression factor z was employed to calculate the gas solubility. However, large pressure changes inside the pressure vessel within a relatively short time inevitably occurred at the beginning of each pressurization or depressurization. Consequently, the system would be temporarily heated by the pressurization or cooled by the depressurization, and then return to the temperature of air bath (30 ^{o}C). In this manner, significant pressure fluctuation would be caused by the temperature change and display inaccurate P_0 for the solubility calculations. Therefore, in order to remove the temperature influence on the pressure reading and estimate the real starting pressure, extrapolation was employed to correct the recorded pressure data within the initial period after each pressurization or depressurization.

The originally recorded pressure data for all the three gases (CO_2, CH_4 and C_2H_6) were analyzed. The solubility of each gas in Brookfield oil was calculated by using the extrapolated pressure data. The dissolving behaviors of both CH_4 and C_2H_6 in Brookfield

oil are found to follow the Henry's law well. However, the observed dissolving behavior of CO_2 in Brookfield oil significantly deviates. Consequently, in the relationship between the calculated gas solubility and the corresponding live oil T_2, deviations were also found in the CO_2 case, while the data trends for the other two gases can extrapolate well to the dead oil value and are closely linear on a semi-log scale.

The investigations on the live bitumen are illustrated in Chapter 4. The measurements show that, the difference in the T_2 distribution between the bitumen with gas solute and the dead bitumen is significant for all three gases, even at the lowest pressure level (~100 psia). The relationship between the equilibrium pressure and the live bitumen T_2 is found to be closely linear on semi-log scale for each reservoir gas. C_2H_6 has the most significant influence on the T_2, while, CH_4 gives the least T_2 change at the same pressure level. Moreover, the data trend from any of the three gases extrapolated well to the dead bitumen T_2. All these findings are similar to the observations in the work on Brookfield oil.

The dissolving of both CH_4 and C_2H_6 in the bitumen sample follows the Henry's law well. However, the behavior of CO_2 is significantly different. This is the same finding obtained in the case of CO_2-Brookfield oil. The relationship between the calculated gas solubility and the corresponding live T_2 of bitumen sample is found to be closely linear on a semi-log scale for all three gases. Deviation was again noted for CO_2. The deviations in the case of CO_2 are possibly due to unexpected phase behavior temporarily occurring at the highest pressure level in this work, resulting in the overestimation of the pressure difference data used in the calculation of solubility. This proposed explanation needs to be verified in the future work.

During the viscosity evaluations of these two heavy oil samples under different conditions, we found that, regardless of the gas type used for saturation, the live oil T_2 correlates with viscosity/temperature ratio on log-log scale. Although the data for the Brookfield oil deviate from the trend of crude oils, both the T_2 and T_1 data obtained from the measurements on bitumen follow the trend of reference data from other crude oils. More importantly, the changes of T_2 and viscosity/temperature ratio caused by solution gas follows the same trend of those caused by temperature variations on the dead oil. These findings hold for both crude bitumen and synthetic Brookfield oil, and create a way for *in-situ* viscosity evaluation of heavy oil through NMR well logging.

5.2 Future Work

On the basis of the work that has been done in this study, the following future work is suggested:

1. Further work needs to be done to better distinguish the T_2 signal of heavy oil from the emulsified water inside the heavy oil. In this manner, the oil saturation can be calculated more accurately.
2. Identification of the phase behavior of CO_2 at the temperature and the highest pressure level used in this work via windowed cell tests to verify the proposed explanation for the deviation of calculated solubilities observed in the CO_2 cases in this study.
3. Investigation of the T_2 response and viscosity change of live heavy oils saturated with gas mixture at various pressures.

4. Study of combining NMR and other logging tools to better characterized the petrophysical properties of various heavy oils.

References

Bassiouni, Z. Theory, Measurement, and Interpretation of Well Logs. SPE Textbook Series, v.4., 1994.

Bouton, J., M.G. Prammer, P. Masak, and S. Menger. "Assessment of Sample Contamination by Down-Hole NMR Fluid Analysis." 2001 SPE Annual Technical Conference and Exhibition Proceedings. 2001.

Bryan, J., A. Kantzas, R. Badry, J. Emmerson, and T. Hancsicsak. "In-situ Viscosity of Heavy Oil: Core and Log Calibrations." 7th Canadian International Petroleum Conference. Alberta, Canada, 2006. Paper 2006-116.

Bryan, J., A. Mai, F. Hum, and A. Kantzas. "Oil- and Water-Content Measurements in Bitumen Ore and Froth Samples Using Low-Field NMR." SPE Reservoir Evaluation & Engineering, 2006, 9: 654-663.

Bryan, J., and A. Kantzas. "Oil-Viscosity Predictions from Low-Field NMR Measurements." SPE Reservoir Evaluation & Engineering, 2005: 8: 44-52.

Coates, G.R., L. Xiao, and M.G. Prammer. NMR Logging: Principles of Applications. Houston, TX: Halliburton Energy Service, 1999.

Cowan, B. Nuclear Magnetic Resonance and Relaxation. Cambridge, UK: Cambridge University Press, 1997.

Curwen, D. W., and C. Molaro. "Permeability fomr Magnetic Resonance Imaging Logs." SPWLA 36th Annual Logging Symposium Proceedings. Society of Petrophysicists & Well Log Analysts, 1995. 1995-GG.

Deleersnyder, M. "In-Situ Heavy-Oils Viscosity Determination Using NMR and Conventional Logs: Application to a Real Example." SPE International Thermal Operations and Heavy Oil Symposium and Western Regional Meeting. Bakersfield, CA: Society of Petroleum Engineers, 2004. Paper SPE 86939.

Dunn, K.J., D.J. Bergman, and C.A. Latorraca. Nuclear Magnetic Resonance Petrophysical and Logging Applications. New York: Pergramon, 2002.

Dunn, K.J., G.A. LaTorraca, J.L. Warner, and D.J. Bergman. "On the Calculation and Interpretation of NMR Relaxation Time Distributions ." 69th SPE Annual Technical Conference and Exhibition. New Orleans, LA: Society of Petroleum Engineers, 1994. SPE 28367.

Enick, R., G.D. Holder, and B.I. Morsi. "Critical and Three Phase Behavior in the Carbon Dioxide/Tridecane System." Fluid Phase Equilibria, 1985, 22: 209-224.

Galford, J.E. "Combining NMR and conventional Logs to Determine Fluid Volumes and Oil Viscosity in Heavy-Oil Reservoirs." 2000 SPE Annual Technical Conference and Exhibition. Dallas, TX: Society of Petroleum Engineers, 2000. Paper SPE 63257.

Galford, J.E., and D.M. Marschall. "Combining NMR and Conventional Logs to Determine Fluid Volumes and Oil Viscosity in Heavy Oil Reservoirs." 2000 SPE Annual Technical Conference and Exhibition Proceedings. SPE, 2000.

Haugen, K.B., and A. Firoozabadi. "Mixing of Two Binary Nonequilibrium Phases in One Dimension." AICHE Journal, 2009, 55: 1930-1936.

Hearst, J.R., and P.H. Nelson. Well Logging for Physical Properties. New York: McGraw-Hill Book Company, 1985.

Hirasaki, G.J., S.W. Lo, and Y. Zhang. " NMR properties of petroleum reservoir fluids." Magnetic Resonance Imaging, 2003, 21: 269-277.

Huang, C.-C. Master Thesis. Houston, TX: Rice University, 1997.

Hürlimann, M.D., L. Venkataramanan, and C. Flaum. "The diffusion–spin relaxation time distribution function as an experimental probe to characterize fluid mixtures in porous media." Journal of Chemical Physics, 2002, 117: 10223-10232.

IUPAC. International Thermodynamic Tables of the Fluid State Carbon Dioxide. London, UK: Pergamon Press, 1973.

Kleinberg, R., and H.J. Vinegar. "NMR Properties of Reservoir Fluids." The Log Analyst, 1996, 37: 20-32.

LaTorraca, G.A., K.J. Dunn, P.R. Webber, and R.M. Carlson. "Low-Field NMR Determinations of the Properties of Heavy Oils and Water-in-Oil Emulsions." Magnetic Resonance Imaging, 1998, 16: 659-662.

LaTorraca, G.A., S.W. Stonard, P.R. Webber, R.M. Carlson, and K.J. Dunn. "Heavy Oil Viscosity Determination using NMR Logs." 40th SPWLA Annual Logging Symposium. Oslo, Norway: SPWLA, 1999. paper PPP.

Lo, S.W., G.J. Hirasaki, W.V. House, and R. Kobayashi. "Mixing Rules and Correlations of NMR Relaxation Time with Viscosity, Diffusivity and Gas/Oil Ratio of Methane/Hydrocarbon Mixtures." SPE Journal, 2002, March: 24-34.

MaCann, K.E., A. Vinegar, and G.J. Hirasaki. "NMR Analysis of Crude Oil and Pure Hydrocarbon Fluids." private communication, 1999.

Masak, P.C., et al. "Field Test Results and Applications of the Down-Hole Magnetic Resonance Fluid Analyzer." 43rd SPWLA Annual Logging Symposium Transactions. SPWLA, 2002.

Miller, K., and B. Erno. "Use and Misuse of Heavy Oil and Bitumen Viscosity Data." 1995 Annual Technical Meeting of the Petroleum Society of CIM. 1995. 14-17.

Mirotchnik, K., K. Allsopp, A. Kantzas, D. Curwen, and R. Badry. "Low-Field NMR Method for Bitumen Sands Characterization: A New Approach." SPE Reservoir Evaluation & Engineering (SPE), 2001, 4(2): 88-96.

Morriss, C.E., R. Freedman, C. Straley, M. Johnston, H.J. Vinegar, and P.N. Tutunjian. "Hydrocarbon Saturation and Viscosity Estimation from NMR Logging in the Belridge Diatomite." The Log Analyst, 1997, 38: 44-59.

Nasrabadi, H., A. Firoozabadi, and T. Ahmed. "Complex Flow and Composition Path in CO_2 Injection Schemes From Density Effects in 2 and 3D." SPE Annual Technical Conference and Exhibition. New Orleans, Louisiana: Society of Petroleum Engineers, 2009. 124803-PP.

NBS. The Thermophysical Properties of Ethane, from 90 to 600K at Pressures to 700 bar. Boulder, Colorado: NBS Technical Note 684, 1976.

Orr, F.M. Jr., A.D. Yu, and C.L. Lien. "Phase Behavior of CO_2 and Crude Oil in Low-Temperature Reservoirs." Society of Petroleum Engineers Journal, 1981: 480-492.

Prammer, M.G. "NMR pore size distributions and permeability at the well site." 1994 SPE Annual Technical Conference and Exhibition Proceedings. SPE, 1994: 55-64.

Syegh, S.G., D.N. Rao, S. Kokal, and J. Najman. "Phase Behaviour and Physical Properties of Lindbergh Heavy Oil/CO_2 Mixtures." Journal of Canadian Petroleum Technology, 1990, 29: 31-39.

Straley, C., D. Rossini, A. Vinegar, P.N. Tutunjian, and C.E. Morriss. "Core Analysis by Low-Field NMR." The Log Analyst, 1997, 38: 84-94.

Tharanivasan, A.K., C. Yang, and Y. Gu. "Measurements of Molecular Diffusion Coefficients of Carbon Dioxide, Methane, and Propane in Heavy Oil under Reservoir Conditions." Energy & Fuels, 2006, 20: 2509-2517.

Upreti, S.R., and A.K. Mehrotra. "Diffusivity of CO_2, CH_4, C_2H_6, and N_2 in Athabasca Bitumen." Canadian Journal of Chemical Engineering, 2002, 80: 116-125.

Vinegar, H.J. "X-ray CT and NMR imaging of rocks." Journal of Petroleum Technology, 1986, 38:115-117.

Vinegar, H.J., P.N. Tutunjian, W.A. Edelstein, and P.B. Roemer. "Whole Core Analysis by 13C NMR." SPE Formation Evaluation, 1991, 183-189.

Yang, Z., and G.J. Hirasaki. "NMR measurement of bitumen at different temperatures." Journal of Magnetic Resonance, 2008, 192(2): 280-293.

Zhang, Q., S.-W. Lo, C.C. Huang, G.J. Hirasaki, R. Kobayashi, and W.V. House. "Some Exceptions to Default NMR Rock and Fluid Properties." SPWLA 39th Annual Logging Symposium. Keystone, Colorado: SPWLA, 1998. Paper FF.

Zhang, Y. PhD Thesis. Houston, TX: Rice University, 2002.

Zhang, Y.P., C.L. Hyndman, and B.B. Maini. "Measurement of gas diffusivity in heavy oils." Journal of Petroleum Science and Engineering, 2000, 25: 37-47.

Appendix A

Main Code:

```
% Lognormal Distribution Fitting for Bitumen, by Elton Yang

clear
clc
clf
load t_and_g.dat
x = t_and_g(2:end,1);
y = t_and_g(2:end,2);
y = abs(y);
Mo = t_and_g(1,2);
a0 = [2,0];   % initial guess

options = optimset ('TolX', 0.000001);
options.Display = 'off';
a = fminsearch ('lognorm', a0, options, x, y);

% For plotting

load t2_and_f_water.txt
t2_wat = t2_and_f_water(:,1);
f_wat = t2_and_f_water(:,2);

n = length(x);     % number of CPMG signal points for fitting
f0 = Mo - sum(f_wat);   % Sum of f for bitumen part
S = a(1);    % Sigma in lognormal distribution
M = a(2);    % Mu in lognormal distribution

Ln_t2_bit(1) = M-2.5*S;

% Lognormal distribution fitting

for i = 2:11

   Ln_t2_bit(i) = Ln_t2_bit(i-1)+S/2;
   g(i) = 1./(S*sqrt(2*pi)).*exp(-(Ln_t2_bit(i)-M).^2/(2*S^2))*abs(S/2);
   t2_bit(i) = exp(Ln_t2_bit(i));

end
g = g';
t2_bit = t2_bit';

% generate new x for plotting

spacing = t_and_g(3,1);
add_x = x(1):0.01:x(round(3/spacing));
x_plot = [add_x'; x((round(3/spacing)+1):end)];
n = length(x_plot);
```

```
for j = 1:n

   % bitumen part
   for k = 1:length(t2_bit)

      amp_bit(k) = f0*g(k)*exp(-x_plot(j)/(t2_bit(k)+eps));

   end
   sig_bit = sum(amp_bit);

   % water part
   for kk = 1:length(t2_wat)

      amp_wat(kk) = f_wat(kk)*exp(-x_plot(j)/t2_wat(kk));

   end
   sig_wat = sum(amp_wat);

   % CPMG signal = bitumen part + water part
   h(j,1) = sig_bit + sig_wat;

end

E = lognorm(a, x, y)

semilogx(x,y,'b+');
hold on
semilogx(x_plot,h, 'r');

axis ([0,20,0,20])
xlabel 'Time (msec)'
ylabel 'Fitting Curve'

fit_dat = [x_plot h];

save t_and_h_fitting_result.dat fit_dat -ascii
```

Subroutine Code for Function "Lognorm":

```
function E = lognorm(a,x,y)
% sum of square residual during log normal nonlinear regression

load t2_and_f_water.txt
load t_and_g.dat

t2_wat = t2_and_f_water(:,1);
f_wat = t2_and_f_water(:,2);

Mo = t_and_g(1,2);
n = length(x);     % number of CPMG signal points for fitting
f0 = Mo - sum(f_wat);  % Sum of f for bitumen part
S = a(1);    % Sigma in lognormal distribution
M = a(2);    % Mu in lognormal distribution
Ln_t2_bit(1) = M-2.5*S;
```

```
% Lognormal distribution fitting
for i = 2:11

   Ln_t2_bit(i) = Ln_t2_bit(i-1)+S/2;
   g(i) = 1/((S+eps)*sqrt(2*pi))*exp(-(Ln_t2_bit(i)-M)^2/(2*(S+eps)^2))*abs(S/2);
   t2_bit(i) = exp(Ln_t2_bit(i));

end
g = g';
t2_bit = t2_bit';

for j = 1:n

   % bitumen part
   for k = 1:length(t2_bit)

      amp_bit(k) = f0*g(k)*exp(-x(j)/(t2_bit(k)+eps));

   end
   sig_bit = sum(amp_bit);

   % water part
   for kk = 1:length(t2_wat)

      amp_wat(kk) = f_wat(kk)*exp(-x(j)/t2_wat(kk));

   end
   sig_wat = sum(amp_wat);

   % CPMG signal = bitumen part + water part
   h(j,1) = sig_bit + sig_wat;

end

E = sum((y - h).^2);
```

Appendix B

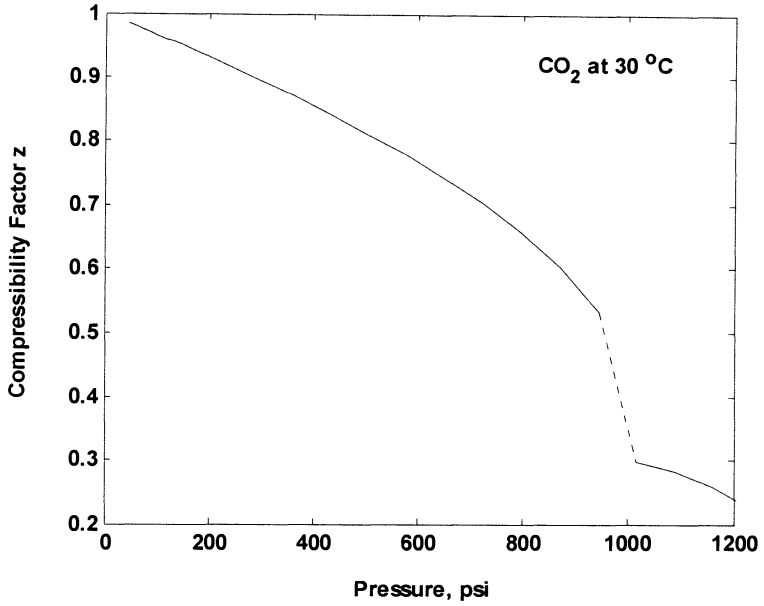
CO_2 at 30 °C
Compressibility Factor z
Pressure, psi
1
0.9
0.8
0.7
0.6
0.5
0.4
0.3
0.2
0
200
400
600
800
1000
1200

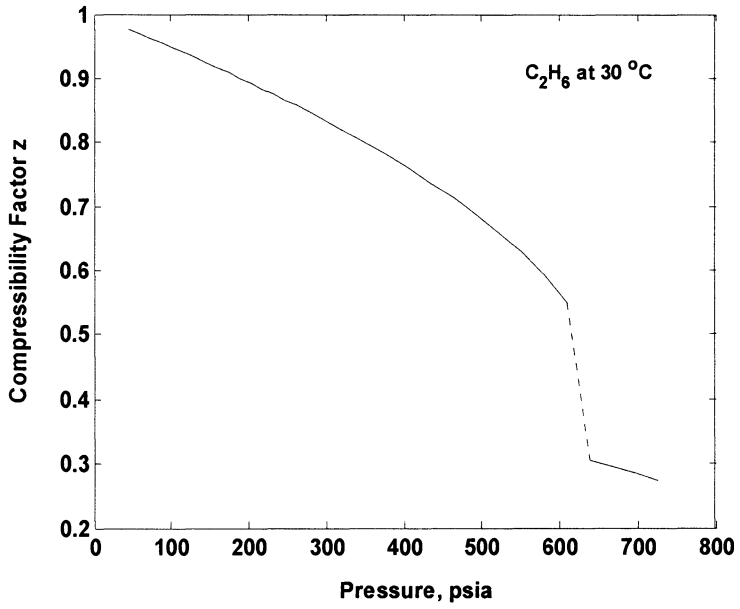
C_2H_6 at 30 °C
Compressibility Factor z
Pressure, psia
1
0.9
0.8
0.7
0.6
0.5
0.4
0.3
0.2
0
100
200
300
400
500
600
700
800

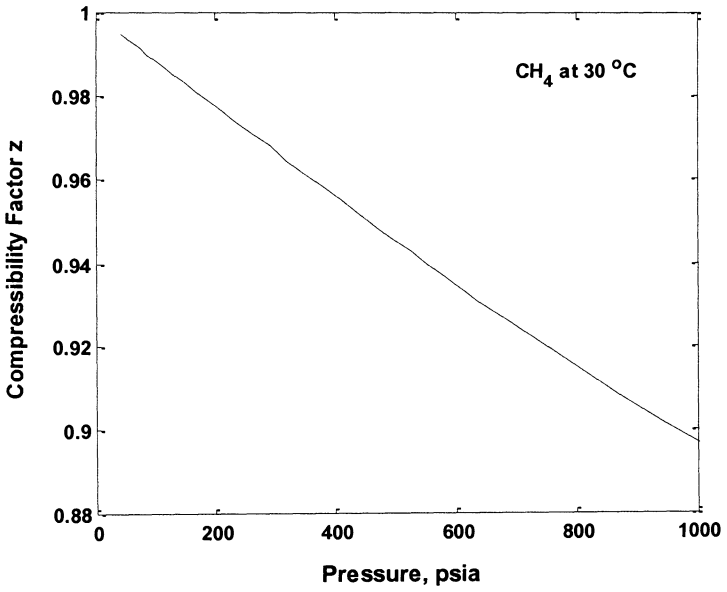
1
0.98
0.96
0.94
0.92
0.9
0.88
0
200
400
600
800
1000
Compressibility Factor z
Pressure, psia
CH4 at 30 °C